ON THE USE OF LAYERED DOUBLE HYDROXIDES IN THE MANAGEMENT OF 129I FROM LIQUID NUCLEAR WASTES

Luis Iglesias Pérez

Dipòsit Legal: T 893-2015

Ph.D. Thesis

On the use of Layered Double Hydroxides in the management of ^{129}I from liquid nuclear wastes

Luis Iglesias Pérez

Department of
Chemical Engineering

Tarragona
April 2015

UNIVERSITAT ROVIRA I VIRGILI

enresa

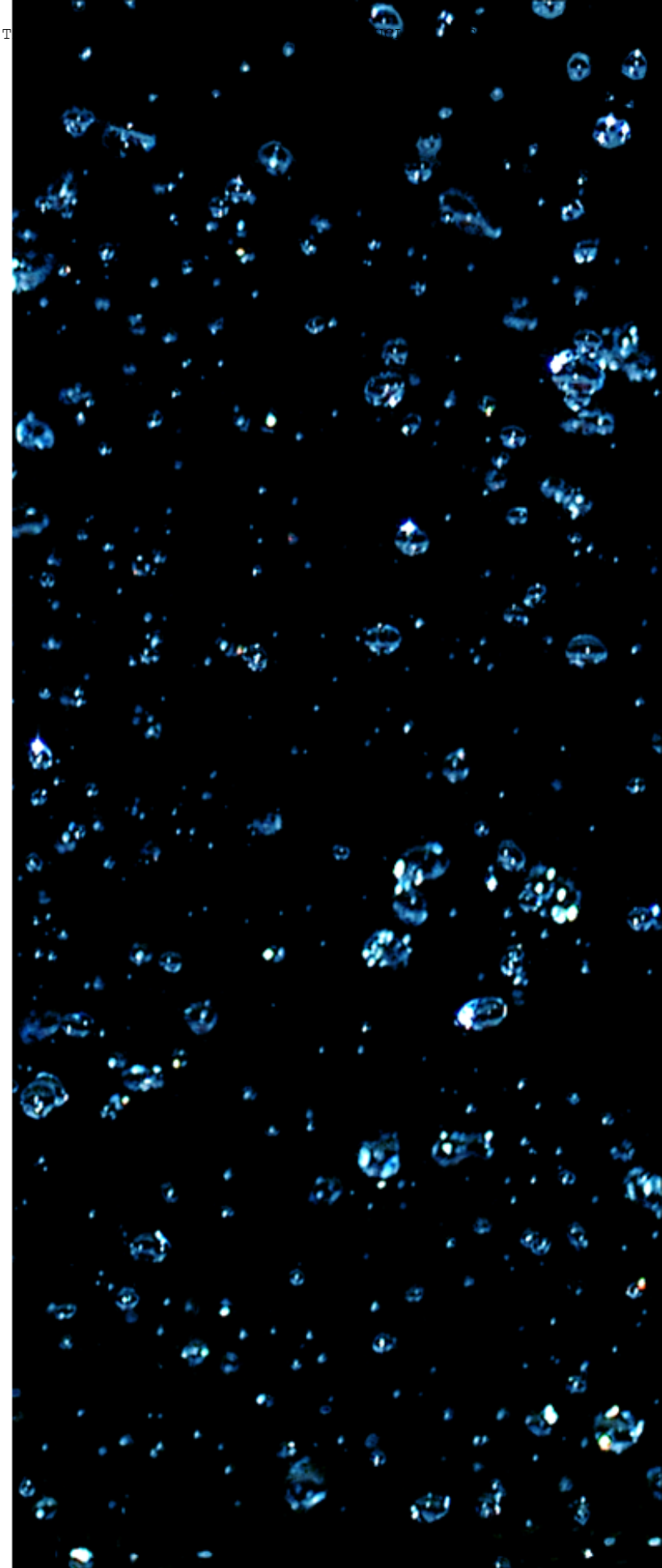

UNIVERSITAT ROVIRA I VIRGILI
ON THE USE OF LAYERED DOUBLE HYDROXIDES IN THE MANAGEMENT OF 129I FROM LIQUID NUCLEAR WASTES
Luis Iglesias Pérez
Dipòsit Legal: T 893-2015

Luis Iglesias Pérez

ON THE USE OF LAYERED DOUBLE HYDROXIDES IN THE MANAGEMENT OF ^{129}I FROM LIQUID NUCLEAR WASTES

Ph.D. Thesis

Department of Chemical Engineering

UNIVERSITAT ROVIRA I VIRGILI

Tarragona

2015

UNIVERSITAT ROVIRA I VIRGILI
ON THE USE OF LAYERED DOUBLE HYDROXIDES IN THE MANAGEMENT OF 129I FROM LIQUID NUCLEAR WASTES
Luis Iglesias Pérez
Dipòsit Legal: T 893-2015

UNIVERSITAT ROVIRA I VIRGILI
ON THE USE OF LAYERED DOUBLE HYDROXIDES IN THE MANAGEMENT OF 129I FROM LIQUID NUCLEAR WASTES
Luis Iglesias Pérez
Dipòsit Legal: T 893-2015

UNIVERSITAT ROVIRA I VIRGILI
ON THE USE OF LAYERED DOUBLE HYDROXIDES IN THE MANAGEMENT OF 129I FROM LIQUID NUCLEAR WASTES
Luis Iglesias Pérez
Dipòsit Legal: T 893-2015

Universitat Rovira i Virgili

Departament d'Enginyeria Química

Escola Técnica Superior d'Enginyeria Química

ON THE USE OF LAYERED DOUBLE HYDROXIDES IN THE MANAGEMENT OF ^{129}I FROM LIQUID NUCLEAR WASTES

Presented by

Luis Iglesias Pérez

To acquire the grade for

The European degree of Doctor

from

Universitat Rovira i Virgili

Supervised by

Dr. Francisco Medina and Dr. Mayra Garcia

UNIVERSITAT ROVIRA I VIRGILI
ON THE USE OF LAYERED DOUBLE HYDROXIDES IN THE MANAGEMENT OF 129I FROM LIQUID NUCLEAR WASTES
Luis Iglesias Pérez
Dipòsit Legal: T 893-2015

UNIVERSITAT ROVIRA I VIRGILI

Department of Chemical Engineering

Avinguda dels Països Catalans, 26
Campus Sescelades
43007 Tarragona (Spain)
Tel. 0034 977 559 603
Fax. 977 559 621
secdeq@urv.cat

WE HEREBY STATE that this work, titled "On the use of Layered Double Hydroxides in the management of ^{129}I from liquid nuclear wastes" presented by Luis Iglesias Pérez for the award of the European degree doctor has been carried out under our supervision in the department of Chemical Engineering, of the Universitat Rovira i Virgili.

Tarragona, 13th February 2015

The directors of the Ph.D. Thesis

Dr. Francisco Medina Cabello

Dra. Mayra García Álvarez

UNIVERSITAT ROVIRA I VIRGILI
ON THE USE OF LAYERED DOUBLE HYDROXIDES IN THE MANAGEMENT OF 129I FROM LIQUID NUCLEAR WASTES
Luis Iglesias Pérez
Dipòsit Legal: T 893-2015

Dedicada a mis padres.

UNIVERSITAT ROVIRA I VIRGILI
ON THE USE OF LAYERED DOUBLE HYDROXIDES IN THE MANAGEMENT OF 129I FROM LIQUID NUCLEAR WASTES
Luis Iglesias Pérez
Dipòsit Legal: T 893-2015

UNIVERSITAT ROVIRA I VIRGILI
ON THE USE OF LAYERED DOUBLE HYDROXIDES IN THE MANAGEMENT OF 129I FROM LIQUID NUCLEAR WASTES
Luis Iglesias Pérez
Dipòsit Legal: T 893-2015

Agradecimientos (Acknowledgements)

Quisiera comenzar agradeciendo al Dr. Francisco Medina el haberme dado la oportunidad de realizar el doctorado en su grupo de investigación y por su supervisión desde el inicio hasta este momento. Este agradecimiento lo hago también extensivo a la Dra. Mayra García que, primero como compañera de laboratorio y después como codirectora, con su consejo y ánimo ha ayudado sin desmayo a fortalecer y mejorar el trabajo. También querría agradecer al Dr. Ricardo José Chimentão su dedicación durante el tiempo que hemos trabajado juntos, así como a Francesc Gispert, Toni, Lukas, Mercè, Mariana y demás miembros del SRCiT de la URV por su inestimable entrega y rigor para mejorar los análisis y la interpretación de mis resultados.

Me gustaría también agradecer a ENRESA haber hecho posible este doctorado con su financiación y su constante colaboración y soporte durante la investigación, especialmente a José Luis Leganés, así como a los demás miembros de ENRESA con los que

hemos colaborado este tiempo por su implicación en el proyecto, así como a Santiago Padilla y los demás miembros del CNA.

También quiero agradecer a mis compañeros de laboratorio haber estado ahí tantas veces para intercambiar ideas, chistes malos o aún peores, críticas lapidarias u opiniones constructivas y compartir experimentos, historias, adicción a la cafeína, horas de escribir (o de intentos de escribir[1]) y momentos en el laboratorio o fuera. La tesis no habría sido lo mismo sin Óscar, Alexander, Dana, Dragos, Carla, Adriana, Iuliana, Shailesh, Pallavi, Kaveh, Beteley, Biniam, Ana, Abel, Anton, Verónica y los demás que han pasado por el laboratorio. No olvidar a Susana, que siempre ha estado ahí para lo que hiciera falta y a todo el personal de la FURV que siempre que ha sido necesaria cualquier gestión me han echado una mano.

I would like to thank Prof. Dr. Clemens for offering me the opportunity to learn with him during my six months research stay in the Institut für Radioökologie und Strahlenschutz of Hannover under his supervision. Special thank goes to Dra. Natallia Torapava for her support and guide, to Alex for his collaboration during the research and to the rest of the laboratory mates: Frank, Stefan, Claudia, amigo Dikey, Laura and all the others for share their work and time with me.

No quiero dejarme en los agradecimientos a Ricardo Ruano, Vicente Rives y Elena Pérez, con quienes me inicié en la investigación y en las hidrotalcitas en 2008 en el departamento de Química Inorgánica de la Universidad de Salamanca, estoy en deuda con ellos: sin su trabajo, dedicación y aportaciones

durante aquellos meses no hubiera continuado en esto para llegar hasta aquí.

Finalizando, quiero mencionar a María, Elena, Tatiana, los demás moradores de la facultad y amigos con los que he compartido cafés, preocupaciones, rosquillas, catorces de abril, curiosidades[2]*, momentos y chistes aún más malos tanto en la universidad como fuera durante este tiempo y que han contribuido y me han trasmitido fuerza y ánimos, desde la cercanía o la distancia, de una forma u otra, para sacar adelante esta tesis, personas que sin que las mencione ya saben quiénes son.*

1 – Upper, D.; The unsuccessful self-treatment of a case of "writer's block"; Journal of Applied Behavior Analysis, 1974, 7, 497

2 – Sokal, A.D; Transgressing the Boundaries: Towards a Transformative Hermeneutics of Quantum Gravity; Social Text, 1996, 46, 217-252

UNIVERSITAT ROVIRA I VIRGILI
ON THE USE OF LAYERED DOUBLE HYDROXIDES IN THE MANAGEMENT OF 129I FROM LIQUID NUCLEAR WASTES
Luis Iglesias Pérez
Dipòsit Legal: T 893-2015

Summary

^{129}I is considered to be a very hazardous radionuclide due to its long half-life, the low interaction that it presents with most geological materials and its biological relevance. The nuclear activity has generated around 5068 kg of ^{129}I, present very diluted in liquid wastes from nuclear power plants. Mg-Al layered double hydroxides (LDHs) with different ratios and interlayer anion have been studied as iodide adsorbent materials. Adsorption capacity was strongly affected by material textural properties, and the carbonate LDH-derived mixed oxides with Mg/Al ratio of 3/1 showed the largest adsorption capacity, increased by applying ultrasound. LDH of different compositions were studied as potential candidates for the immobilization of iodine (as iodate or iodide) using different incorporation methods: coprecipitation, anionic exchange and reconstruction. The reconstruction gave the highest iodate incorporation, ca. 54 % vs. ca. 40 % reached by coprecipitation. The thermal stability of the materials and the anionic release in contact with a solution was also studied. The iodine loss by heating at 453 K was very significant as well as and the release of iodine in contact with MilliQ water and brine solution. At the present stage of the research we may conclude that LDHs can be considered as iodine scavengers for a short-term storage, but they are not suitable for a long-term disposal of radioactive iodine.

UNIVERSITAT ROVIRA I VIRGILI
ON THE USE OF LAYERED DOUBLE HYDROXIDES IN THE MANAGEMENT OF 129I FROM LIQUID NUCLEAR WASTES
Luis Iglesias Pérez
Dipòsit Legal: T 893-2015

Resumen

El radioisótopo ^{129}I está considerado un radionucleido peligroso debido a su largo tiempo de vida media, la baja interacción que presenta con la mayoría de los materiales geológicos y su relevancia biológica. La actividad nuclear ha generado alrededor de 5068 kg de ^{129}I, apareciendo muy diluido en las desechos acuosos de las centrales nucleares. Los hidróxidos dobles laminares (HDLs) de Mg-Al con diferentes ratios y diferentes aniones interlaminares han sido estudiados como materiales adsorbentes de yoduro. La capacidad de adsorción se vio fuertemente afectada por las propiedades texturales del material, y los óxidos mixtos derivados de las HDLs de carbonato con relación Mg/Al 3/1 tienen la mayor capacidad de adsorción, la cual se incrementa con la aplicación de ultrasonidos. HDLs de diferentes composiciones se estudiaron también como posibles candidatos para la inmovilización de yodo (como yodato o como yoduro) usando diferentes métodos de incorporación: coprecipitación, intercambio aniónico y reconstrucción. La reconstrucción da la mayor incorporación de yodato, aproximadamente 54% frente al 40% aprox. que alcanzó por coprecipitación. También se estudió la estabilidad térmica de los materiales y la pérdida de yodato en contacto con una solución. La pérdida del al calentar a 453 K fue muy relevante y también lo fue la pérdida de yodato en contacto con agua MilliQ o salmuera. En la etapa actual de la investigación se pueden considerar a los HDLs como aptos para adsorber yoduro de una solución pero no son adecuados para un almacenamiento a largo plazo de yodo radiactivo.

UNIVERSITAT ROVIRA I VIRGILI
ON THE USE OF LAYERED DOUBLE HYDROXIDES IN THE MANAGEMENT OF 129I FROM LIQUID NUCLEAR WASTES
Luis Iglesias Pérez
Dipòsit Legal: T 893-2015

Resum

El ^{129}I està considerat un radionúclid perillós a causa del seu llarg temps de vida mitjana, la baixa interacció que presenta amb la majoria dels materials geològics i la seva rellevància biològica. L'activitat nuclear ha generat al voltant de 5068 kg de ^{129}I, apareixent molt diluït en les deixalles aquoses de les centrals nuclears. Els hidròxids dobles laminars (HDLs) de Mg/Al han estat estudiats com materials adsorbents de iodur, fent proves amb diferents ràtios i diferents anions interlaminars. La capacitat d'adsorció es veu seriosament afectada per les propietats texturals del material, i els òxids mixtes derivats de les HDLs de carbonat amb ràtio Mg/Al 3/1 tenen la major capacitat d'adsorció, la qual s'incrementa amb l'aplicació d'ultrasons. HDLs de diferents composicions es van estudiar també com a possibles candidats per a la immobilització de iode (com iodat o com iodur) utilitzant diferents mètodes d'incorporació: coprecipitació, intercanvi aniònic i reconstrucció. La reconstrucció dóna la major incorporació de iodat, aproximadament el 54% enfront del 40% aprox. que va aconseguir per coprecipitació. També es va estudiar l'estabilitat tèrmica dels materials i la pèrdua de iodat en contacte amb una solució. La pèrdua en escalfar a 453 K les mostres va ser molt significativa i també ho va ser la pèrdua de iodat en contacte amb aigua MilliQ o salmorra. En l'etapa actual de la investigació es poden considerar els HDLs com a aptes per adsorbir iodur d'una solució però no són adequats per a un dipòsit a llarg termini de iode radioactiu.

UNIVERSITAT ROVIRA I VIRGILI
ON THE USE OF LAYERED DOUBLE HYDROXIDES IN THE MANAGEMENT OF 129I FROM LIQUID NUCLEAR WASTES
Luis Iglesias Pérez
Dipòsit Legal: T 893-2015

Figure caption

1. Introduction

2. Materials and experimental methods

3. Layered Double Hydroxides

Contents

He donned his suit of armour, mounted Rocinante with his patched-up helmet on, braced his buckler, took his lance, and by the back door of the yard sallied forth upon the plain in the highest contentment and satisfaction at seeing with what ease he had made a beginning with his grand purpose.

The Ingenious Gentleman
Don Quixote of La Mancha

Se armó de todas sus armas, subió sobre Rocinante, puesta su mal compuesta celada, embrazó su adarga, tomó su lanza, y, por la puerta falsa de un corral, salió al campo con grandísimo contento y alborozo de ver con cuánta facilidad había dado principio a su buen deseo.

El Ingenioso Hidalgo
Don Quijote de la Mancha

Miguel de Cervantes

1. Introduction

UNIVERSITAT ROVIRA I VIRGILI
ON THE USE OF LAYERED DOUBLE HYDROXIDES IN THE MANAGEMENT OF 129I FROM LIQUID NUCLEAR WASTES
Luis Iglesias Pérez
Dipòsit Legal: T 893-2015

1.1. Radioactivity

1.1.1. Nuclear power reactors and nuclear wastes

Power generation is the main source of nuclear waste worldwide. There are two forms of power generation based on nuclear reactions: nuclear fission, where a fissionable nucleus is induced to division for a neutron and gets divided and splits into smaller parts (lighter nuclei and often free neutrons and photons)[1]; and nuclear fusion, a process that generates heavier atomic nuclei from two or more lighter atoms; but only the former has been deployed commercially[2]. A nuclear fission reactor harnesses a nuclear chain reaction, normally using as uranium enriched in ^{235}U as fuel, a fissile uranium isotope that can be induced to fission with low-energy thermal neutrons.

Actually, they are 434 nuclear power reactors in operation in 30 countries (and 69 under construction) and there are a variety of different fission reactors in use[3], the map shown their distribution in Figure 1-1. Approximately, a 81% are light water moderated and cooled reactors; 11% are heavy water moderated and cooled reactors, 3.5% are light water cooled, graphite moderated reactors, 3.5% are gas cooled reactors and two reactors are liquid metal cooled fast reactors[3]. All the major reactor manufacturers have developed third-generation reactors that are designed to be safer than those operating today. The construction of new nuclear power plants get slowed after Fukushima accident but the expansion continues nowadays, especially in China.

However, nuclear energy remains a controversial source of electric power because of the potential danger in case of accidental release of radioactive material. There is, moreover, no generally accepted means of disposing of nuclear waste and this is a growing problem across the world[4 5].

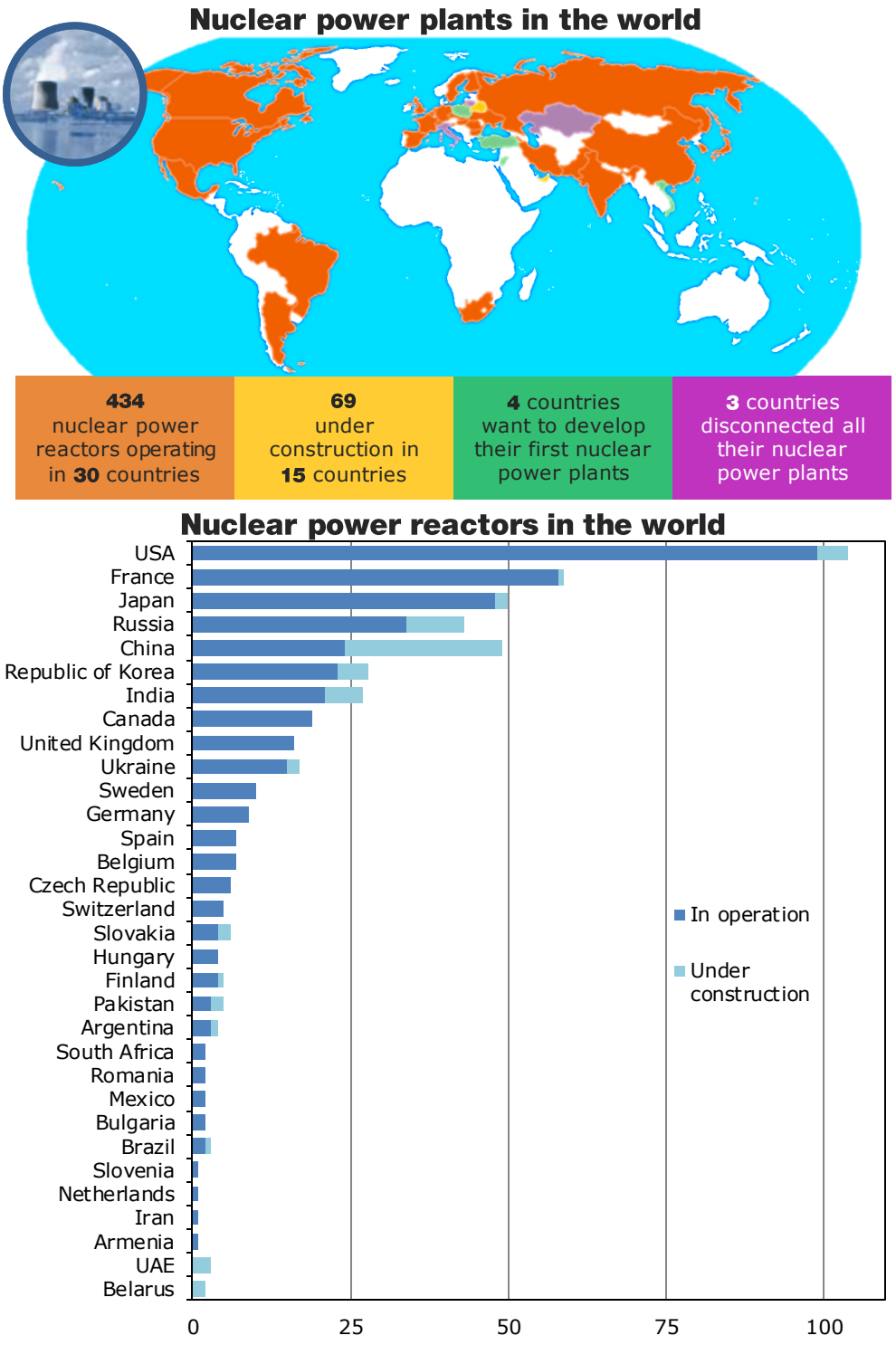

Figure 1-1 –Nuclear Power Reactors distribution in the world[3].

1.1.2. Radioactivity and radioactive contamination

Radioactivity (or radioactivity decay) is the physic process where unstable or excited atomic nuclei lose energy by emitting particles spontaneously. Quantum mechanics does not allow predicting when such a radioactive decay will take place, but only the probability of it would happen in a given time. The standard unit of activity of a radioactive substance is the Becquerel (Bq) and it corresponds to one decay per second. All radioactive decays are then characterized by a time known as the mean life, which is the average lifetime of a nucleus before it decays[6]. Another used unit is the Sievert (Sv), which is a derived unit of ionizing radiation dose, a measure of the health effect of low levels of ionizing radiation on the human body.

1.1.2.1. α-decay

In 1897-1898, Marie and Pierre Curie found a form of charged particle radiation (α radiation) which is now known to consist of ionized helium (He^{2+})[7]. The helium nucleus is a very stable structure and, when it is ejected from a heavy nucleus, a great deal of energy is released. Since nuclear systems are always seeking to be in the lowest energy state possible, one way of achieving this for an excited or very heavy nucleus may be by ejecting two protons and two neutrons in the form of a helium nucleus, the energy released in forming the helium nucleus being used to enable it to escape from the 'parent' nucleus. In this escape the α-particle has to penetrate a potential barrier. To conserve energy, the α-particle and the 'daughter' nucleus in such decay carry away a definite amount of kinetic energy between them equal to the difference in mass-energy between the parent nucleus and the daughter nucleus plus the helium nucleus. Alpha particles as well as other types of charged particles dissipate their energy during collisions mainly by two mechanisms: ionization and electron excitation. The high mass and charge of an alpha particle, relative to other forms of nuclear radiation, gives it greater ionization power by coulombic interaction or even direct collision of the alpha particle with atomic electrons; but it gives a poorer ability to penetrate matter.

1.1.2.2. β-decay

In 1896 Becquerel discovered that uranium compounds emitted a form of radiation (β^- radiation) which could be deflected by a magnetic field. This implied that the radiation consisted of a stream of charged particles and these were subsequently identified to be electrons. Afterwards, positron emission (β^+) was also observed.

This similarly involves the emission of a charged particle-an electron (e^-) or a positron (e^+). This happens when there are respectively too many neutrons or protons in a nucleus for it to be stable. Pauli suggested in 1930 that in β-decay two particles were emitted so that the definite energy released was shared between them. Since all the electric charge released in β-decay is carried away by the electron or positron it follows that the new particle is electrically neutral, the neutrino[6]. β particles can penetrate much deeper than α radiation[8].

1.1.2.3. γ-decay

In 1900 Villard identified a third form of highly penetrating radiation (γ radiation) which was not deflected by a magnetic field and turned out to be akin to x-rays but of much shorter wavelength, so much more energetic.

The nucleus has a series of energy levels and if the nucleus is excited to a higher one, for example in a nuclear reaction or following radioactive decay, it will be produced a series of jumps down to lower energy levels finally ending up in the 'ground' state. Each jump involves the release of energy and in form of a photon, it means, γ-radiation. Since nuclear energies are on a much larger scale than atomic energies (millions of electron volts rather than electron volts), the corresponding frequencies of the emitted photons (energy hν) are some millions of times larger than those of visible radiation and the wavelength of the radiation some millions of times smaller (even smaller than for x-rays) as observed[7]. γ-radiation has a higher penetration power, can penetrate several centimeters in concrete or lead[8], penetration capacity is represented in Figure 1−2.

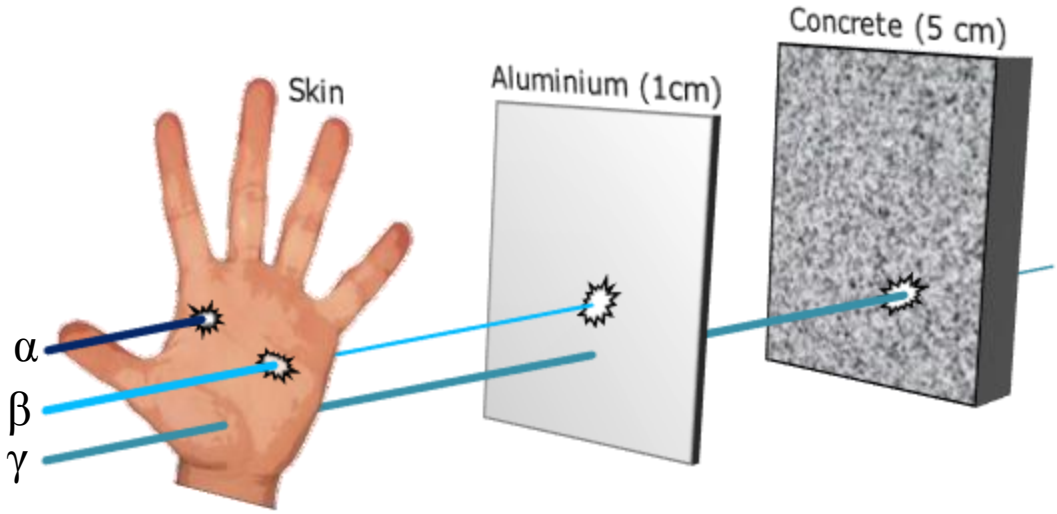

Figure 1-2 – Penetration power of alpha, beta and gamma radiation[8].

1.2. Radioactivity effects on human health

Even through the effects of ionizing radiations are known from the discovery of X-rays by Röntgen (who suffered burns that have been reported by Stevens[9] and Gilchrist[10]) the danger of radioactive elements as radium was not well reported during the early nuclear age and some commercial products included small amounts of radium, such as table games, watches or devices that were used by medical practitioners in wide variety of uses (Figure 1–3).

Figure 1-3 – Advertisements of products with radioactive compounds[11,12].

Nevertheless, at the end of 20's, radioactivity began to be considered dangerous[13] and, since this moment, hundreds of studies were developed

about it[14], especially reporting the radioactivity effects on population after the nuclear explosions in Hiroshima and Nagasaki (Japan) during the II World War[15,16].

Radioactivity effects on human health depend of several factors such as radioactivity intensity, exposition time, affected tissue and its capability to absorb radioactivity. In addition, some radioisotopes have associated other added effects, such as the chemical toxicity (e.g., the case of plutonium[17]).

Effects on humans are divided in two main groups:

- deterministic effects, the ones caused by intense exposures to a high radioactivity dose in a short period of time, and
- stochastic effects (mostly cancer), caused by much lower exposures prolonged during long times[18].

1.2.1. Deterministic effects

Deterministic effects are caused by direct energy damage to tissues and cells. This is usually caused by an intense dose of more than 0.5 Sv delivered over a short time (seconds or minutes). Acute doses greater than 10 Sv often are lethal effects. A graphical resume is shown in Figure 1–4.

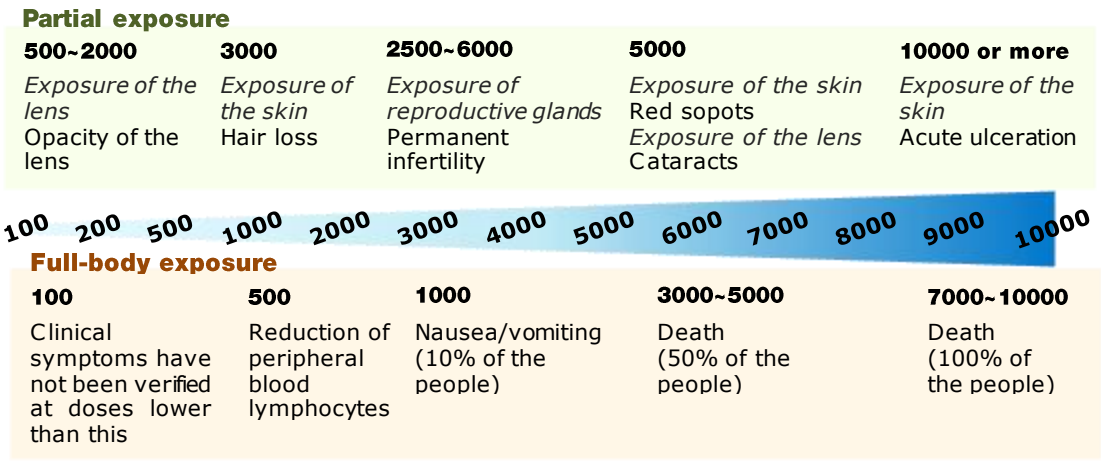

Figure 1-4 – Health effects of instantaneous exposure to large doses of radiation. Units: millisieverts[19].

The effects are much less, or negligible, if the exposure is at a much lower dose rate but extended over a longer period (years). This is because sub-lethal damage is reparable at the cellular level, the body can repair itself and new cell proliferation will replace lethally damaged cells.

Some of the severe effects include suppression of bone marrow function, damage to the gastrointestinal tract, skin burns, cataracts, and reduced lymphocytes. Symptoms include nausea, pain, vomiting, and reddening of the skin. In some cases, peripheral blood stem-cell transplants have been successful at improving recovery following exposure.

Data on deterministic effects are taken from side effects of radiotherapy, exposure of the early radiobiologists without conscience about radioactivity damage, atomic bomb injured in Japan (1945) and a from severe nuclear accidents as Chernobyl (1986, former Soviet Union).

1.2.2. Stochastic effects

Stochastic effects include cancer and genetic damage (mutation). Cancer results when cells multiply out of control, and certain types of cancer are linked to exposure to ionizing radiation at high sublethal doses.

Data for stochastic effects are most of times based in epidemiological studies on the survivors of the atomic bombs in Japan, on patients exposed to medical treatments, and on industrial exposures to workers. Animal studies are also used to evaluate human effects.

It is important to remark that cancer might not be expressed until decades after receive the exposure. The data from a study of the Japanese bombs survivors, which includes a study group of about 80 000 individuals, indicate a statistical increase in malignancies at doses above 0.2 Sv delivered at high dose rates.

There is a large uncertainty about incidence of cancer caused by low dose rates in the range of background exposures. For example, no increase in the frequency of cancer has been documented in populations residing in areas with a high natural background radioactivity. A linear, non-threshold hypothesis is used to estimate stochastic effects from radiation exposure. This hypothesis assumes as correct a linear extrapolation of data collected at high doses to zero exposure, so that all doses are assumed to cause an effect that is linearly related to the amount of dose.

The International Commission of Radiological Protection (ICRP) estimates fatal cancer risk at a rate of 0.04 per Sv for adult workers and 0.05 per Sv for the general population[20]. Greater risk for the general population is caused because it includes the risk for younger people. This means that a dose of the order of 20 μSv (i.e., 1% of the natural background exposure) is assumed to cause a risk of about one in one million that an individual member of the general public will receive a fatal cancer. An additional risk of nonfatal cancer is also estimated.

1.3. Radioactive contamination

Around 88% of the total radiation dose arrives from natural sources, but the level of exposure of population to radiation depends on climatic factors, fertilizing, local geology, drainage patterns and nutrition, which are different at each region in the world[21,22]. A scheme is shown in Figure 1−5.

Radioactivity exists in various geological formations such as soils, rocks and sediments, also in vegetation, water and air, while 12% is of anthropogenic origin[23]. Rocks and soils contribute considerably to indoor and outdoor exposure to the environmental radioactivity by γ and β radiation emitting mainly from ^{40}K, ^{226}Ra, ^{232}Th, ^{238}U.

The 17% of incoming radiation comes from foods and drinks, in the time between two heart beats, decay in our body 10000 atomic nuclei; in one hour

30000 atoms decay in human lungs, 15 millions of ^{40}K and 7000 of uranium from the ingested food decay in the stomach and intestines[24]. In Spain, 26.2% of bottled water have an α-activity higher than 100 mBq/L, and a β-activity no higher than 1000 mBq/L[25].

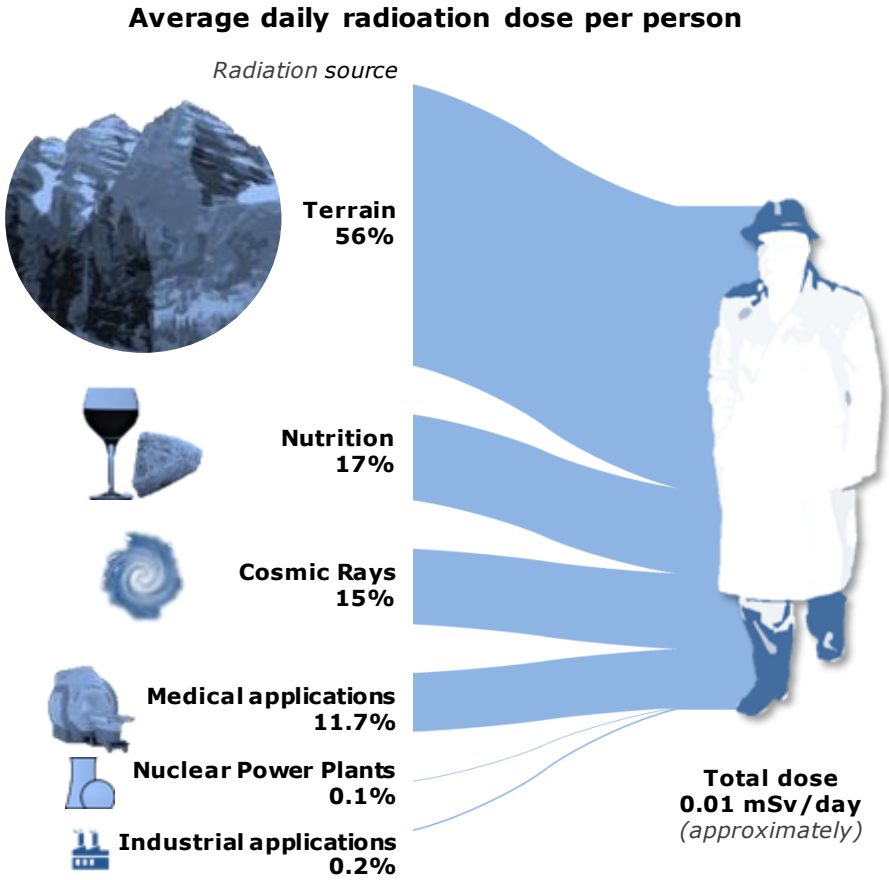

Figure 1-5 – Average daily radiation dose per person and its source distribution[23].

1.3.1. Diffusion on environment

Industrial activity affects also to radioactivity levels measured, in Ebro river the presence of a factory using sedimentary phosphate rocks as a raw material in an industrial process leads to the input of several different radionuclides, mainly ^{238}U, that influenced in higher radioactivity levels[26].

There is no a detailed knowledge about biological effects of radionuclides in plants. Biermans *et al.* tried it working with ^{90}Sr, at the physiological level in seedlings of Arabidopsis thalina. The obtained results show that, in some circumstances, the plants increased their leaf area and the weight of roots, suggesting significant repair of radiation-induced damage[27].

Trying to predict the soil/sediment-to-plant transfer of radionuclides, Willey studied the transfer and fate of radionuclides, investigating many confounding factors which could potentially influence such transfer at different levels of biological organisation[28]. The article assesses the utility of a meta-analysis of phylogenetic effects on alkali earth metals. Due to the great importance of studying how radioisotopes are introduced into food chains and its inherent limitations, there would be necessary more work to investigate if phylogeny may indeed explain differences in radionuclide transfer.

Significant escape of gaseous radio-iodine, ^{129}I, has been reported during the reprocessing of used nuclear fuel. Miller and Wang proposed an original method prevent iodine escapes to the environment it with an innovation that involves the fluoridation of the surfaces of nano-porous clay minerals to capture the radio-iodine, showing results of an increase in ^{129}I capture of 10–100 times per unit surface area, although the amount of fluoride appeared not to influence the quantity of radio-iodine sequestered[29].

^{99}Tc arrives to the Irish Sea from the Sellafield nuclear fuel reprocessing plant (Cumbria, United Kingdom) discharges in the period from 1994 to 2004. The distribution and behaviour of the radioisotope in the subtidal sediments was studied and a significant quantity appears to have accumulated in the sediments. Jenkinson *et al.* reports their results from the analysis of two deep sediment cores showed that the activity concentrations were variable and the highest values were largely associated with the fine-grained particles. The 98% of ^{99}Tc discharged has been dispersed[30].

During the Fukushima accident they occurred inputs of radionuclides into the atmosphere and in adjacent catchment, groundwater and coastal waters, in terms of radiation scape, which has been higher than that produced in Chernobyl and, because Fukushima power plant is close to the coast, radioisotopes have widely spread in the Pacific, with unexpected consequences[31]. A subsequent investigation concerning the radiation doses received by the Japanese population was realized, monitoring their hormonal and radioactive levels[31], the conclusions was that those living in the Fukushima prefecture had effective doses (considering both internal and external exposure) under 10 mSv, which are acceptable according to current criteria. However, some subjects (especially children) have had higher effective doses in the range 10–50 mSv, outside the accepted limit and will have to be monitored and medicated forever.

1.3.2. Nuclear wastes

The radiotoxicity of a waste can be defined as the sum of the radiotoxicity of each individual radio-nuclide. Radiotoxicity is time-dependent because of decay and buildup of the radio-nuclides. Nuclear wastes in Spain are mainly classified in function of their activity:

- Low and Intermediate Level Waste (L&ILW, or ILW). They can be managed, conditioned and stored definitely in the near-surface repository of "El Cabril" (see section 1.4.1.1.), including in this category a subdivision of Very Low Level Waste (VLLW). They do not produce heat.
- High Level Waste (HAW), composed mainly by spent nuclear fuel. They may be included in this category those ILW which due to their characteristics cannot be managed by storing them in the repository at "El Cabril".

Besides the activity, conditioning depends of the state of the wastes.

- Liquid wastes are separated in aqueous and organic wastes and then they are treated using several physical and chemical methods to reduce the contamination and the volume as filtration or evaporation. For their transport and storage they must be solidified.
- Solid wastes are separated in function of their activity and their physicochemical properties with the main purpose of reducing their volume, with different procedures of decontamination, chopping, crushing and compacting. Organic residues are incinerated to solidify them. Finally they are immobilized making a concrete block.

The main source of radioactive waste is related to the power generation using nuclear reactors and their dismantling. The nuclear reactor is placed in a pool and the spent fuel coming from nuclear power plants are continuously stored after being exhausted in the reactor (in terms of energetic economy). Storing is made, initially in reactor pools, in waiting for either reprocessing or other treatment.

Spent fuel contains almost all the radioactivity produced inside the reactor by fission, neutron capture and radioactive decay. When it is loaded in the reactor, nuclear fuel contains fresh uranium enriched in ^{235}U at around 3.5%. When is discharged, the fuel composition changes. In this exhausted fuel uranium represents a 96% in weight, but is now less enriched (approximately 0.8% in ^{235}U). The fuel contains now a 3% of highly radioactive fission products and minor actinides (^{237}Np, $^{241/243}Am$, $^{242/244}Cm$) as well as around 1% of several isotopes of plutonium. Its chemical composition is displayed in Table 1-1.

Most of these radioisotopes have short lifetimes (with few exceptions such as ^{99}Tc, ^{135}Cs or ^{129}I). Their radiotoxicity (essentially due to ^{137}Cs and ^{90}Sr) remains during few centuries. However, most of the transuranians (neptunium, plutonium, americium and curium) produced inside the reactor, as well as their decay products are α-emitters with lifetimes that can extend to

millions of years and their radiotoxicity is much higher than those of fission products. The long lifetimes and the potential risk that these nuclei entail force to plan a long-term management.

Table 1-1 - Half-life, activity and weight of the major transuranians and of the fission products inside one metric ton of spent fuel, discharged from a light-water reactor; the initial fuel enrichment in ^{235}U is 3.25% and the burn-up is 33000 MWd per ton[32].

Isotope	Emission	Half-life (years)	Activity (Ci/ton)	Weight (g/ton)
^{90}Sr	β	25.15	$7.34 \cdot 10^{3}$	520
^{99}Tc	β, γ	$2.14 \cdot 10^{5}$	130	772
^{129}I	β, γ	$1.57 \cdot 10^{7}$	0.03	185
^{135}Cs	β, γ	$2.95 \cdot 10^{6}$	0.19	218
^{137}Cs	β, γ	30.15	$1.06 \cdot 10^{5}$	1223
^{234}U	α	$2.45 \cdot 10^{5}$	0.95	153
^{235}U	α	$7.04 \cdot 10^{8}$	0.02	7861
^{236}U	α	$2.34 \cdot 10^{7}$	0.29	4451
^{237}Np	α	$2.14 \cdot 10^{6}$	0.34	482
^{238}Pu	α	87.7	$3.01 \cdot 10^{3}$	176
^{239}Pu	α	$2.41 \cdot 10^{4}$	358	5768
^{240}Pu	α	$6.55 \cdot 10^{3}$	507	2226
^{241}Pu	β	14.4	$1.38 \cdot 10^{5}$	1335
^{242}Pu	α	$3.76 \cdot 10^{5}$	2.10	533
^{241}Am	α	432.6	112	33
^{243}Am	α	$7.38 \cdot 10^{3}$	17.90	90
^{242}Cm	α, n	0.45	$4.04 \cdot 10^{4}$	12
^{244}Cm	α, n	18.11	$1.69 \cdot 10^{3}$	21

1.4. Nuclear waste in Spain

In Spain, the first nuclear reactor, a fast breeder reactor named Coral-1, was installed in 1967 in the former Nuclear Energy Committee facilities (in Spanish, *Junta de Energía Nuclear*), actually named CIEMAT, and in 1969 the first nuclear power plant started the power production.

Through the *Real Decreto* 1522/1984 of July 4th, 1984, was stablished the public company '*Empresa Nacional de Residuos Radioactivos S.A.*', (succeeded by the actually named ENRESA after the 24/2005 Law[33]) to manage the spent fuel and other nuclear waste generated in Spain, control the dismantling process of nuclear facilities and store them definitely[34], according to the General Plan for Radioactive Waste approved by the Spanish government[23]. The *Real Decreto* 5/2005 establish the state ownership of the nuclear waste after their definitive storage, lately reapproved in the article 38 bis of the 25/1964 Law about nuclear energy[35] (introduced as 9th final disposal in the 11/2009 Law about regulation of Real Estate Investment Trust[36]).

The spent fuel in the nuclear power plants, after being recovered from the reactor, is stored into the named Spent Fuel Pools (SFP) located inside the power plants. In a future, spent fuel is planned to be stored for a few decades in a Centralized Temporally Repository (nowadays still not available) to then, being managed to be disposed in a final repository. A diagram of the whole process is showed in the Figure 1-6, where L&ILW means Low and Intermediate Level Waste; ILW is Intermediate Level Waste; HLW is High Level Waste; ITR is Individual Temporary Repository; L&ILWCR is Low and Intermediate Level Waste Centralized Repository; SF is Spent Fuel and TR is Temporal Repository. In yellow there are represented the infrastructures that are not yet operational, blue arrows indicate the actual processes and the orange ones the designed processes to be implemented in the future.

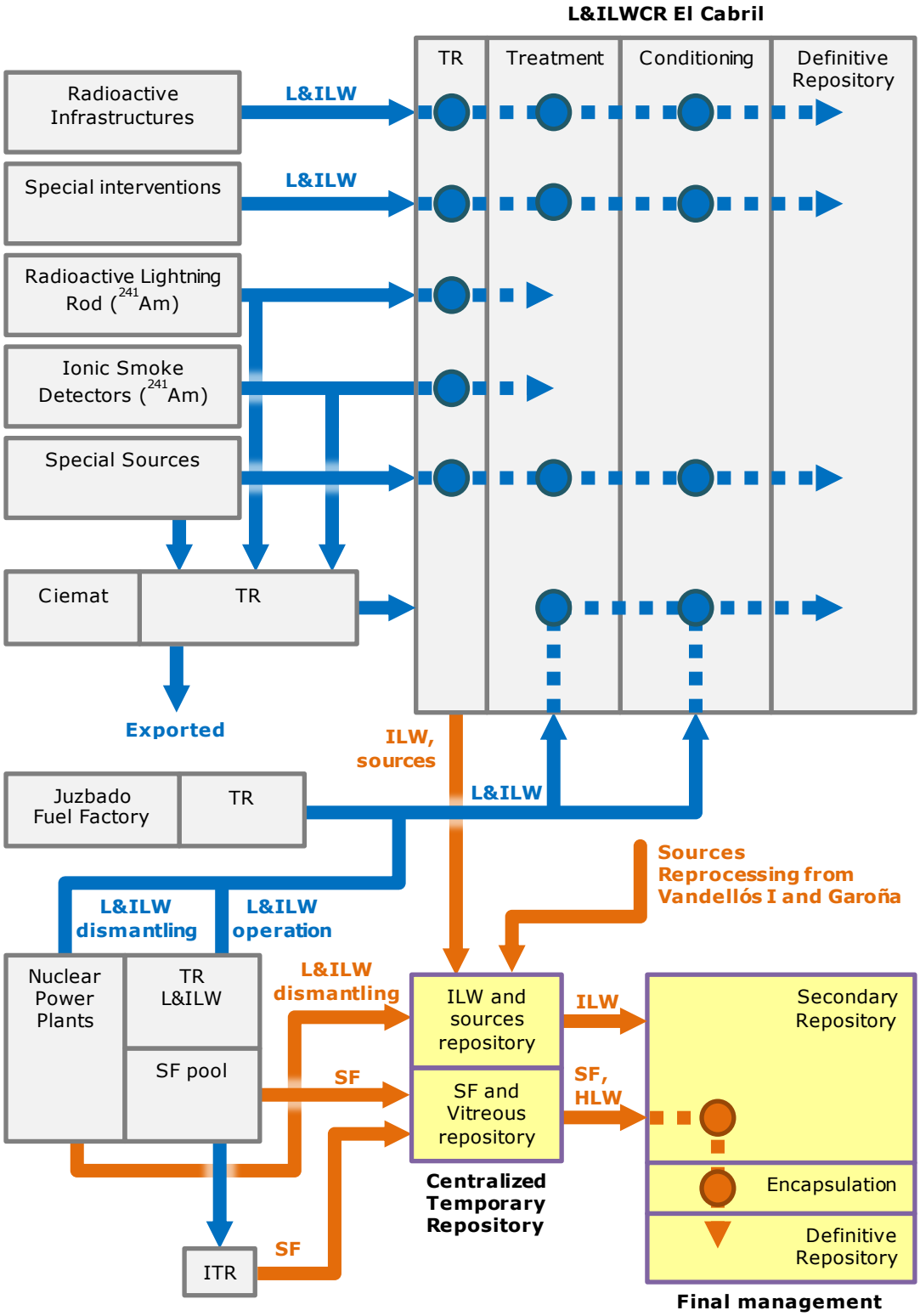

Figure 1 6 – Scheme of the management process for nuclear wastes in Spain. Adapted from *Sexto Plan General de residuos radiactivos*[23].

Waters of the SFP present several risks. Radioisotopes are present in these hundreds of cubic meters of water. Radioactivity in pool waters come from activation and fission products. The sources of the activation products are crud deposits and corrosion films on the fuel bundle surfaces. The fission products arise from bundles with rods which failed in-reactor or from intact bundles which adsorbed circulating fission products. Cesium, tritium, cerium, strontium and iodine are the principal fission products in reactor pools.

To prevent the formation of iodine volatile compounds, hydrazine is added to some pools to convert it into water-soluble species, thereby reducing the concentration of air-borne iodine[37]. Boric acid is also added as a reactivity control agent.

The water pools are considered I&LLW during the time that the spent fuel is stored there and VLLW after their displacement. Cooling systems using heat exchangers are used to cool them and provides shielding from radiation.

Liquids waste treatment aims to decontaminate sufficiently, so that the decontaminated water bulk volume could be either released to the environment or recycled.

Attending to the general considerations in R+D and the planned actions of the strategic guidelines defined in the Sixth general plan of radioactive waste, it was supported a project for the design, synthesis and characterization of new selective adsorbent materials. The objective of this study, at laboratory scale, deals with investigating on the adsorption capacities of different materials of radioactive elements which are present in very low concentration in aqueous effluents, in order to concentrate them and facilitate the subsequent quantification by a suitable method. (R+D Plan 2009-2013 designed by ENRESA, area of ‘technology and processes of treatment and conditioning, dismantling section).

1.4.1. Managing of nuclear waste

Theoretically, there are three main options for long term management of nuclear waste: storage in a safe emplacement, transmutation to non-radioactive isotopes and separation of actinides and fission products from other components of the waste.

1.4.1.1. Disposal

The long timescales over which some of the radioisotopes remain active led to the idea of deep geological disposals: hundreds of meters under surface in repositories to isolate and contain radioactive waste. This isolation would be endowed by a combination of engineered and natural barriers (rock, salt, clay) and no obligation to actively maintain the facility is passed on to future generations. A repository is comprised of mined caverns or tunnels where the packaged waste would be placed indefinitely into[38]. Deep geological disposal is the preferred option for waste management of long-lived radioactive waste in several countries, included Spain[23].

Near-surface repository is an adequate installation for low and intermediate activity waste. This is enough to ensure the protection of both people and environment against ionizing radiation and it allows the facility's reuse after a period of 300 years. An example of near-surface disposal facility is "El Cabril", located in Spain. El Cabril is in operation since 1992, and it is estimated that the 91% of the volume of generated waste will be managed there[39], preferably in solid state. The rest of the nuclear waste's volume cannot be disposed into this kind of repository due the presence of long half-life time radioisotopes as ^{94}Nb or ^{99}Tc make impossible the disposal of an important part of the waste into this kind of repository.

Liquid radioactive waste injection consists in the direct injection of liquid radioactive waste into an underground layer of rock several hundred meters deep. The place is chosen considering the natural ability to trap the waste, i.e. rocks with adequate porosity and surrounded by impermeable layers that must

act as a natural seal[40]. This technique has been developed and implemented in Russia, where it is carried out since 1960 to nowadays. Some optimistic data are already reported on the success of the already existing systems of deep injection[41,42].

Cask storage facilities has been proposed as an alternative system for accumulating spent fuel after cooling treatment in the nuclear power plants pools for several years. In the case of Spain, several nuclear power plants have developed Individual Temporal Repositories using concrete cask storage, as Zorita or Trillo. In the future, the spent fuels stored in these facilities will required to be moved to another repository. Hence, cask storage is considered just an interim storage for the nuclear waste management and this is no considered as a definitive option in any nuclear management plan.

Deep boreholes have been proposed as a potential solution for nuclear waste storage. This alternative is supported by the advances in drilling technologies and a better understanding of extremely long fluid residence times in deep bedrock. Deep boreholes may have programmatic and economic advantages but more studies and experience will be required[43].

Throwing the wastes to the sea has been a routine between 1949 and 1982 at sites in the North East Atlantic[44]. In 1972 the London Convention banned the dumping of high activity nuclear wastes to the sea. The medium and low radioactivity wastes were included in 1983. Finally, in 1993 the managing of wastes was ruled[45], totally prohibiting the dumping of any nuclear waste to the sea. Unfortunately, it continued happening[46].

Another option studied was to place the nuclear wastes into shallow drillholes in the ice at South Pole. In this case, the nuclear waste tanks can be either anchored with cables to the surface or let to sink downward to the bedrock by melting the ice[47]. This option is currently forbidden by the Antarctic Treaty[48].

Disposal to outer space was also proposed as an alternative to waste storage, but discarded due to the high costs and the potential risks of an accident during launching[47].

1.4.1.2. Transmutation

Transmutation is a technique proposed to transform long live radioisotopes in short half-life ones or another stable isotopes[49]. Currently, it is being discussed the viability of transmutation processes using either reactors or high-energy particle accelerators. Because of its relatively long half-life combined with a high mobility in the environment, ^{129}I is a particularly important nuclide in the study of transmutation of fission products. The proposed mechanism is neutron capture, producing ^{130}I, with a much shorter half-life of 12.36 h and decay to stable ^{130}Xe[50].

1.4.1.3. Separation

In the spent nuclear fuel and other radioactive waste there are potentially useful components with several latent applications. Among such applications we can found radioactive waste that could be used again as nuclear fuel or in industrial, military or medical applications. Another part of this waste belongs to the category of high, medium or low activity waste and it will require different treatments or storages. Separating them would make easier am efficient management, i.e., Pu is separated using the PUREX process[51].

Having a smaller volume of the high activity fraction would also permit a cheaper management. In addition, chemical separation and recovering of elements allows improving the management of the spent fuel[52].

Inorganic ion exchangers have the advantages to be applied in ion exchange and adsorption processes of radioactive waste. They have good radiation and chemical stability and high capacity for some radioactive components in nuclear wastes. Zeolites, titanium phosphate and clays are among these materials. They have also potential as final waste form for geological storage[51].

Electrochemical separation, also known as electrorefining, has been adapted to the purification of Pu and U for both weapons and the breeder reactor fuels programs. The spent fuel recovered from the Experimental Breeder Reactor was successfully processed by the electrometallurgical process developed by Argonne National Laboratory[51].

Molten salt separation has been considered an interesting process due to the high resistance of these materials to nuclear damage. Salt Transport Process is a pyrochemical method for recovering U and Pu from residues of fast reactor fuels[51].

1.4.1.4. General considerations

Concerning the long term management, there is a general consensus on the deep geological repositories, but there are still only a few number of experiences about this kind of repositories, as they are the management of the actually closed Asse II and Morsleben in Germany as nuclear repositories[53] and the Waste Isolation Pilot Plant in New Mexico, USA[54]. Shared solutions with regional or international repositories are currently capturing more attention, but it is necessary to get a consensus.

Separation and transmutation of long live radioisotopes to reduce volume and toxicity of the wastes are not sufficiently technologically developed and they would require storing a significant volume of waste. Nonetheless, support the investment in research to increase the knowledge about these alternatives is considered in the strategic plan of Spanish government about radioactive wastes, including participation in international research programs.

The combined option of separation and transmutation (S+T), in its different versions, makes mandatory the international collaboration due to the needs of the research programs in this area. We can highlight the European Commission programs and the Nuclear Energy Agency projects.

1.5. Radionuclide ^{129}I

^{129}I decays by emitting β^- particles with a maximum energy of 154.4 keV and γ-rays of 39.6 keV as well as X-rays (29–30 keV)[55] in ^{129}Xe. The natural abundance of this radioisotope has been altered drastically by human actions since 1945.

In nature, ^{129}I is produced in three different ways, by cosmic rays interactions with Xe in the atmosphere, as a spontaneous fission product of ^{238}U and ^{235}U in the lithosphere[56] and, to a minor extend, by neutron-induced reactions on ^{128}Te and ^{130}Te[55].

The natural abundance of ^{129}I has been estimated to be around 230 kg[57]. From these, natural earthy abundance is estimated to be approximately 80 kg and pre-anthropogenic ^{129}I in oceans is estimated to be approximately 130 kg, while ^{129}I in non-marine water represents approximately 11 kg[58].

Anthropogenic sources of this radionuclide in the environment comprise fallouts from nuclear explosions and accidents as well as liquid and gaseous releases from the spent nuclear fuel reprocessing facilities. ^{129}I is produced as a fission product in nuclear reactors and gets accumulated in the reactor fuel proportionally to its fission[59]. Also, iodine radioisotopes are volatile fission products presents in the reactor waters or in cooling system. In case of nuclear accident, it supposes an environmental and biological risk[60].

Since the first test (Trinity nuclear test in July 16th 1945) more than 2400 nuclear devices has been detonated for 8 countries; currently, they are 434 nuclear power reactors working in 30 countries[3,61] and, although major nuclear disasters are low-frequency events, after Chernobyl and Fukushima accidents it has been reported major levels of ^{129}I around the damaged power plants and in their fallout region[62-64].

Anthropogenic ^{129}I is estimated in more than 5068 kg. Among them, 50-150 kg came from nuclear weapons testing, 6 kg from Chernobyl nuclear disaster,

1.2 kg from Fukushima[64] and the rest from nuclear reprocessing facilities. With a half-life of 15.7 million years, ^{129}I is the longest lived major fission product present in irradiated nuclear fuel.

In environment, ^{129}I is mainly located in upper and deep ocean (in both of them their concentration is increasing from last decades) and in soils, with the lowest concentration in stratosphere (near 0 at the end of the last century)[65].

1.6. General context

Throughout this chapter it has been introduced some of the aspects involving nuclear waste management. Radionuclides present in nuclear waste of particular importance to the environment and risk assessment are ^{99}Tc, ^{129}I, and ^{237}Np, because of their long half-lives and presumably high mobility. These nuclides are present in high abundance in underground nuclear test, fuel reprocessing, and in spent reactor fuel.

Focusing on iodine, its radiological impact on the biosphere has been largely discussed. According to Oscarson *et al.*[66], ^{129}I is the "greatest hazard to man and environment of the different radionuclides generated throughout the storage of HAW". Therefore, several HAW studies are focused on iodide adsorption and immobilizing as well as on the identification of possible materials and admixtures for trapping this radionuclide. Such materials would require, in addition, a high selectivity towards iodide since "radioisotopes are generally a trace species in a soup of far more abundant, common groundwater anions"[67]. Additionally, stability towards temperatures of approximately 373 K and radiation stability are required features.

^{129}I has a complex chemistry in the environment. The fate and transport of ^{129}I is dictated by its chemical speciation. Aqueous iodine usually occurs as the highly mobile iodide anion (I^-). Under more oxidizing conditions, iodine may be present as the iodate anion (IO_3^-), which is more reactive than iodide and

could be adsorbed onto positively charged sites existing locally in clays and organic matter.

During the last decades, different materials have been tested for selective ^{129}I adsorption from nuclear effluents. Organoclays OCB and OCM, activated carbon GAC 830 can adsorb iodide but such adsorption is not selective. They showed also adsorption capacities for TcO_4^- and Cs^+ [68].

Argentite (AgS), a natural sulfide mineral, has been reported as iodide adsorption material[68,69] but detailed studies would be necessary to know if it is a suitable material. It has been proposed that oxidation, reduction, and mineral replacement affect iodide adsorption on sulfides[70]. Obviously, iodide adsorption by sulfides is complex and still not fully understood.

Some authors[71] compared the iodide adsorption capacity of different oxides, hydroxides, sulfides, silicates, and lignite coal. Interestingly, the adsorption capacity of lignite coal decreased with time. Moreover, they found that active carbon selectively adsorbs I_2 rather than I^-. The I_2 is produced by oxidation of I^- with the dissolved oxygen in the waste water; so that, active carbon, presumably, would be ineffective under anaerobic conditions as expectedly present in a HAW repository.

Silicates are not supposed to significantly influence iodide adsorption at near neutral pH, and iodide adsorption on silicates is attributed to the variable surface charge and hence strongly dependent on pH[72]. In the same manner, specific cement phases have shown to possess a high iodide adsorption capacity (particularly calcium monosulfate aluminate hydrate) which, again, strongly depends on pH[71].

Cu-, Bi-, Fe phases and hydrotalcite have been also investigated as additives for geotechnical barriers but discarded due to low iodide adsorption capacity[66].

A fairly large number of publications exist up to now regarding iodide adsorption by organoclays[73,74]. In them, it is concluded that organoclays (particularly bentonites which were treated by hexadecylpyridinium) are effective for iodide retention in the geotechnical barrier of HLRW repositories and they proved long term structural stability under elevated temperature. In contrast to structural stability it was found a decrease of iodide adsorption capacity of organoclays after exposure to 413 K for 70 days[74].

Therefore, as has been stated in this section, they are a big concern on iodine sequestering and they are a large list of comparable results of iodide adsorption capacity obtained by the investigation of a set of different materials. This is only a summary of some of the different studies published. However, it is difficult to establish comparisons among the different materials since the results of the adsorption experiments are very susceptible of the conditions used in the different experimental setups (e.g., pH, Eh, concentration, time, precursor material, solid liquid ratio…).

Due to the anionic form that iodine has in waste waters, in this work we wanted to take profit of this fact and to study the interactions (adsorption-immobilization-desorption processes) of these anions on different solids with very well know anionic exchange and scavenger properties, such as layered double hydroxides.

1.7. Objectives

As remarked along this chapter, iodine adsorption in the major concern of this dissertation. From a general point of view, this work has been focused on two studies:

i) Iodide adsorption capacity and behavior of the selected prepared materials.

ii) Iodide and iodate adsorption capacity of selected prepared materials and study of their suitability to be used as "getters" in repositories.

More specifically the objectives of this thesis work were:

- To synthesize and characterize suitable adsorbent materials for selective iodide adsorption.
- To study the iodide adsorption capacity of the material and the possibilities of improving, using common reagents (no actives).
- To study the retention capacity of iodide of the different materials.
- To determine if they are suitable materials for iodide adsorption in waste waters from nuclear power plants.

My present design, then, is not to teach the method which each ought to follow for the right conduct of his reason, but solely to describe the way in which I have endeavored to conduct my own.

Discourse on the method of rightly conducting the reason, and seeking truth in the sciences

René Descartes

2. Materials and experimental methods

UNIVERSITAT ROVIRA I VIRGILI
ON THE USE OF LAYERED DOUBLE HYDROXIDES IN THE MANAGEMENT OF 129I FROM LIQUID NUCLEAR WASTES
Luis Iglesias Pérez
Dipòsit Legal: T 893-2015

2.1. Structural Analysis

2.1.1. X-ray diffraction

X-Ray Diffraction (and more specifically Powder X-Ray Diffraction, PXRD) is a non-destructive technique for materials characterization that provides information about the samples such as phase identification, crystal structure and defects, strain, crystallite size, phase quantification, determination of amorphous phase, and determination of unit cell parameters of new materials[75].

The diffraction method utilizes the interference of the radiation scattered by atoms in an ordered structure and is therefore limited to studies of crystalline materials, being amorphous excluded[76].

The incoming X-ray beam can be characterized as a plane wave of radiation interacting with the electrons of the material under study. The interaction between the beam and the material is composed of both absorption and scattering. The scattering can be thought of as spheres of radiation emerging from the scattering atoms[76]. If the atoms have long-range order, the separate 'spheres' interfere constructively and destructively producing distinct spots, i.e. Bragg reflections, in certain directions. The information provided by specific scattering angles, θ_{hkl}, is about the long-range ordering dimensions, the intensity gives information on the location of the electrons within that order. The basis for material science studies using X-ray diffraction is Bragg's law (Equation 2-1):

$$\lambda = 2d_{hkl}\sin(\theta_{hkl}) \qquad \text{(eq. 2-1)}$$

where λ is the wavelength of the incoming radiation, d_{hkl} is the spacing of the (hkl) atomic plane and θ is the angle of the diffracting plane where constructive interference occurs (Figure 2-1.b).

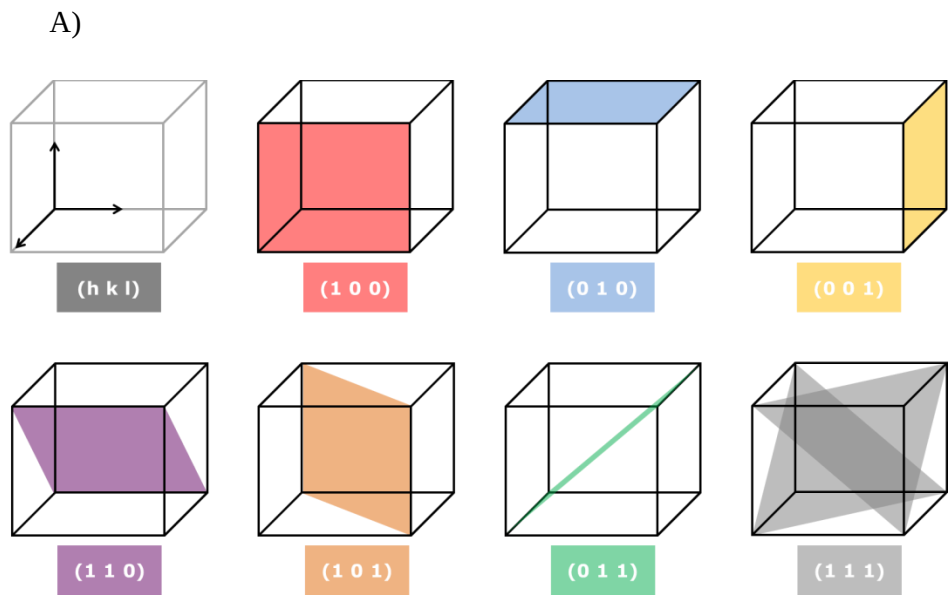

Figure 2-1 – a) Examples of the Miller indices of planes in the unit cell of a crystalline structure. b) Diffraction scheme. λ: wavelength of the incoming radiation; d: spacing of the (hkl) atomic plane; θ: angle of the diffracting plane where constructive interference occurs.

The PXRD analysis of the solid samples prepared during the implementation of this thesis work were recorded by a Siemens D5000 diffractometer with Bragg–Brentano geometry (See Figure 2-2) using nickel-filtered Cu Kα radiation (λ = 0.1541 nm) and a Bruker D8 Discover. The diffractograms were collected in the 2θ range of 5–70° with an angular step of 0.05° at 3 seconds per step, which resulted in a scan rate of 1º/min. The identification of phases was performed by means of the Committee for Powder Diffraction Sources (JCPDS) data base.

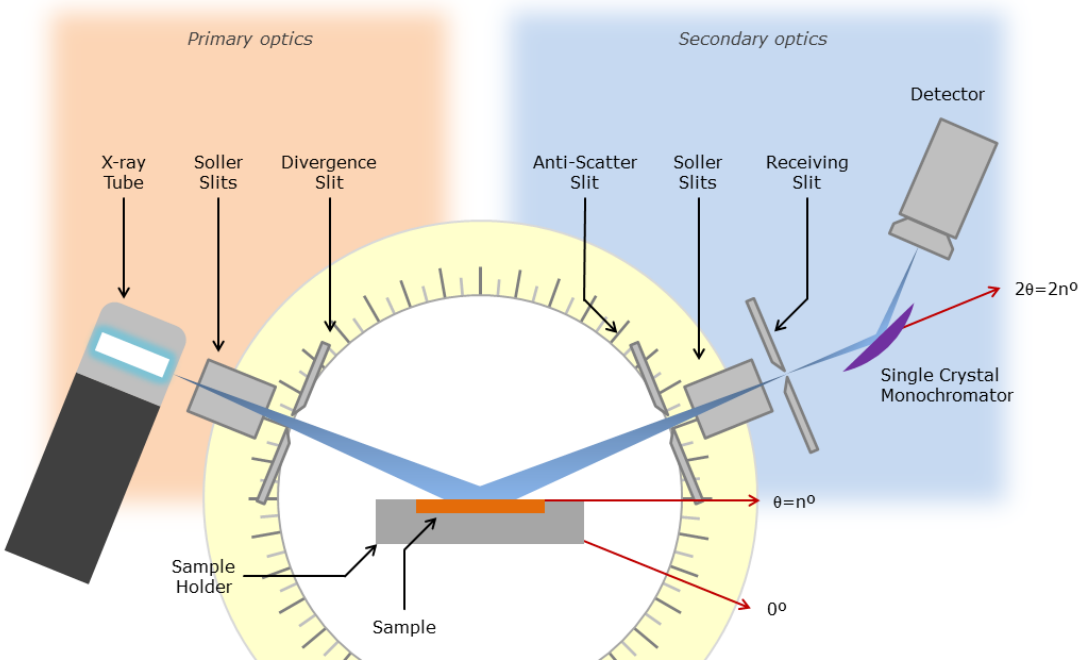

Figure 2-2 – Scheme of a diffractometer with Bragg-Brentano geometry such as that of Siemens D5000.

2.1.2. EXAFS (XAFS)

Extended X-Ray Absorption Fine Structure (EXAFS) is a X-ray materials analysis technique performed in synchrotron, designed specifically to produce very intense photon beams that provides information about the chemical composition and local structure of the sample[77].

Whilst XRD depend on the constructive interference of radiation that is scattered by relatively large parts of the sample, on the other hand EXAFS is due to creation of photoelectrons which are either excited to holes in the valence levels, or to unbound states and scattered by nearby atoms in a lattice[77-79], as shows Figure 2-3. Considering how is the X-ray absorption of a free atom, where an electron with a binding energy E_b is irradiated with an energy hν (being $h\nu \geq E_b$), the electron leaves the atom with a kinetic energy represented in equation 2-2. The spectrum shows edges corresponding to the binding energy of electron core levels in the atom, but contains no further structure. When this happens in an atom bound in a lattice, the local nucleus in the environment of the excited electron modulates the absorption and fine structure arises in the spectrum containing information about surrounding atoms.

$$E_k = h\nu - E_b \qquad \text{(eq. 2-2)}$$

In a XAFS spectrum, there are three important regions to be considered: pre-edge, XANES region (X-ray absorption near edge spectroscopy) and EXAFS region (extended X-ray absorption fine structure). The pre-edge is the zone of the spectrum after producing the electron excitation (i.e., after the absorption edge). XANES region provides information on the valence state of the exited atom and its bonding geometry, whereas EXAFS deals with the interference effects visible in the absorption spectrum beyond the edge, and provides detailed information on the distance, number, and type of neighbours of the absorbing atom (after mathematical treatment and Fourier transformed).

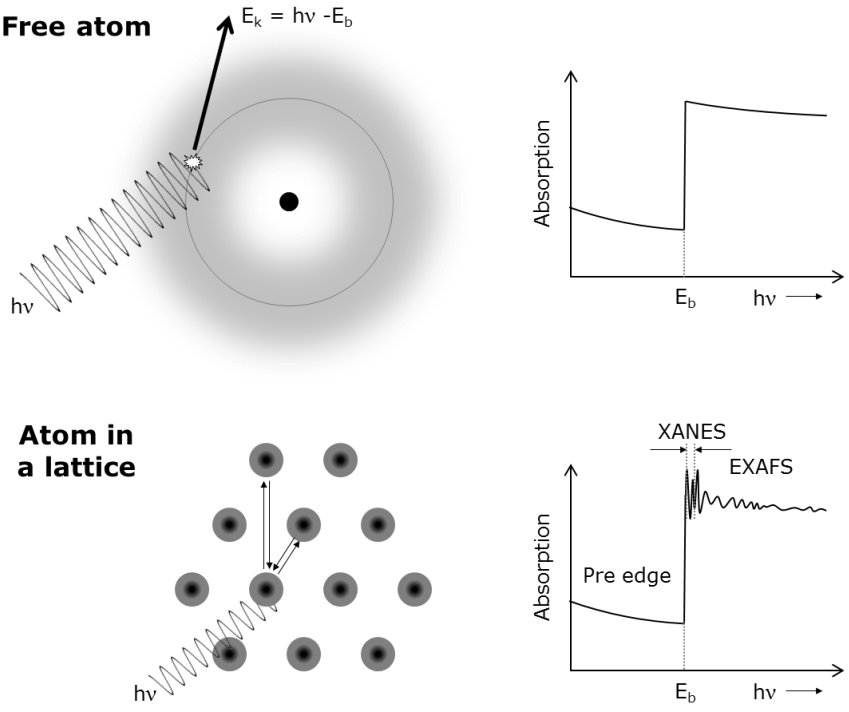

Figure 2-3 – Absorption of X-rays as a function of photon energy, E=hν by a free atom and by atoms in a lattice.

EXAFS measurements of samples and references were performed at the I K X-ray absorption edge at 33169 eV. The data were collected at the Rossendorf Beamline (RoBL) 20 at the European Synchrotron Radiation Facility (ESRF), located in Grenoble (France) which operated at 6.0 GeV and a maximum current of 185.43 mA. RoBL is important because it has been the first experimental station dedicated to XAFS spectroscopy on radioactive elements using synchrotron light source in Europe. In addition to the advantages offered by a third-generation synchrotron light source it also gives the possibility of sample manipulation in a specially designed glove box before or during the measurement[80].

The EXAFS station was equipped with a Si (111) double crystal monochromator. The EXAFS data were collected in cryostat filled with He,

the reference samples were diluted with boron nitride (BN). The samples were also measured without dilution in the plastic sample holder covered with Kapton film. The powder was filled into the sample holder. Higher order harmonics were suppressed by the use of two mirrors. The standard beam size at the sample is $20\times3mm^2$ (hν). The size of the focused beam is $\leq 0.5\times0.5mm^2$. The calculated integrated flux for the focused beam is 6×10^{11} photons/s at an energy of 20 keV and 200 mA electron-beam current[80]. Internal energy calibration was made against potassium iodide. All measurements were performed in transmission mode. The EXAFSPAK program package was used for the data treatment. For each sample a minimum of 2 scans were merged after energy calibration by means of the EXAFSPAK.

2.2. Textural analysis

2.2.1. N_2 Physisorption

N_2 physisorption is a common technique to determine the textural parameters of a solid. In catalysts or adsorbents materials, both specific surface area and pores size and distribution are important parameters to determine because the capacity of catalyze a reaction or adsorb may be related with the surface or porosity of the material[81-83].

The used method is that of Brunauer, Emmet, Teller (BET)[84], that is an extension of the Langmuir theory which takes their suppositions and introduces the concept of multilayer adsorption following three additional hypothesis:

- Gas molecules are going to be physically adsorbed into a solid surface in layers tending to infinite.
- There are no interactions between layers.
- This theory is applied to all the layers.

And, similar to Langmuir theory, BET method requires supposing some idealized mechanisms derived from previous hypothesis:

- The adsorption of a gas molecule into the surface of the solid is related with only one defined adsorption energy.
- The only considered interaction between molecules is that a molecule can act as a single adsorption site for a molecule of the upper layer.
- The uppermost molecule layer is in equilibrium with the gas phase, having similar adsorption and desorption rates.
- The desorption is a process limited kinetically, adsorption heat is needed and:
    - this phenomenon is homogeneous in the same layer,
    - the adsorption heat is E_1 for the first layer,
    - the other layers are assumed to be similar and they can be represented as condensed species (liquid phase). Hence, the heat of adsorption is E_L (heat of liquefaction).
- If the pressure is the saturation pressure, the molecule layer number tends to infinity.

The following equation 2-3 is the adsorption isotherm equation of the Brunauer, Emmet, Teller method:

$$\frac{1}{\left[V_a\left(\frac{P_0}{P}-1\right)\right]} = \frac{C-1}{V_m C} \times \frac{P}{P_0} + \frac{1}{V_m C} \qquad \text{(eq. 2-3)}$$

Where P is the partial vapor pressure of adsorbate gas in equilibrium with the surface at 77.4 K (b.p. of liquid nitrogen), in pascals; P_0 the saturated pressure of adsorbate gas, in pascals; V_a is the volume of gas adsorbed at standard temperature and pressure (STP) (273.15 K and atmospheric pressure ($1.013 \cdot 10^5$ P_a)), in milliliters; V_m the volume of gas adsorbed at STP to produce an apparent monolayer on the sample surface, in milliliters and C the dimensionless constant that is related to the enthalpy of adsorption of the adsorbate gas on the powder sample.

The textural properties of the synthesized samples reported in this work were measured by N_2-physisorption at 77 K using a Quadrasorb SI surface analyzer. All the samples were degassed in vacuum at 393 K for 15 h prior to analysis. The BET specific surface area was calculated from the range P/P_0= 0.05–0.35 in the adsorption branch, while BJH pore size distribution was calculated from the desorption branch.

2.3. Electron microscopy

The electron microscopy is a group of popular techniques in the field of inorganic materials. It comprehends several techniques as SEM, TEM, AFM, EDX among others, to routinely take pictures using an electron beam to form the images. This allows to obtain great magnifications, thereby revealing details of the texture and shape of a given material with a resolution of 0.1 nm[77,85]. During the development of this thesis work, three different electron microscopy techniques have been used: environmental scanning electron microscopy (ESEM); transmission electron microscopy (TEM) and energy dispersion X-ray analysis (EDX).

2.3.1. Environmental Scanning Electronic Microscopy

Environmental Scanning Electronic Microscopy (ESEM) is a type of electron microscope that produces images of a sample by scanning it with a focused beam of electrons. ESEM pictures are produced by detection of either secondary and backscattered electrons and contrast is produced by the orientation that the surface of the materials has with respect to the detector. ESEM micrographies reveal details of the material's shape, particle size and particles organization. One of the main differences between SEM and ESEM lies in the capacity of ESEM to work with wet samples and in low vacuum or gas, because it is possible to maintain a gaseous pressure in the specimen chamber, as well as allows to work with non-conductive samples without coating them; however, SEM cannot be used in these conditions because

requires high vacuum to work[86]. A scheme of an ESEM is reproduced in Figure 2-4.

Compared with TEM, because the SEM and ESEM images relies on surface processes rather than transmission, it is able to image bulk samples up to many centimeters in size and can have a great depth of field, and so can produce images that represents the three-dimensional shape of the sample.

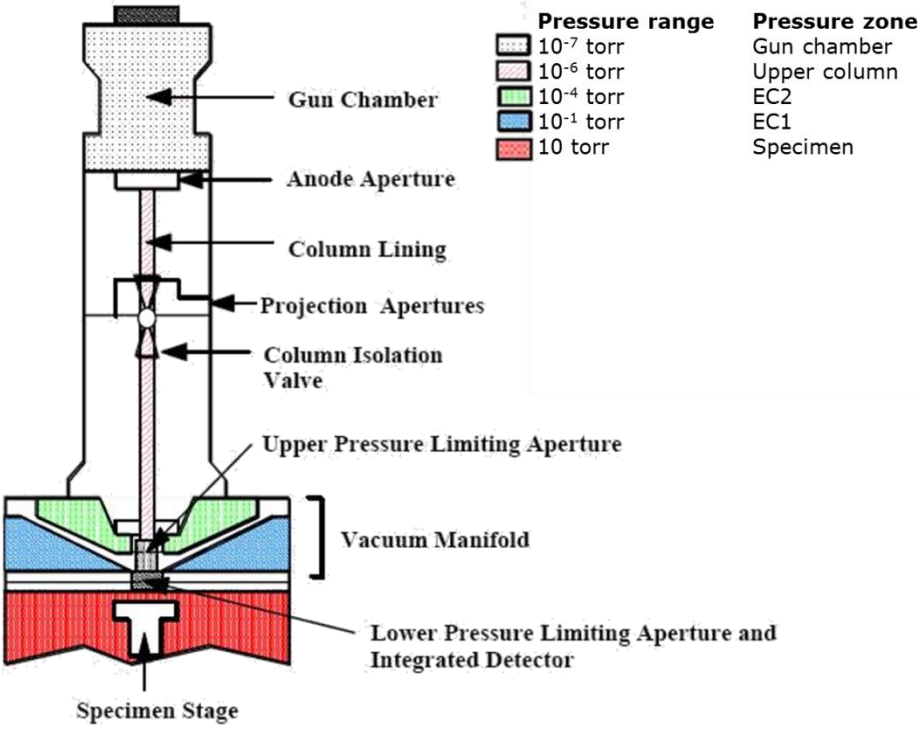

Figure 2-4 – Scheme of an environmental scanning electron microscope[87].

Here, environmental scanning electron microscopy (ESEM) was carried out on the samples using a FEI Quanta 600microscopewith INCA microanalysis from Oxford Instruments operating at high vacuum, using a carbon or gold sputtering; and at low vacuum without sputtering with an accelerating voltage of 20 kV and a working distance of 6.6 mm.

2.3.2. Transmission Electron Microscopy

Transmission Electronic Microscopy (TEM) is a useful tool for investigating the atomic structure and morphology of nano- and micro-objects, being necessary use very thin samples to be transparent for the electron beam[88].

A TEM has several components as showed in Figure 2-5, which include a vacuum system where the electrons move, an electron emission source for generation of the electron stream, a series of electromagnetic lenses, as well as electrostatic plates. The latter two allow the operator to guide and manipulate the beam as required. It is also required a device to allow the insertion into, motion within, and removal of specimens from the beam path. Imaging devices are subsequently used to create an image from the electrons leaving the system. Generally, the image resolution of a TEM is at least an order of magnitude higher than that of a SEM.

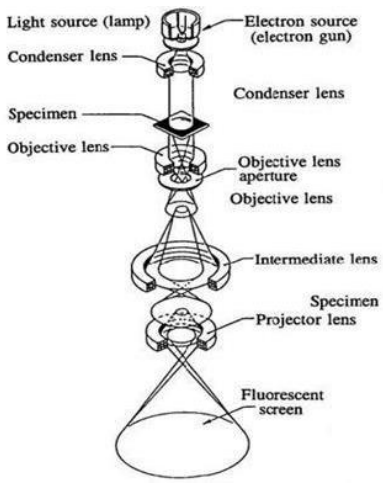

Figure 2-5 – Scheme of a Transmission Electron Microscope[89].

TEM analysis was performed in a JEOL 1011 apparatus using 100 kV accelerating voltage. The samples were dispersed in ethanol and then deposited on a standard 3 mm holey carbon-coated copper grid.

2.3.3. Energy Dispersive X-ray Spectroscopy

Energy Dispersive X-ray Spectroscopy (EDX) is a semi-quantitative X-ray micro analytical technique that provides information about the chemical composition of a sample for elements with Z > 3 as long as the sample has not been modified by coating. Frequently, samples need to be coated with a thin film of gold or carbon to improve their conductivity and diminish the charging suffered under the electron beam in SEM.

Its characterization capabilities are due in large part to the fundamental principle that each element has a unique atomic structure allowing unique set of peaks on its X-ray emission spectrum[90]. The energy of the electron beam is determined by the accelerating voltage of the microscope, and therefore this energy defines which X-rays are excited during the interaction with the material. SEMs typically work with high accelerating voltages, ~20 kV approximately, in order to excite the well-known K lines in the atomic spectra (even L lines are also produced at these energies they have the problem that the information in the low-energy part of the atomic spectra is frequently neglected). Energies of at least 12 kV are necessary to excite the K lines while simultaneously minimizing of the interaction volume[91].

As X-rays are among the "by-products" of electron microscopy, we can use it to determine the chemical composition of materials on a submicron scale and, with spatial resolution.

2.4. Chemical analysis

2.4.1. Ionic selective electrodes

Potentiometric sensors offer an inexpensive and convenient method for fast analysis with high sensitivity and selectivity compared with other analytical methods to determine low concentration levels of anions. In view of such advantages, efforts have been made to make selective sensors for different anions[92].

An ionic selective electrode is a sensor that converts the activity of a specific ion dissolved in a solution, in the present cases chloride or iodide, into an electrical potential. The voltage is dependent on the logarithm of the ionic activity, according to the Nernst equation (eq. 2-4)[93]. The sensing part of the electrode is usually made as an ion-specific membrane, along with a reference electrode, as shown Figure 2-6.

$$E = E^0 + (2.303RT/ nF) \times Log(a) \qquad \text{(eq. 2-4)}$$

Where E is the total potential (in mV) developed between the sensing and reference electrodes; E^0 is a constant which is characteristic of the particular ISE/reference pair (i.e., the sum of all the liquid junction potentials in the electrochemical cell); 2.303 corresponds to the conversion factor from natural to base10 logarithm; R is the Gas Constant (8.314 joules/degree/mole); T is the Absolute Temperature; n is the charge on the ion (with sign); F is the Faraday Constant (96.500 coulombs per mole); and Log(a) is the logarithm of the activity of the measured ion.

Liquid phases were analyzed using a pH & Ion-meter GLP 22^+. Crison selective chloride and iodide electrodes, 96 52 in case of chloride and 96 56 in case of iodide, both with a sensitive membrane composed by a mixture of salts, with Ag/AgCl reference system in case of 96 56 electrode; and a 50 44 Crison reference electrode with lithium acetate 0.1 M as intermediate electrolite. The solid state membrane electrodes as used are constructed using a robust body, with a membrane in contact with the solution. The main advantage of them is that there is no solution to evaporate or leak away[94]. A diagram of the system is represented in Figure 2-6.

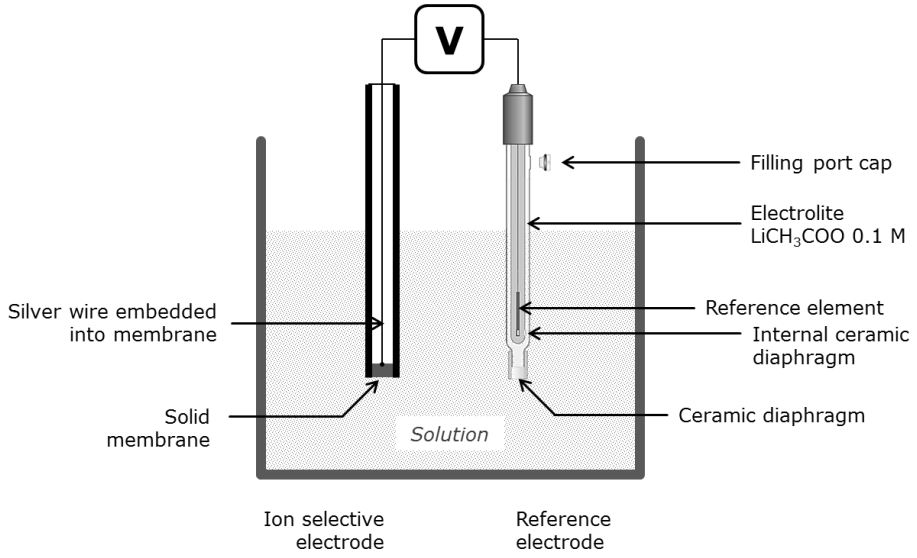

Figure 2-6 – Diagram of a measuring system using ion selective electrode and a reference electrode[93 94].

Some limitations, such as interferences of other anions and the detection limit must be considered during the use of selective electrodes. For instance, analyzing iodide, absence of Br^-, CN^-, Ag^+ y S^{2-} is required because they interfere in the I^- response. In other cases, irreversible damage of the membrane can be caused by other ions (for instance, iodine in the chloride electrode). Working with any type of electrode requires an ionic strength adjuster ($NaNO_3$ 5M solution) added to both the standard solutions and samples in a proportion of 2:100.

The calibration standards were prepared by dissolving NaCl (Fluka, 99.50%), dried during 2 hours at 393K, in MilliQ water, in the case of chloride, and NaI (Sigma Aldrich, 99.999%) treated in the same conditions as NaCl in case of iodide. Standards and samples were measured in the same conditions of ionic strength, temperature and stirring avoiding bubbles, colloids or suspended solids in the solution.

2.4.2. Ion chromatography

Ion chromatography (IC) is a useful method to separate and determine simultaneously and with precision very low concentrations (in the level of ppb) of several ions (in this case, iodide and iodate) in a single run[95]. It is needed to take into consideration the interference with other anions such as nitrate (e.g. from digestion of solids) or chloride (from brine solution).

Ion-chromatography, IC, was performed using a Dionex ICS-2000 apparatus with gradient eluent concentration of potassium hydroxide to determine iodate and iodide concentration in both the filtered solutions (after adsorption tests) and the solutions after digestion of the solid samples with concentrated HNO_3 using conductivity detection.

2.4.3. ICP-OES and atomic absorption

Inductively coupled plasma - optical emission spectrometry (ICP-OES, showed in Figure 2-7) and atomic absorption it is possible to determine qualitatively and quantitatively the chemical composition of both digested materials and waters.

ICP-OES is considered a powerful analytical tool for the determination of elements in concentrations in order of ppb or higher. It is simple and fast due to its high sensitivity and versatility, and it can be used to analyze multiple elements simultaneously.

A peristaltic pump carries the sample (aqueous or organic) into the nebulizer and is changed into aerosol in the spray chamber where is mixed with argon and introduced inside the torch. The sample is divided into their respective atoms which then lose electrons and recombine in the plasma, giving off radiation at the characteristic wavelengths of the elements involved[96].

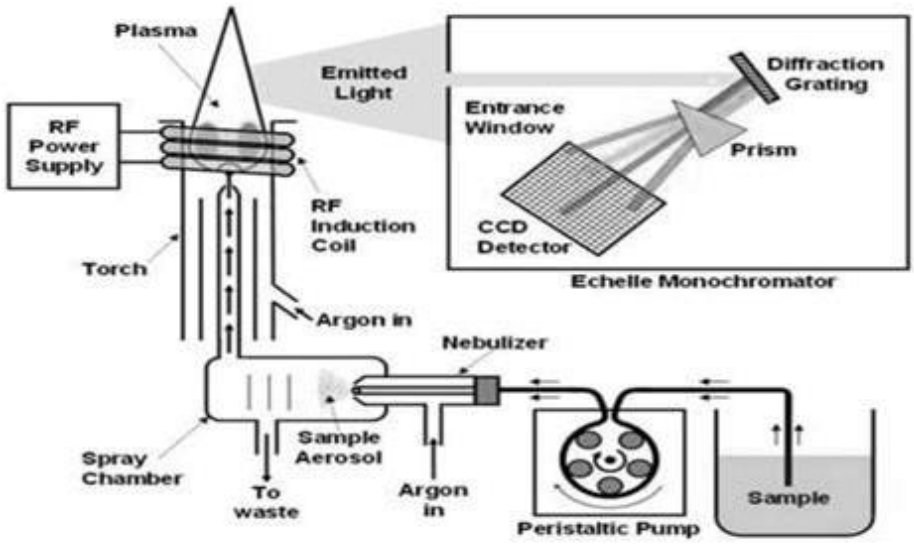

Figure 2-7 – ICP-OES scheme[97].

The concentration of the elements contained in the samples should be in a range higher than 0.001 ppm, to assure precise measurements and reproducibility.

Inductively coupled plasma optical emission spectrometry, ICP-OES, Thermo Scientific iCAP 6000 Series, was used to measure iodine concentration in the digested in HNO_3 solid LDH samples. 45 mL of aqueous samples were used in each measurement. The used standards were the Al standard 1000 mg/L ± 5 mg/L from certiPUR; Mg standard 1000 mg/L from certiPUR; Ca standard 1000 mg/L from certiPUR; Fe standard 1000 mg/L from certiPUR; iodate standard KIO_3^- solution 1/60 M from Fluka; iodide standard of I^- 1000 mg/L ± 15,3 mg/L from Fluka. ICP spectrometer Spectro Arcos FHS16 was also used to simultaneous determination of several elements in digested samples with a 1% of HNO_3 in total volume, using Multi element Standard Ultra Scientific ICM-103 1000 µg/ml to identify Fe, Cu, Ni, Mn, Cr, Zn, Ca, K, Mg, Na, Al, Ag, among others.

ICP-OES has a wide number of applications that has increased significantly in the past decade. The types of biological samples analyzed by ICP-OES include whole blood[98], internal organs[99,100], bones[101], hair[102] and more; it is used in environmental analysis of waters[103] and digests of sewage sludge[104] and soils sediments[105].

2.5. Ultrasonication

Ultrasound are the acoustic waves transmitted through any physical medium with frequencies over the human perception (approximately, 20000 Hz). The waves compress and stretch the molecular spacing of the medium through which it passes, as the ultrasound cross the medium the average distance between the molecules will vary as they oscillate about their mean position. When the negative pressure provoked for an ultrasonic wave crossing a liquid is large enough, the distance between the molecules of the liquid exceeds the minimum molecular distance required to hold the liquid intact, and then the liquid breaks down and voids are created. Those voids are the named cavitation bubbles[106,107].

The behaviour of cavitation bubbles is represented in Figure 2-8, it can be stable cavitation, when bubbles formed at fairly low ultrasonic intensities (1-3W·cm^{-2}) oscillate about some equilibrium size for many acoustic cycles; or transient cavitation when bubbles are formed using sound intensities in excess of 10 W·cm^{-2}. The transient bubbles expand through a few acoustic cycles to a radius of at least twice their initial size before collapsing violently on compression, being considered for that the main source of the chemical and mechanical effects of ultrasonic energy, depending of the parameters frequency, intensity, temperature, the solvent and how the ultrasounds are applied. Each collapsing bubble can be considered as a micro-reactor where are created instantaneously pressures higher than one thousand atmospheres and temperatures of several thousand degrees[108]. If this transient cavitation effects are being applied to a solid, the particle size of the sample is

diminished by solid disruption, increasing the total solid surface in contact with the solvent, as no other method of treatment of samples can reproduce[106,109,110]. For that, ultrasound have applications speeding up enzymatic reactions, accelerating liquid-liquid extraction techniques, enhancing the performance in solid-phase extraction and microextraction and others.

The used ultrasonic bath is a JP Selecta Ultrasons without heating that works at one frequency (50 Hz) and power (150W).

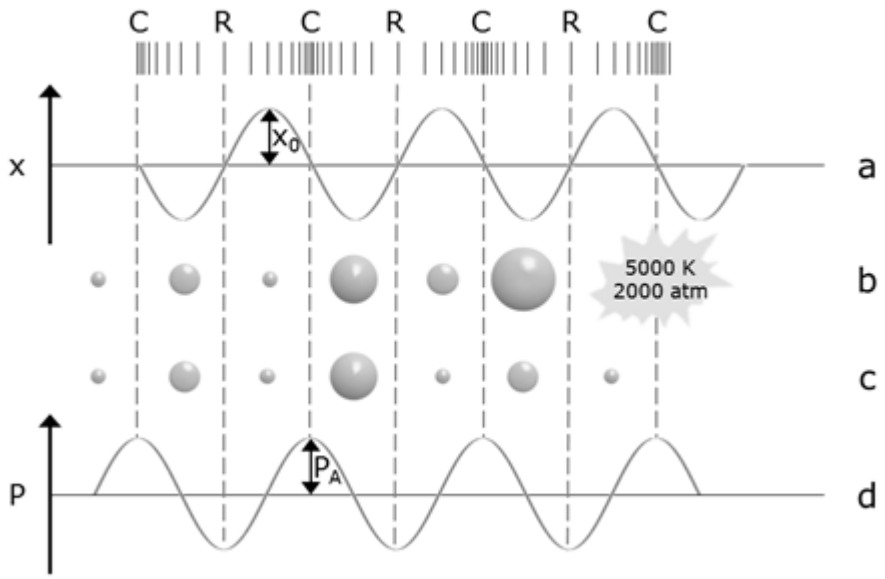

Figure 2-8 – Creation of stable cavitation bubbles and creation and collapse of transient and stable cavitation bubbles. (a) Displacement, (x) graph; (b) transient cavitation; (c) stable cavitation; (d) pressure (P) graph[107].

I am among those who think that science has great beauty. A scientist in his laboratory is not only a technician: he is also a child placed before natural phenomena which impress him like a fairy tale.

Pronounced during 'The future of culture' debate in Madrid, 1933
Marie Curie

3. Layered Double Hydroxides

UNIVERSITAT ROVIRA I VIRGILI
ON THE USE OF LAYERED DOUBLE HYDROXIDES IN THE MANAGEMENT OF 129I FROM LIQUID NUCLEAR WASTES
Luis Iglesias Pérez
Dipòsit Legal: T 893-2015

3.1. Introduction

Layered double hydroxides (from now on, LDHs) are a family of clay minerals that has been widely studied, partly because they are materials with reasonable crystallinity that can be easily prepared (for example by coprecipitation methods[111]). They present an extended list of applications, with special relevance as anion-exchangeable matrices in material chemistry[112], adsorption[113], catalysts[114-116], pharmaceuticals[117,118] and others[119-121].

In the present chapter, several LDH are used as adsorbent materials for iodide retention from aqueous solutions as well as host materials to accumulate iodate or iodide in a stable and safely manner.

3.1.1. LDH structure

LDHs materials are represented by the general formula $[M^{2+}_{x}M^{3+}(OH)_{2(x+1)}]^{+}[A^{n-}_{(1/n)} \cdot mH_2O]^{n-}$, where M^{2+} and M^{3+} are divalent and trivalent metal ions, respectively; A^{n-} is the charge-balancing anion of valence *n*; $x = (5 \leq x \leq 2)$. The M(II)/ M(III) LDH category (M(II): Mg^{2+}, Fe^{2+}, Co^{2+}, Ni^{2+}, Zn^{2+}, *etc.*; M(III): Al^{3+}, Fe^{3+}, Cr^{3+}, *etc.*).

LDH have positively charged brucite-type layers. This mineral, with formula $Mg(OH)_2$, is composed by divalent magnesium cations octahedrally surrounded by hydroxide anions[122]. These octahedral units are linked by edge-sharing, forming layers as shown in Figure 3-1, with hydroxide groups sitting perpendicular to the plane of the layers that are stack on top of one another to form the three-dimensional structure.

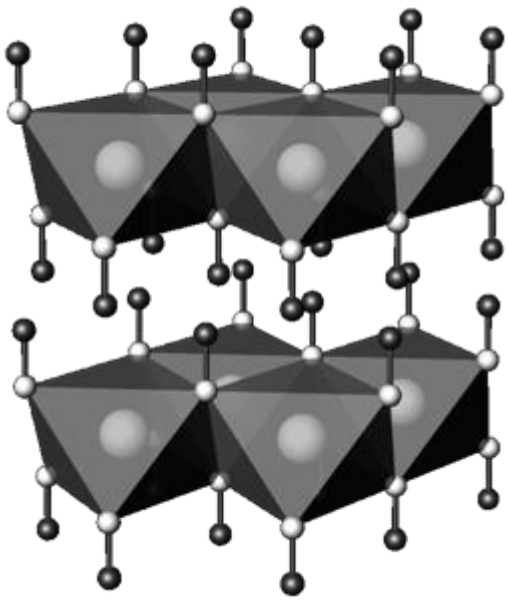

Figure 3-1 – Brucite layer structure. Taken from reference[123].

The basic structure of LDH may be derived by partial substitution of divalent cations by trivalent ones, with a possibility of varying the identity and relative proportions of di– and trivalent cations, being possible to use Mg^{2+}, Ca^{2+}, Mn^{2+}, Fe^{2+}, Co^{2+}, Ni^{2+}, Zn^{2+}, Cd^{2+}, *etc*. as divalent cations[124] and Al^{3+}, Cr^{3+}, Co^{3+} or Fe^{3+} as the trivalent ones[125]. LDHs incorporating Li^{+} monovalent cation have also been reported by Besserguenev *et al.*[126] but LDH synthesis incorporating tetravalent cations in its structure has not been successful so far[127,128].

Cavani *et al*. have reported, in their ample review article of 1991, that pure LDH phases can only be formed for M(II)/M(III) ratios in the range of 2–4[129]. For $x > 0.33$, x=M(III)/(M(II)+M(III)), the presence of M(III)–O–M(III) linkages is unavoidable and this is energetically unfavorable due to the strong repulsion between the adjacent trivalent cations[130]. Thus, x>0.33 may lead to the formation of $Al(OH)_3$ (usually not detected by PXRD) due to the increment of neighboring M(III) octahedra. Similarly, x<0.2 may lead to a

high density of Mg octahedra in the brucite-like sheet, acting as nuclei for the formation of Mg(OH).

Some authors have faced the cation ordering in LDH layers by means of either theoretical models[131] or experimental studies[132,133]. For instance, the structure suggested by Xiao *et al.* and showed in Figure 3-2 is the result of computational calculations on a two-dimensional discrete Coulomb alloy with formula $A_{1-x}B_x$, in which A and B have different charges and are free to move on the sites of a triangular lattice in order to achieve the lowest energy configuration[134].

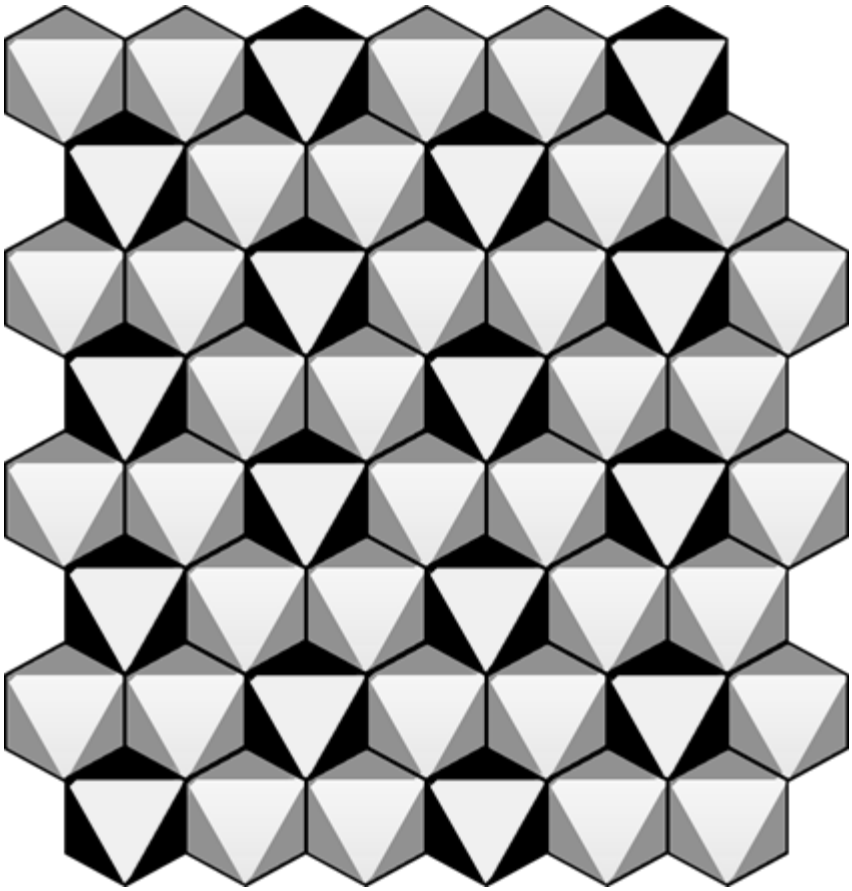

Figure 3-2 – Simulation of a regular triangular superlattice of a Coulomb alloy with x = 1/3. Taken from reference[134].

The interlayer galleries of the LDH structure contain both interlayer anions and water molecules. In consequence, there is a complex network of hydrogen bonds between layer OH^- groups, interlayer anions and water molecules, provoking a disorder space where hydrogen bonds are in a continuous state of flux causing a very complex structure[135]. The interlayer anion is neutralizing the excess of positive charges from the layers[136] and it has been suggested that charge compensation in LDHs has many of the characteristics of resonance effects[132].

The affinity for the interlayer space of LDH was determined to be $OH^- > F^- > Cl^- > Br^- > NO_3^- > I^-$ for monovalent anions, while that for divalent anions is in the sequence $CO_3^{2-} > NYS^{2-} > SO_4^{2-}$ being affected the affinity by the charge and the diameter of the anion[137].

As claimed by Britto *et al.*[138], they are three different approaches to explain the thermodynamic stability of LDHs.

- As the LDHs are obtained by alkali precipitation from a mixed metal (M(II) + M(III)) salt solution, it has been measured the solubility products of LDHs and related it to their thermodynamic stability; the lower the solubility product, greater being the thermodynamic stability.
- the calorimetric measurement of the enthalpy of formation.
- An electronic structure approach can be envisaged taking into consideration such factors as the octahedral crystal field stabilization energies of the metal ions and the mode of coordination of the anions.

3.1.2. Synthesis of LDHs

LDH have been discovered in Sweden in 1842[129], but the majority of LDHs actually used are obtained by synthesis. It exists a wide variety of procedures for LDH synthesis. The selected method will depend on the purpose for which the LDH is to be used.

3.1.2.1. Coprecipitation

Coprecipitation is the most widely used method to prepare LDHs, a versatile procedure to prepare materials containing a variety of layer cations and interlayer anions[139] and is also adequate to produce large quantities of material. Coprecipitation methods are generally faster and less laborious than others[140] and offer some dynamic control of synthesis conditions[141]. Salt solutions of the corresponding divalent and trivalent cations in a determinate ratio and the desired interlayer anion are used in this procedure.

The mechanism of coprecipitation relies upon the condensation of hexa-aquo complexes in solution in order to build brucite-like layers having a uniform distribution of both metallic cations and solvated interlamellar anions.

A thermal treatment process is often performed in order to increase the yields and/or the crystallinity of amorphous or poorly crystallized materials. These procedures can be classified according to reached temperature: a conventional process consists of heating the reactor containing the aqueous suspension of LDH at a temperature between 273-373 K over a few hours or days. The other procedure is known as hydrothermal treatment, which involves higher temperatures and pressures, ranging from 10 to 150 MPa, generally in stainless steel autoclave[142].

3.1.2.1.1. Precipitation at Low Supersaturation

It is performed by slow addition of mixed solutions of the corresponding salts of divalent and trivalent cations into a reactor containing an aqueous solution of the desired interlayer anion. Simultaneously, an alkali solution is added to keep the pH at the selected value, thus provoking the coprecipitation of the LDH[143].

3.1.2.1.2. Precipitation at High Supersaturation

In this procedure, a mixed salt solution of di- and trivalent cations is added to an alkaline solution containing the desired interlayer anion. This method generally gives rise to less crystalline LDHs, because of the wide number of

crystallization nuclei. Thermal treatment performed following coprecipitation may help to increase the crystallinity[144-146].

3.1.2.1.3. Incorporating separate Nucleation and Aging Steps

The formation of LDH crystallites involves two different stages: nucleation and aging. The processes that take place while a crystal is undergoing aging in its mother liquor are fairly complex. It may involve crystal growth, agglomeration, breakage as well as other phenomena as Ostwald ripening[129,139,147-149].

3.1.2.1.4. Urea Hydrolysis Method

Urea, $COO(NH_2)_2$, has several properties that make it useful as precipitant agent and has been largely used to precipitate metal ions as well as hydroxides and insoluble salts[150,151]. Urea is a weak Brønsted base, highly soluble in water and with a hydrolysis rate which can be easily controlled by setting the temperature. Its hydrolysis proceeds in two steps: first ammonium cyanate is formed, being the rate determining step; then takes place a fast hydrolysis of the cyanate to ammonium carbonate as follows:

$$CO(NH_2)_2 \rightarrow NH_4CNO \rightarrow NH_3CNO + 2H_2O \rightarrow 2NH_4^+ + CO_3^{2-}$$

The hydrolysis of ammonium ions to produce ammonia and carbonate to yield hydrogen carbonate results in a pH around 9, conditioned by temperature, which is a suitable pH to precipitate a large number of metal hydroxides[140,152]. This method has also applications in gravimetric analysis[153].

3.1.2.2. Ion-exchange method

This method results appropriate when coprecipitation is inapplicable such as when, for example, the divalent or trivalent metal cations or the anions involved are unstable in alkaline solution, when there is another competitive reaction or there are anions with higher affinity to the interlayer space present in the solution, as previously described.

In ion-exchange method, anions in solution are exchanged with the anions presented in the interlayer regions of LDHs to produce specific anion pillared LDHs. Thermodynamically, ion exchange in LDHs depends mainly on the electrostatic interactions between the positively-charged host sheets and the exchanging anions and, to a lesser extent, on the free energy involved in the changes of hydration[154,155].

Affinity for incoming anion[156], exchange medium[157], pH value[158] or chemical composition of the layers[159] are factors determining the extent of ionic-exchange in any given case.

3.1.2.3. Rehydration using structural "memory effect"

When a LDH is calcined at temperatures around 773 K[160] the interlayer water, interlayer anions and the layer hydroxyl groups are removed, resulting in the formation of a mixed metal oxide[161]. The mixed oxide materials are able to regenerate the original layered structure when they are exposed to liquid water or a water saturated atmosphere[129,160,162-164]. The hydroxyl layers are reformed by absorbed water. In addition, water molecules and anions are incorporated into the interlayer galleries in a process named as reconstruction, regeneration or "memory effect".

The incorporated anions are not necessarily the anions existing in the former LDH, being this a useful method to efficiently incorporate anions to the LDH structure, as well as to obtain pillared structures[114,165,166].

3.1.2.4. Other synthesis methods

Hydrothermal synthesis methods are adequate to intercalate organic guest species with low affinity for LDH[129,143,167,168]. To avoid competing anions with higher affinity for interlayer space insoluble hydroxides of the metals are used as cations sources.

Salt-oxide (or hydroxide) method was first proposed by Boehm *et al.*[169], using salts and oxides as metal sources to synthetize ZnCr-Cl LDH, being a useful

way to obtain other LDH such as CuCr-Cl LDH which are difficult to obtain by coprecipitation[170].

In the non-equilibrium aging method, the salt and alkali solutions are rapidly mixed and nucleated in a colloid mill previously to the aging step. After the aging period, another portion of salt and alkali solutions is added simultaneously to the mixture to ensure that metal ions are supersaturated in every moment. In this conditions, increasing the concentration of ions as well as decreasing the temperature favor the nucleation over crystal growth[171].

Other methods have been reported to prepare LDH, such as the use microwaves, that has been found as a rapid and convenient tool for material synthesis[172,173]; or ultrasound, that can improve the crystalline properties compared LDHs prepared without ultrasonic treatment[174,175].

LDH synthesis on different supports allows the materials to get better mechanical performance, thermal stability and degree of dispersion. Supported LDHs syntheses have been reported using, for example, α-Al_2O_3[176,177], γ-Al_2O_3[178-180], carbon nanofibers[181-183] and mesoporous silica[184,185] as supports.

3.1.3. Properties and applications of LDH

The great versatility of LDHs, which has been stated in the different sections of this chapter, makes these materials as one of the most studied and technologically interesting. LDHs are a cheap, versatile, relatively easily synthesizable, and a potentially reusable source of a variety of catalyst supports, catalyst precursors or actual catalysts. In particular, mixed oxides obtained by calcination of LDHs present relatively large specific surface areas (100-300 m^2/g) with a homogeneous and thermally stable dispersion of the metal ion components. They present marked acid-base properties, and characteristic synergistic effects between the elements with the possibility of

reconstruction of the structure under mild conditions[168]. Some examples of the applications of LDHs are resumed below:

- As catalysts support:

LDH materials can be used as support for organic compounds (what is known as heterogeneization of homogeneous catalysts). For instance, L-Leucine has been immobilized in LDH by intercalation or by replacing of hydroxyl ions at the edge sites of the LDH layers. The individual components, i.e., L-leucine and the LDH, showed very poor activity and lack of enantioselectivity in the epoxidation reaction of α,β-unsaturated ketones such as chalcone. Nevertheless, the hybrid catalysts presented high activity and even enantioselectivity towards the trans-(R,S)-epoxide depending on the L-leu location on the nanohybrid catalyst[118].

MgAl LDHs has been studied by Choudary *et al.*[186] as support for metals, e.g. nanopalladium (0). These catalysts were prepared by ion-exchange with $PdCl_4^{2-}$ followed by reduction. Choudary *et al.* found that using this material in ionic liquids the catalysts has higher activity and selectivity than the homogeneous $PdCl_2$ system in the Heck olefination of electron-poor and electron-rich chloroarenes. In addition, these catalysts showed higher activity in the C-C coupling reactions of chloroarenes than other heterogeneous catalysts with nanopalladium (0) on supports as alumina or silica[186]. Additionally, LDH supported rhodium(0) catalyst was effectively used in the Heck, Suzuki and Stille cross-coupling of haloarenes. Catalyst could be easily removed and reused in several cycles[187].

-Hybrid LDHs:

It is possible to improve LDHs features such as mechanical performance, thermal stability and degree of dispersion by using either inorganic or organic supports during the LDH synthesis. As an example, it has been reported the

use of α-Al_2O_3[176,177] to produce a material adequate to be used in flow reactors.

LDHs supported on γ-Al_2O_3[178-180] allow obtaining a homogeneous distribution of the cations, being impregnation a convenient method to prepare alumina supported hydrotalcite-type mixed hydroxides.

LDHs supported on carbon nanofibers[181,182] have been obtained by a coprecipitation method using either a regular maturation stage or a colloid mill process. The solid obtained resulted to be a valuable base catalyst for the synthesis of glycerol carbonate and dicarbonate as well as for the self-condensation of acetone exhibiting highly improved catalytic performance in both reactions. For instance, one of the CNF supported LDH catalyst presented 300 times higher activity compared to bulk activated hydrotalcites in the case of glycerol transesterification with diethyl carbonate.

Other LDH hybrid inorganic materials were prepared with zeolites[185], obtaining microcrystals tightly attached onto the LDH monolayer and where the zeolite monolayer has a preferred orientation.

With polymers[188] it was possible to obtain homogeneous poly-methyl methacrylate (PMMA)-LDH nanocomposites with a structure consisting of PMMA nanobeads uniformly embedded into the LDH nanocrystals. This material is interesting for the development of well-defined nanocomposites, possessing the specific requirements for a given application, combined with the advantage of LDHs, such as a large variety of compositions, tunable layer charge density and high compatibility with biomaterials.

- As catalysts and catalyst precursors:

LDHs have been reported as efficient catalyst precursors for the synthesis of carbon nanotubes by chemical vapor deposition of acetylene[189].

Numerous works have reported the use of both calcined and rehydrated LDHs in a large number of organic reactions performed in liquid phase, including epoxidation of styrene using MgAl LDH[190], Knovenagel condensation and aldolysations using MgAl or NiAl LDHs[191], or LDHs containing fluoride as efficient, selective and environmentally attractive catalysts for C-C bond formation[192], hydroxylation of phenol over CoNiAl LDHs[193] and liquid-phase carbonylation of methanol to methyl acetate catalyzed over tin-promoted NiAl LDH avoiding the formation of acetic acid in appreciable levels[194].

Many reports have studied the use of LDHs as precursors of mixed oxide catalysts formed by thermal decomposition. Such metal oxides are known to promote a wide variety of industrially important base-catalyzed reactions[195]. MgAl LDH have been reported as catalyst in reactions such as Claisen-Schmidt condensation[196], Meerwein-Ponndorf-Verley reduction[197], Henry reaction of aldehydes[198], isomerizations[199] and diasteroselective synthesis, MgAl LDH has been found to catalyze the reaction between aldehydes and nitroalkanes very efficiently affording threo nitroalkanols in a highly diastereoselective manner[198].

During last decades, several types of LDHs as suitable precursors for transition metal-containing heterogeneous catalysts have been reported[200-205]. Mixed oxides from calcined CuMgAl LDHs have been studied as potential catalysts for hydrogenation of cinnamaldehyde[206]. It was reported that Cu^{2+} ions embedded in the MgAl oxide matrix are the key redox site for this reaction. Rives *et al.* reported the use of V(III)-substituted LDH as precursors of MgV mixed oxides as catalysts for the oxidative dehydrogenation of propane and n-butane[207]. Their results indicated that the performance of the catalysts is determined by the relative amounts of Mg_3VO_4 and MgO, which depends on the content of V(III) of the starting LDHs.

LDHs have been investigated for their potential as materials for the reduction of SO_x and NO_x emissions in the Fluid Catalytic Cracking Units in oil

refineries [208,209]. Mixed oxides obtained from Cu/Mg/Al LDH precursor were the most effective at catalyzing both the oxidation of SO_2 to SO_4^{2-} and the reduction of sulfates to H_2S[209].

- Catalysis in natural gas conversion:

A part of the future of electric power generation is expected to give importance to hydrogen as fuel[210]. Therefore, applications of Ni/Al, Ni/Mg/Al or Ni/Ca/Al catalysts obtained from LDH precursors in the preparation of syngas by catalytic partial oxidation of methane have been widely investigated, with promising results[211-215].

- Pillared LDHs as catalysts:

The intercalation of anionic species into LDHs is a potential alternative for the immobilization of catalytic complexes. LDHs containing bulky and stable anions are rather interesting, since they can give rise to a wide range of microporous materials[216]. Also, it has been proposed the use of LDHs as layered host systems for intergallery immobilization of anionic photocatalysts[217].

- Medical applications:

The first medical applications of LDHs were associated with their use as antacids and antipepsin agents[218,219]. Several studies are focused on the intercalation and controlled release of pharmaceutically active compounds from LDH materials, taking advantage of their biocompatibility, variable chemical composition, alkaline character[220] and their ability to intercalate anionic drugs. Nevertheless, because of the LDHs basic character, they are unsuitable as an oral drug delivery system without any modification because they will be destroyed in the stomach where the pH is 1.2. Hence, Duan *et al.*[221] prepared a core-shell material as a drug delivery system.

Currently, the incorporation of biologically essential molecules in the LDH interlayer space has become a topic of interest and LDH has been shown to stabilize materials such as DNA[222], ATP[223], aminoacids[224], enzymes[225] and vitamins[226].

- Applications in nuclear industry:

L. Aimoz *et al.*[227] analyzed the applicability of MgAl-I, ZnAl-I and ZnAl-IO_3 as potential matrices to store ^{129}I. Theiss *et al.*[228] studied the iodine and iodide adsorption capacity of previously calcined ZnAl LDH and its thermal decomposition and suggested that iodine species may form non-removable anions by thermal decomposition of the LDH structure when these anions are intercalated into the LDH structure. Bastianini *et al.*[229] studied the ZnAl-I and ZnAl-I_3 LDHs obtained via intercalation of molecular iodine from non-aqueous solution and described a mechanism of iodine diffusion into the interlayer space to combine with iodide.

One of the factors that can significantly affect the iodine retention capacity of LDHs is the presence of carbonate in the interlayer space, an anion with higher affinity than iodide or iodate[137]. Therefore, several studies[230,231] investigate diverse intercalation methods involving dissolution and re-coprecipitation procedures to obtain MgAl LDHs avoiding any presence of carbonate in the material. Prasanna *et al.* showed that iodide-containing MgZnAl LDHs lost the intercalated iodide by leaching even at neutral pH, since hydroxide ion (coming from the aqueous medium) can displace the former[232].

MgAl LDH has been used by Kulyukhin *et al.*[233] as adsorbent materials for ^{137}Cs and ^{90}Sr with poor results; however, a material based on MgNd LDH may be used for ^{90}Sr recovering.

LDHs applications in adsorption and ion exchange processes are also important; there is a considerable interest in the use of LDHs to remove

negatively charged species. LDHs can take up anion species from solution by three different mechanisms: surface adsorption, interlayer anion-exchange and reconstruction of a calcined LDH precursor by the memory effect[234]. Both uncalcined and calcined LDHs have also been used as sorbents for decontamination of radioactive wastewater, Toraishi *et al.*[235] reported the adsorption behavior of IO_3^- anions from radioactive wastewater by LDHs, concluding that IO_3^- is weakly adsorbed on the external surface of carbonate−LDH, whereas IO_3^- is exchanged for interlayer NO_3^- in nitrate−LDH.

- Other applications:

The interlayer region of LDHs can provide a novel environment for photochemical reactions of guest molecules[236-239]. Also, inorganic materials such as clays or microporous solids are attractive as replacements in modified electrodes since they have much better stability, tolerance to high temperatures and oxidizing conditions and chemical inertness than organic polymers. Due to the capability of clays to exchange intercalated ions, clay modified electrodes have been extensively studied[240-247].

LDHs have also potential as additives in polymeric materials with several functions such as PVC stabilizing[114,248-250] or flame retardants as well, leading to reduced quantities of smoke during polymer combustion[251].

Furthermore, calcination of LDHs leads to highly dispersed metal oxides with interesting colorimetric parameters to be used as ceramic pigments when they have a very specific composition using transition metals[121,252].

3.2. LDH as adsorbent materials

In this section, it is presented the adsorption of iodide on Mg/Al calcined LDHs with different Mg/Al molar ratios (2/1 and 3/1) and two different interlayer anions (carbonate and nitrate). It is known that the interlayer anion of the parent hydrotalcites influences the textural properties of their

corresponding mixed oxides[253], which may have an effect on the uptake capacity of the adsorbent material. Our purpose was, once deeply studied the existent literature on the topic, to study the influence of the LDH composition (i.e. the M(II)/M(III) molar ratio ant the interlayer anion) the adsorption behavior, as well as the influence of the ultrasound (US) application against conventional stirring as a method to improve the adsorption processes.

3.2.1. Experimental

3.2.1.1. Reagents

All reagents used were analytical grade. MilliQ water was obtained using a Q-Gard 1 Purification Pack. Degasified water was prepared by heating water up to 363 K and flowing argon during 30 minutes.

3.2.1.2. LDH synthesis

Nitrated and carbonated LDHs with Mg/Al molar ratios of 2 and 3 were synthesized using the co-precipitation method as follows: an aqueous solution (100mL) containing the appropriate amount of magnesium nitrate (20–30 mmol) and aluminum nitrate (10 mmol) (Sigma Aldrich 98% and Fluka 98% respectively) was added dropwise into a beaker containing 100 mL of deionized and decarbonated water with vigorous stirring at room temperature. The pH of the solution was kept constant at pH = 10.0 ± 0.2 by adding either a 2 M NaOH (Sigma Aldrich 98%) solution (for nitrated HT) or a 2 M NaOH and Na_2CO_3 (Sigma Aldrich 99%) 0.05 M solution (for carbonated HT). The resulting mixture was aged under stirring overnight, then filtered and thoroughly washed with deionized water and dried at 373 K for 12 h. The preparation and aging of the nitrated HT were performed under Argon flow. The obtained solids were denoted as 21C-as and 31C-as (for carbonated HT) or 21N-as and 31N-as (for nitrated HT).

3.2.1.3. Calcination

Calcination of LDH was performed as a standard calcination method as follows: LDH materials were placed in crucibles and calcined by heating at 10 K/min up to 723 K during 5 hours in an oven to obtain the corresponding mixed oxides. Samples were stored in argon atmosphere until their use.

3.2.1.4. Adsorption process

The adsorption tests were performed with the mixed oxides from calcined LDHs. Batch experiments were carried out in 40 mL polypropylene tubes using 35 mL of KI (Sigma Aldrich, 99%) solutions with a range of concentrations from 100 to 3000 ppm and 0.160 g of calcined LDH. The mixture was magnetically stirred (1000 rpm) at controlled temperature (298 K) for 25 h. Previous experiments had shown that this is time enough to reach the equilibrium. After 25 h the adsorbent was separated from the solution by centrifugation. The liquid phase was filtered and analyzed using a selective iodide electrode connected to a reference one. All measurements were carried out in triplicate and the results shown correspond to the mean values. The resultant adsorption data were fitted to Langmuir and Freundlich equations to check the degree of fitting to these both models.

Iodide adsorption was also performed with 21N-c and 31N-c samples while applying ultrasound treatment. The batch experiments were carried out in an ultrasonic bath at a frequency of 50 kHz. The mixture was submitted to ultrasonication for 1 h and then magnetically stirred (1000 rpm) at a controlled temperature (298 K) to complete 25 h. The procedure was applied in accordance with results obtained in previous experiments.

3.2.1.5. Recycling studies

Recycling tests were also conducted with the 31C-c sample. After every adsorption run, the resulting material was recovered from the solution by centrifugation, washed with water and dried overnight at 353 K. The solid was

then calcined at 723 K for 5 h in static air and submitted to a new adsorption experiment. The sample was used in three consecutive runs.

3.2.1.6. Leaching experiments

After the adsorption process, the recovered solids were used in releasing tests, performed on sample 31C-I at a neutral and acidic pH, which are the types of pH generally found for these kinds of wastewaters. The pH of the solutions was adjusted with HNO_3 to 7, 5 and 3.

3.2.1.7. Brucite synthesis

Brucite was obtained following the synthesis procedure described by Moreira *et al.*[254]. Typically, 1M sodium hydroxide solution was added to dropwise to a 0.5M magnesium nitrate solution and stirred vigorously during the entire procedure. Once a precipitate was formed, the stirring was continued for 1 h to age the sample in the mother liquid.

After this, the solid was filtered, washed with MilliQ water (1L by 10 grams of brucite), dried at 343 K and stored. A part of the synthetized brucite was calcined during 5 hours at 723 K.

Batch experiments were carried out in 40 mL polypropylene tubes using 35 mL of KI (Sigma Aldrich, 99%) solutions with concentrations of 3000 ppm I^-, and 0.160 g of either as prepared or calcined brucite, respectively. The mixture was magnetically stirred (1000 rpm) at controlled temperature (298 K) for 25 h.

3.2.2. Study of adsorption capacity

3.2.2.1. I^- adsorption equilibrium

Preliminary experiments were conducted for different periods of time to determine the equilibrium time. The sample 21N-c was the representative sample used in the tests of adsorption. The obtained results are shown in Table 3-1, revealing that 25 h are enough to reach the equilibrium. The

amount of I^- adsorbed was determined by difference between the initial and the final iodide concentration.

Table 3-1 – Variation of adsorption capacity of 21N-c with time.

Time	Q_e	Adsorbed I^-	Theoretical adsorbed I^{-a}
h	mg I^-/g_{HTc}	%	%
5	85	28	9
10	111	36	11
20	126	42	13
25	156	51	16
30	155	51	16
35	154	51	17

[a] I^- adsorbed respect to the theoretical maximum uptake capacity

3.2.2.2. Brucite adsorption capacity

Iodide adsorption was performed with brucite materials as a blank test. The adsorption results of brucite samples showed no differences in iodide concentration before and after the contact with the material. The I^- uptake found was 1% for brucite while calcined brucite (723 K) did not presented I^- adsorption at all. XRD analysis of synthetized brucite, brucite after iodide uptake and previously calcined brucite after iodide are showed in Figure 3-3. The three samples correspond to brucite (JCPDS 44-1482). Any structural change was observed after keeping the materials in contact with the iodide solution. In addition, there was no presence of crystalline iodine-containing structures.

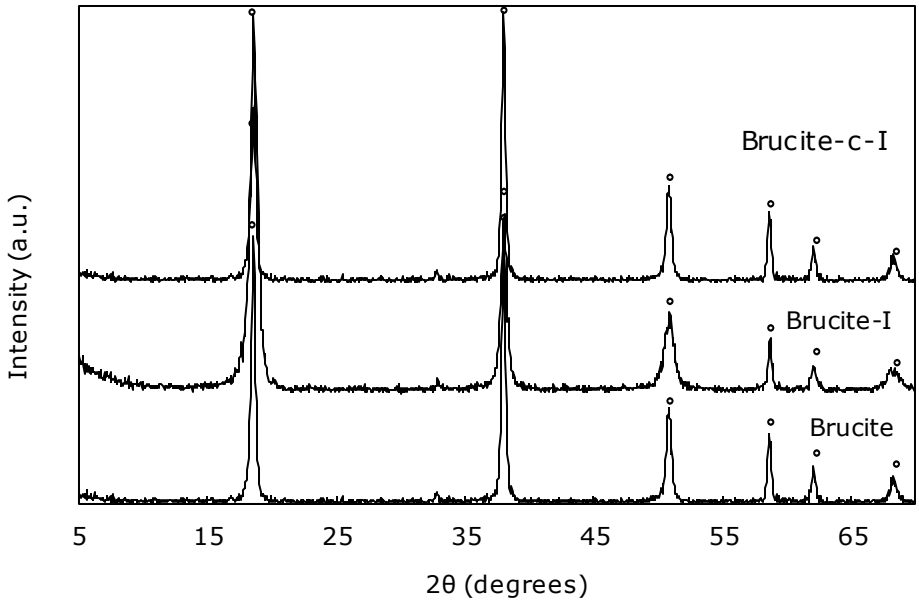

Figure 3-3 – PXRD patterns for the brucite, brucite after iodide uptake (Brucite_I) and calcined brucite after iodide uptake (Brucite_c_I). Brucite (JCPDS 44-1482) mark: °.

3.2.2.3. Effect of molar ratio and interlayer anion of parent hydrotalcite

The effect of the Mg/Al molar ratio as well as the effect of the interlayer anion of the parent LDH was investigated on the removal of the iodide anions. A clear influence of the Mg/Al molar ratio on the uptake capacity of the adsorbent (Table 3-2) was observed. Thus, those materials with Mg/Al molar ratio equal to 3 (31C-c and 31N-c) presented the highest iodide adsorption (392 and 266 mg I^-/g respectively). The higher adsorption capacity of these samples is due to their lower layer charge density and is in agreement with previous studies on adsorption with LDHs[230,255]. In addition, mixed oxides with a Mg/Al molar ratio of 3 undergo the fastest reconstruction process due to the structural ordering of their cations[256], which may help the adsorption process. However, it is important to note that carbonate derived mixed oxides presented higher adsorption capacities in comparison to the nitrate derived ones. This may be related to the textural properties of the adsorbent materials. In this case, the calcined carbonate LDHs presented a larger surface area, pore

size and pore volume than the corresponding calcined nitrate materials, as shown in Table 3-2. Nitrates thermally stabilize the hydrotalcite-type structure[257] compared to other anions such as CO_3^{2-}, allowing the formation of more crystalline structures and thus reducing their specific surface area. This makes it more difficult for the iodide species to access the calcined LDH and consequently the adsorption capacity of these samples decreases.

Table 3-2 – Maximum adsorption capacities and theoretical adsorption capacity estimation for the different adsorbents

Sample	Max. uptake mg/g	Adsorbed I^- meq I^-/g	Theoretical ads. I^{-a} %	Ratio Al/(Mg+Al)
21C-c	139	1.09	27	0.34
31C-c	392	3.09	57	0.23
21N-c	113	0.89	23	0.34
31N-c	266	1.94	66	0.26
21N-cUS	232	1.79	24	0.34
31N-cUS	439	3.46	60	0.26

[a] I^- adsorbed respect to the theoretical maximum uptake capacity

A porosity study of the parent MgAl–NO_3 and MgAl–CO_3 as well as the final materials (after iodide adsorption) confirms the absence of microporosity (t-plot method). Their surface areas were between 50 and 90 m^2/g. There is a noticeable decrease in the specific surface area of samples after iodide adsorption compared to the parent materials and the calcined ones (Table 3-3). For instance, the specific surface area of sample 21N-c after iodide adsorption dropped from 51 m^2/g (for 21N-as) to 18 m^2/g (for 21N-I) and its pore volume was reduced drastically from 0.26 cm^3/g to 0.04 cm^3/g. All the iodide-containing samples presented comparable surface areas with values about 15 m^2/g. This surface area is created by the outside surface of the different stacks (assembly of the layers), which are packed in an irregular way.

The pore size distribution (PSD) curves (Figure 3-4) point out modifications in the pore size range of the samples. For instance, sample 21N-as presented a broad peak with a maximum around 3 nm. This shows that small mesopores establish the porosity characteristics of this material. Slightly larger

Table 3-3 –Chemical analysis, textural properties and crystal parameters for the adsorbents in their different stages

Sample	c	d_{006} Å	S_{BET} m^2/g	Pore V cm^3/g	ICP ratio Al/(Mg+Al)	ICP ratio Mg/Al	EDX ratio* Mg/Al
21C-as	23.11 (40)	3.85	87	0.55	0.34	1.95	-
21C-c	-	-	261	0.78	-	-	-
21C-I	23.06 (5) / 23.77 (-)	4.00 / 3.80	17	0.26	-	-	2.25
21N-as	23.94 (-)	3.95	51	0.06	0.34	1.95	-
21N-c	-	-	176	0.33	-	-	-
21N-I	24.20 (-) / 23.52 (-)	4.20 / 3.95	18	0.04	-	-	2.00
21N-IUS	24.12 (-) / 23.52 (-)	4.10 / 3.98	36	0.06	-	-	2.04
31C-as	23.60 (40)	3.93	56	0.19	0.23	3.28	-
31C-c	-	-	204	0.66	-	-	-
31C-I	25.60 (1) / 23.67 (-)	4.26 / 4.01	14	0.09	-	-	3.23
31N-as	23.55 (-)	3.93	-	-	0.26	2.87	-
31N-c	-	-	174	0.27	-	-	-
31N-I	23.59 (10) / 23.10 (-)	4.21 / 3.99	14	0.03	-	-	3.14
31N-IUS	24.66 (-) / 23.55 (-)	4.11 / 3.95	50	0.12	-	-	2.81

* EDX values have been obtained after 3 measurements in 3 different points for each sample

mesopores were produced in the sample after the iodide adsorption. The PSD curve of 21N-I presented a sharp and high peak which is also shifted to a larger size with a maximum at about 4.5 nm. Compared with the corresponding resultant material after adsorption with ultrasonication (21N-IUS), an interesting change in the pore size distribution can be observed. A broad peak with a maximum at around 11 nm is observed, while the peak at 4.5 previously found in sample 21N-I seems to decrease in this case. In addition, the S_{BET} of sample 21N-IUS is 36 m^2/g, whereas the surface area for the 21N-I material is 18 m^2/g. This is an interesting result, which can be explained by the fact that the physical shear forces generated during acoustic cavitation may break down the larger aggregates to smaller ones leading to an increase in surface area[258].

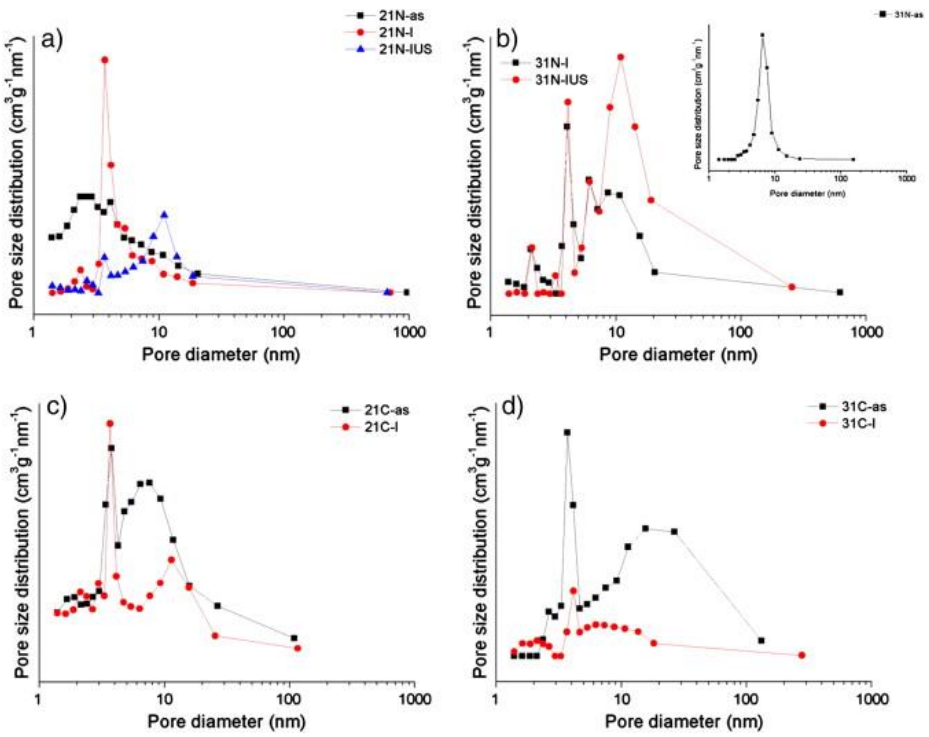

Figure 3-4 – Pore distribution in as-synthesized LDHs (black) and LDHs after iodide adsorption without ultrasonication (red) and with ultrasonication (blue) of samples 21−N (a); 31−N (b); 21−C (c); and 31−C (d).

Compared to 2/1 MgAl-NO_3 LDHs, those with a molar ratio of 3 show similar behavior; however, they present peaks shifted towards larger sizes. As in the previous case, the application of ultrasonication during the adsorption process results in the formation of larger pores. On the other hand, both 2/1 and 3/1 carbonated LDHs show very similar PSD curves presenting two different pore sizes: one sharp peak at about 4 nm and one broad peak at higher values with their maximum in the 11–15 nm range. In any sample, neither micropores nor macropores are detected, revealing that the uniformity of the porous structure is accentuated.

Taking into account only the molar ratio and the interlayer anion of the parent LDHs, the results for the adsorption capacity of the materials were as follows (Table 3-2): 21N-c < 21C-c < 31N-c < 31C-c. The effect of the ultrasound treatment will be discussed later.

The iodide adsorbed by these materials represents only a fraction of the theoretical adsorption capacity estimated, taking into account the adsorption sites available (see Scheme 3-1) and considering that all the Al^{3+} will be forming the structure of the iodide-reconstructed HT. Table 3-2 gives the I^- adsorption capacity of these materials according to their theoretical adsorption values. As mentioned earlier, the adsorption process is more efficient in those samples with lower Al/(Mg+Al) ratios. Furthermore, the I^- adsorption found was in a range from about 1 to 3 meq I^-/g, comparable to that shown by anion exchange resins [129].

$$[M^{2+}_{1-x}M^{3+}_{x}(OH)_2](A^{m-})_{x/m}\cdot nH_2O \xrightarrow{\Delta} MgO - Al_2O_3\left(Mg_{1-3x/2}Al_xO\right) + A(O/H) + H_2O$$

(Hydrotalcite) *(Mixed Oxide)*

$$MgO\cdot Al_2O_3\left(Mg_{1-3x/2}Al_xO\right) \xrightarrow{I^-_{aq.}} [M^{2+}_{1-x}M^{3+}_{x}(OH)_2](I^-)_{x/m}\cdot nH_2O$$

Scheme 3-1 – Process of calcination and reconstruction of hydrotalcite-like compounds.

The XRD patterns of the parent LDHs along with the mixed oxides and reconstructed LDHs are shown in Figure 3-5. The XRD pattern of the parent LDHs (31N-as, 31C-as, 21N-as and 21C-as) shows reflection lines typical of a layered structure. The peaks disappear after calcination at 723 K, indicating the collapse of the layered structure of the LDH, and new peaks typical of MgO (periclase, JCPDS 45-0946) were observed. After the adsorption experiment the four samples seem to recover their original layered structure. However, all the reflection peaks become broader than in the parent material, indicating a poorer degree of crystallinity. In addition, the disappearance of the (012) plane (around $2\theta = 35°$) in all diffractograms, except in 21C-I, demonstrates that the stacking of the structure changes after iodide adsorption and the materials obtained present high structural disorder. This effect is attributed to the fact that iodide is unable to form H-bonds between the metal hydroxide layer and the interlayer, and hence the (hkl) reflections practically disappear[232,259]. This effect was observed in all the materials after iodide adsorption. Since I^- presents higher size (0.432 nm) than the other species co-existing in the interlayer space (such as H_2O, OH^-, and CO_3^{2-}), one could expect that the materials PXRD analyses after iodide uptake will differ mostly in the (003) and (006) reflections. PXRD analysis of these materials revealed a shift of the (003) and (006) peaks at lower 2θ values positions (Table 3-4) which are in agreement with the presence of intercalated iodide species as compensating anions[260].

The existence of various layered phases can be concluded for some of these iodide-rehydrated samples, since the PXRD patterns showed (00l) harmonics at approximately 7.9 and 3.9 Å, corresponding to diffraction by planes (003) and (006) respectively. As the adsorption experiments were conducted in an inert atmosphere, these distances should correspond to the intercalation of hydroxyl species in the interlayer that compete with iodide species during the adsorption.

The scanning electron microscopy (SEM) of samples after iodide adsorption (Figure 3-6) shows the typical morphology of LDHs with a random distribution of platelets, which demonstrates the existence of the reconstructed LDH as previously shown by PXRD. The ESEM image of those samples reconstructed after ultrasound-assisted iodide adsorption (Figure 3-6 c) presents nearly uniformly plate-like structures, which are clearly much less agglomerated than those presented by the as-synthesized sample (Figure 3-6 a) and the sample after adsorption with mechanical stirring (Figure 3-6 b). At a first glance, these samples (21N-as and 21N-I) consist in highly interconnected plate-like particles forming irregular agglomerations. This fact makes it difficult to obtain an accurate size value from the SEM micrographs. The lateral sizes of these LDHs are in a large range from, approximately, 100 to 300 nm. In contrast, the samples submitted to adsorption with ultrasound displayed dispersed plate-like crystals in the range between 150 and 250 nm, with an average size of 190 nm. The low degree of agglomeration presented by these samples is attributed to the effect of ultrasound, which results in the separation of the crystallites. Even though the platelet size is rather similar in all the samples (ultrasonicated and non-ultrasonicated), it has been seen that those submitted to adsorption with ultrasound presented higher specific surface areas. This fact is consistent with the higher degree of dispersion displayed by these samples.

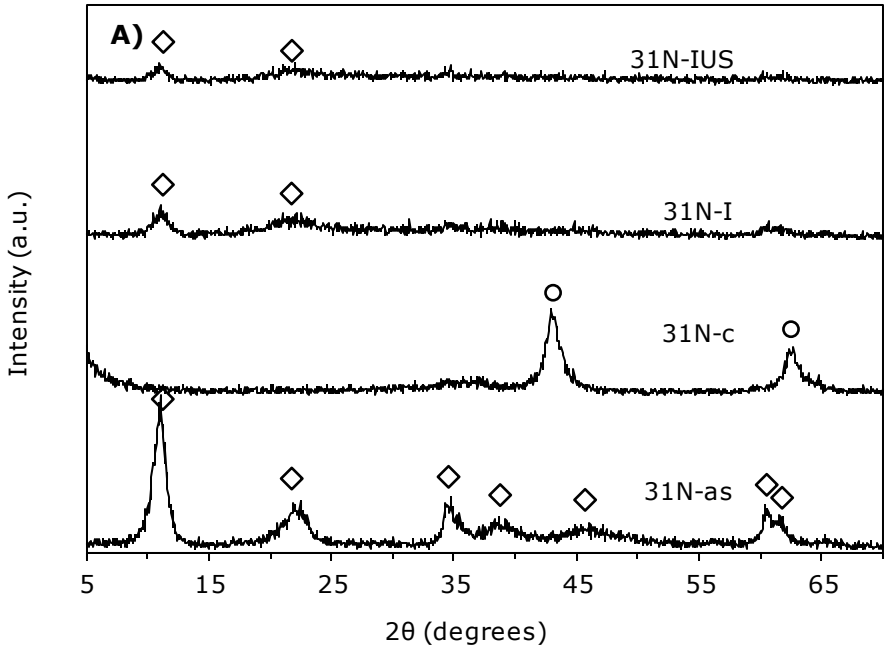

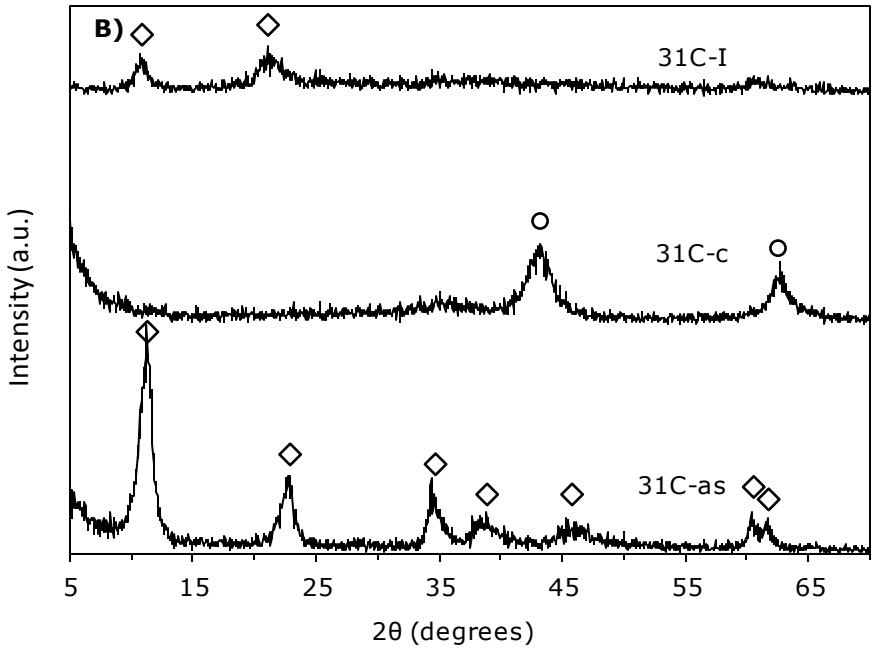

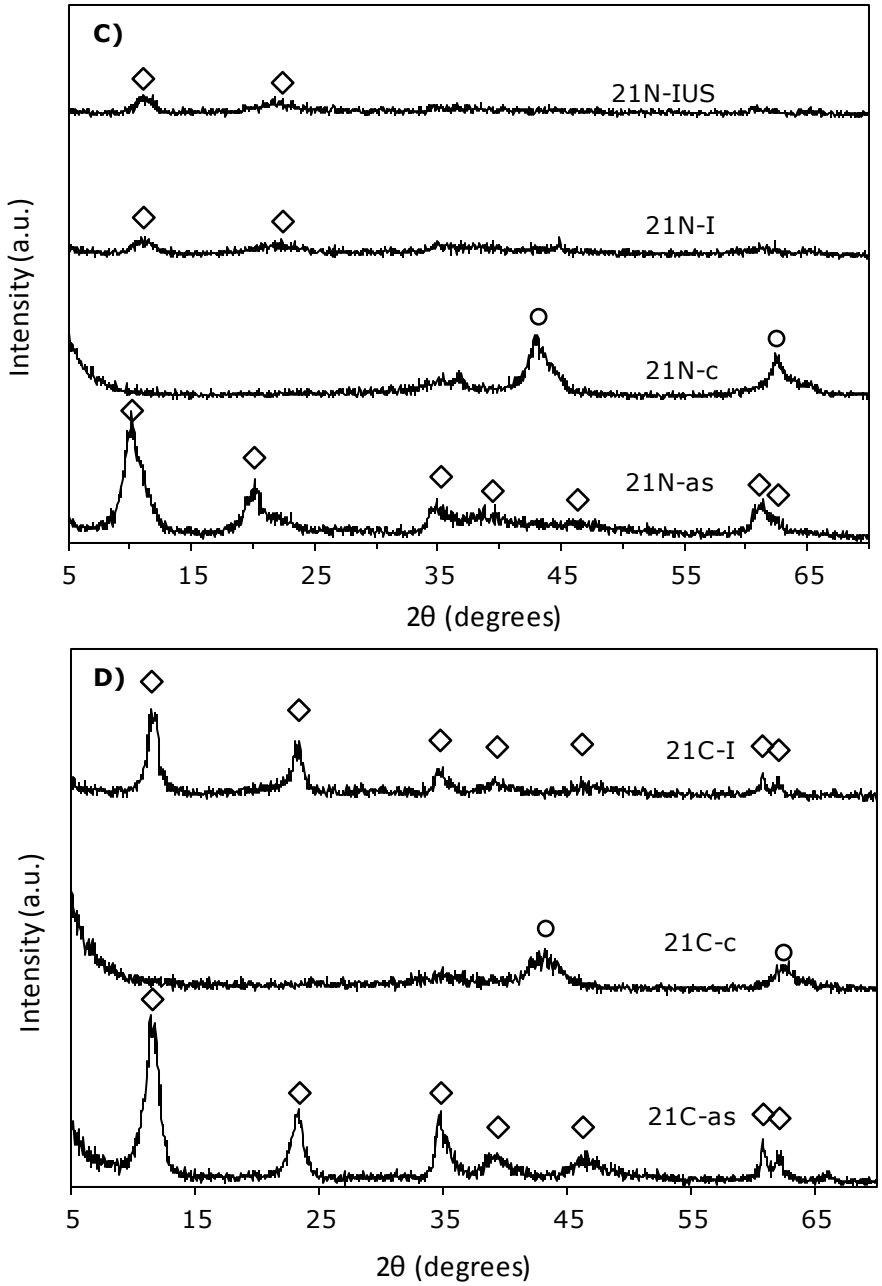

Figure 3-5 – PXRD patterns for the nitrate (A) and carbonate (B) 31 MgAl LDHs and nitrate (C) and carbonate (D) 21 MgAl LDHs. As-synthesized sample as X-as; calcined samples as X-c; samples after the iodide uptake as X-I and X-IUS the samples after the iodide uptake applying ultrasounds. Simbols: ◇ , periclase; ○ , hydrotalcite.

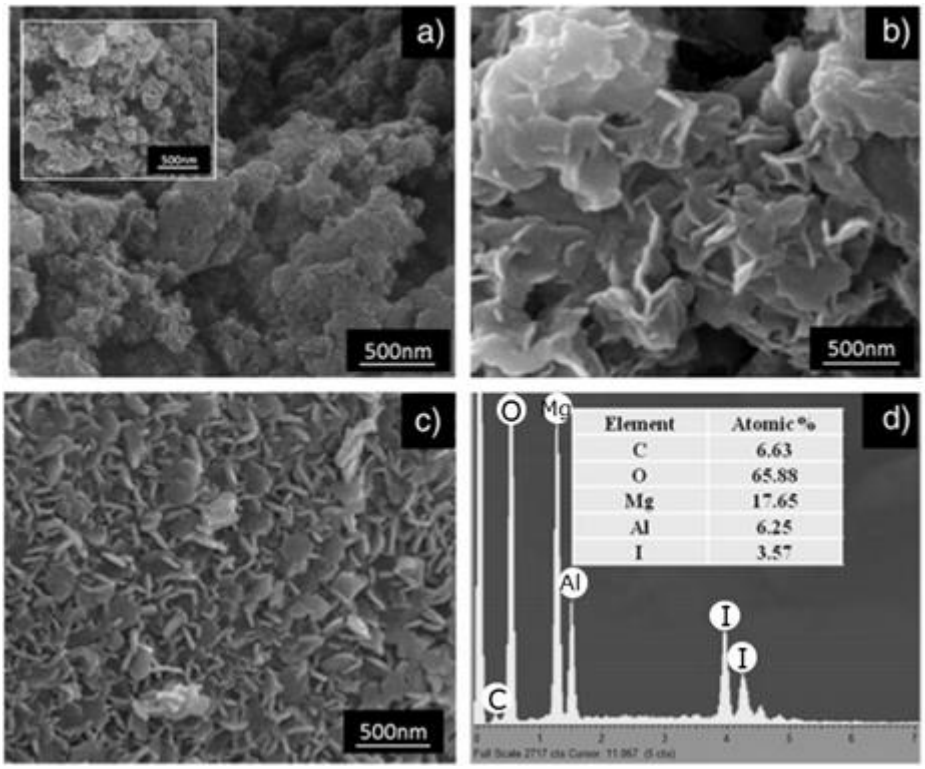

Figure 3-6 – Scanning electron microscopy of hydrotalcites MgAl–NO3: a) as-synthesized (21N-as); b) after the iodide adsorption (21N-I); c) after the iodide adsorption with ultrasounds (21N-IUS); and d) EDX analysis for 31N-IUS.

On the other hand, the Mg/Al molar ratio was maintained after the adsorption experiment, as confirmed by EDX analysis (Figure 3-6 d). The presence of iodide species was also ascertained by this technique.

Figure 3-7 shows the effect of varying the initial concentration of iodide species on the uptake capacity of the calcined HT samples. As expected, it can be seen that iodide adsorption increased with the increasing initial iodide concentration. These data were fitted to the Langmuir and Freundlich equilibrium models (Table 3-4), expressed as Eqs. (3-1) and (3-2) respectively:

$$\frac{C_e}{Q_e} = \frac{1}{Q_m K_L} + \frac{C_m}{Q_m} \qquad \text{(Eq. 3-1)}$$

$$\ln(Q_e) = ln(K_F) + \frac{1}{n} ln(C_e) \qquad \text{(Eq. 3-2)}$$

Q_e represents the amount of iodide adsorbed per gram of adsorbent (mg I^-/g HTc) at equilibrium, C_e is the equilibrium solution concentration (mg I^-/L) and Q_m is the maximum adsorption capacity of the material expressed in terms of mg I^-/g HTc. K_L is the adsorption equilibrium constant from Langmuir equation (3-1). K_F (mg/g) and 1/n are Freundlich constants (3-2). The parameter *n* is related to the distribution of bonded ions on the adsorbent. Values of *n* in a range between 1 and 10 indicate a favorable adsorption.

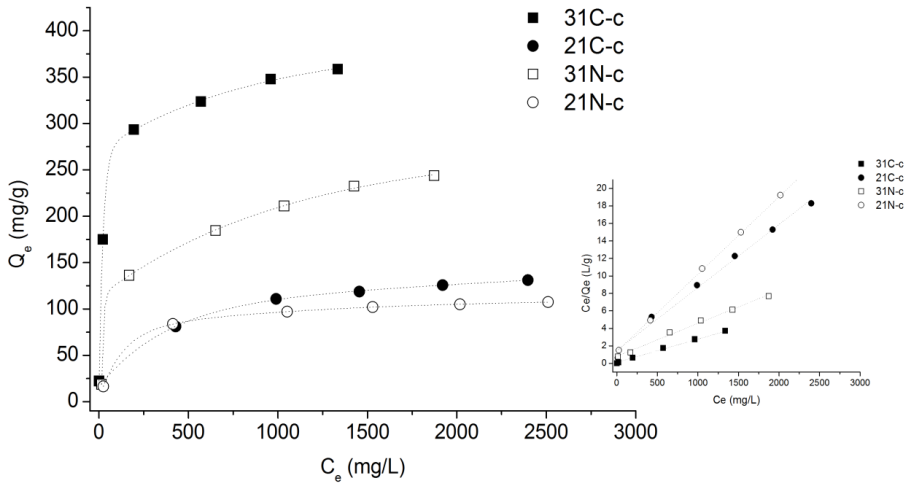

Figure 3-7 – Adsorption capacity (Q_e) of iodide adsorbed at equilibrium vs. equilibrium concentration (C_e). Inset: linearization of experimental data.

Table 3-4 – Langmuir and Freundlich isotherm parameters for adsorption of iodide on calcined MgAl hydrotalcites.

Adsorbent	Langmuir				Freundlich		
	Q_m mg I^-/g $_{HTc}$	K_L L/g	R^2	ΔG^0	K_F mg/g	n	R^2
21C-c	139	0.0049	0.998	-0.63	7.92	2.56	0.940
31C-c	392	0.0071	0.994	-2.24	34.12	2.78	0.907
21N-c	113	0.0065	0.999	-1.35	4.53	2.42	0.937
31N-c	266	0.0047	0.993	-1.21	5.93	1.92	0.931
21N-cUS	232	0.0069	0.994	-1.50	12.18	2.56	0.972
31N-cUS	439	0.0105	0.999	-3.23	64.71	3.56	0.959

As can be seen in Table 3-4, the experimental data were satisfactorily fitted with the Langmuir equation with R^2 values of 0.99 for all cases. The higher K_L value obtained indicates its better affinity for the adsorbate. This is observed particularly for the samples containing a higher Mg/Al molar ratio due to their low charge density. Moreover, the free Gibbs energy calculated (Table 3-4) indicates that the adsorption process takes place spontaneously under the experimental conditions, and the increment in the negative direction also indicates higher affinity between the iodide and the adsorbent.

The essential characteristics of a Langmuir isotherm can be expressed in terms of a dimensionless constant (equilibrium parameter), R_L[261]. This parameter is expressed as Eq. (3-3):

$$R_L = \frac{1}{1 + K_L C_0} \qquad \text{(Eq. 3-3)}$$

Calculations of the R_L parameter give information about whether an adsorption system is favorable or unfavorable. R_L values equal to 0 indicate irreversible adsorption and R_L values between 0 and 1 indicate favorable adsorption. When $R_L > 1$ the adsorption is unfavorable. All the experimental R_L values obtained for the iodide adsorption were within the 0-1 range, which indicates a favorable adsorption. Table 3-4 reveals that higher the initial

iodide concentrations lower the R_L parameter, indicating a more favorable adsorption at lower concentrations. This might be related with the larger ionic strength generated at higher iodide concentrations, which may hinder the motion of the iodide species to the surface of the adsorbent.

Table 3-5 – Values of equilibrium parameter R_L with different initial iodide concentration

C_0	R_L					
mg/L	31C-c	21C-c	31N-c	21N-c	21N-cUS	31N-cUS
3000	0.0426	0.0637	0.0662	0.0488	0.0461	0.0308
2500	0.0507	0.0755	0.0784	0.0579	0.0548	0.0366
2000	0.0627	0.0926	0.0962	0.0714	0.0676	0.0455
1500	0.0818	0.1198	0.1242	0.0930	0.0881	0.0597
800	0.1433	0.2033	0.2101	0.1613	0.1534	0.1064
100	0.5706	0.6711	0.6803	0.6061	0.5917	0.4878

3.2.2.4. Effect of ultrasound application

Several studies are focused on how ultrasonication alters the crystallinity and texture of hydrotalcite-like materials; however, fewer studies are published focused on the effect of ultrasound on adsorption capacities of this calcined material.

Figure 3-8 shows the iodide uptake of nitrate derived mixed oxides while applying ultrasonication. A representation of the uptake capacity for the same samples without ultrasonication treatment was also displayed for comparative purposes. As can be seen in Figure 3-8, iodide adsorption increased when ultrasonication was used. The uptake capacity shown by these two samples was around 232 mg/g and 439 mg/g (21N-IUS and 31N-IUS respectively), a factor about 2 times higher than that presented by their non-sonicated counterparts. These samples also presented higher adsorption values than those derived from carbonated LDHs, which showed the greatest adsorption capacity in the previous stage studied. These sonicated samples and sample 31C-c showed the highest K_L values (Table 3-4), indicating greater interaction with the absorbate.

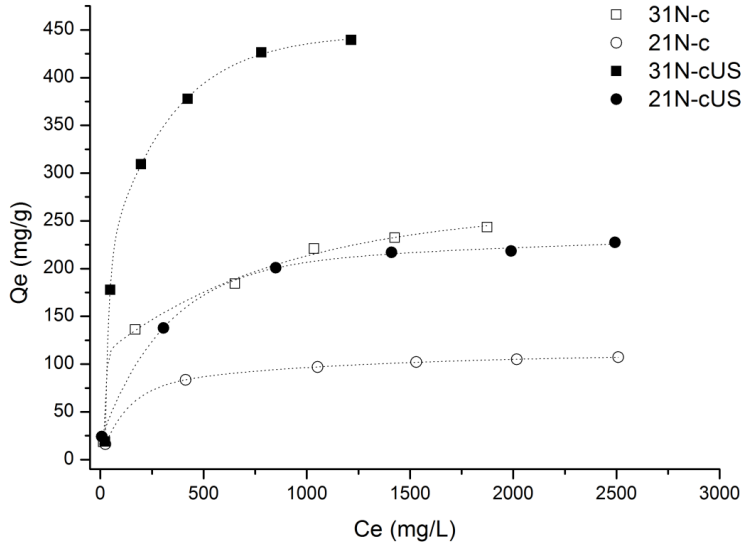

Figure 3-8 – Adsorption capacity (Q_e) of iodide adsorbed at equilibrium vs. equilibrium concentration (C_e) with ultrasonication (21N-cUS and 31N-cUS) and without ultrasonication (21N-c and 31N-c).

The better adsorption of iodide species can be explained by different effects. First, ultrasonication produces a rapid movement of the liquid which accelerates mass transfer throughout the adsorbent, favoring both the reconstruction of the material and the adsorption of the anions. However, the micro-streaming produced by vibrational energy encourages the incorporation of the iodide species into the interlayer of the LDH during reconstruction.

Differences in surface area were also found after adsorption for the ultrasonicated samples (Table 3-3), which present a surface area significantly larger than that shown by the adsorbents after iodide adsorption under mechanical conditions. For example, the sample 21N-IUS presented a surface area of 36 m^2/g against 18 m^2/g displayed by sample 21N-I. Likewise, the sample 31N-IUS presented a surface area of 50 m^2/g against 14 m^2/g found by sample 31N-I. In addition, ultrasonication produced the formation of greater pores, as previously seen in the PSD curves. The application of ultrasound

also affected the crystal material structure after adsorption, diminishing the degree of agglomeration of the LDHs formed, and, despite the crystal size being rather similar in both series of samples; this effect may be responsible for the increase in surface area.

TEM analyses were also performed in order to find some differences in the morphology of the adsorbents. As previously found by ESEM, the samples presented a high degree of agglomeration which made it difficult to observe significant differences in their morphology. In Figure 3-9 are displayed the TEM micrographs of samples 21N-I (Figure 3-9 a) and 21N-IUS (Figure 3-9 b & 3-9 c). At a first glance we can observe that sample 21N-I (non-ultrasonicated) presents higher disorder orientation of crystallites than 21N-IUS (ultrasonicated). The crystal size is coherent with that found by ESEM. In contrast, sample 21N-IUS seems to have certain preferential orientation and crystals are rather aligned parallel with the surface of the copper grid. Moreover, it is possible to distinguish some hexagonal platelets (Figure 3-9 c) which present lateral sizes around 100 nm. On the other hand, the thickness of the layers (marked with arrows in Figure 3-9 c) resembles to be lower in the case of ultrasonicated sample (21N-IUS) than the non-ultrasonicated one (21N-I).

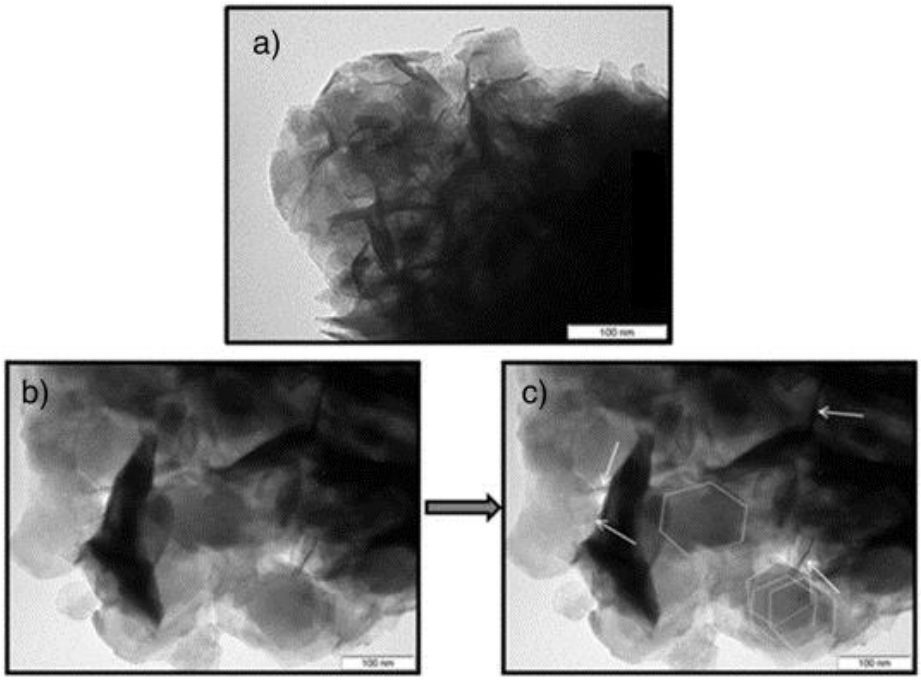

Figure 3-9 – TEM micrographs of samples after iodide adsorption: a) 21N-I (without ultrasound); b and c) 21N-IUS (with ultrasound).

In a liquid–solid system, the uptake of the solute in a particle varies according to the $D_0t^{0.5}/r^2$. Hence, there is a linear relationship between the uptake and $t_{0.5}$ for most of the adsorption processes[262].

The diffusion rate of I^- in a particle can be calculated following the equation (3-4):

$$q_e = k_i t^{0.5} \qquad \text{(Eq. 3-4)}$$

where k_i is the intraparticle diffusion rate expressed in mg g^{-1} $min^{0.5}$ and q_e represents the adsorption capacity of I^- (mg/g) at equilibrium time.

Table 3-6 presents the diffusion rates calculated for those experiments carried out in the presence of ultrasound and also their non-ultrasonicated analogs. The highest diffusion rates were found for those adsorbents where iodide adsorption was assisted by ultrasound. The phenomena produced during ultrasonication (cavitation, microagitation, microstreaming…) enhance the

transport of the adsorbent to the surface of the adsorbate particles. The mass transfer rate is increased by reducing the diffusion resistance[263]. In addition, ultrasonication brings about the partial exfoliation of the adsorbent (i.e. LDH), reducing the internal diffusion of the iodide species through the particles of the adsorbent. Therefore equilibrium was more easily achieved and higher iodide adsorption capacity can be attained. This is clearly observed for sample 31N-cUS, which presents a higher iodide adsorption capacity (Table 3-2) than its non-ultrasonicated analog, and the corresponding reconstructed material (31N-IUS) showed a larger surface area and pore volume (Table 3-3).

Table 3-6 –Interparticle rate diffusion constant parameters

	Adsorbent			
	21N-c	31N-c	21N-cUS	31N-cUS
Diffusion rate (k_i) (mg g^{-1} $min^{0.5}$)	3.75	3.53	4.32	10.33

3.2.2.5. Study of reversibility of the process. Desorption and recycling

After the adsorption process, releasing tests were performed with sample 31C-I under neutral and acidic conditions, which are the pH generally found for this kind of waste waters. The pH of the solutions was adjusted with HNO_3 to 7, 5 and 3. In all the cases, leaching of iodide was observed as showed in Figure 3-10.

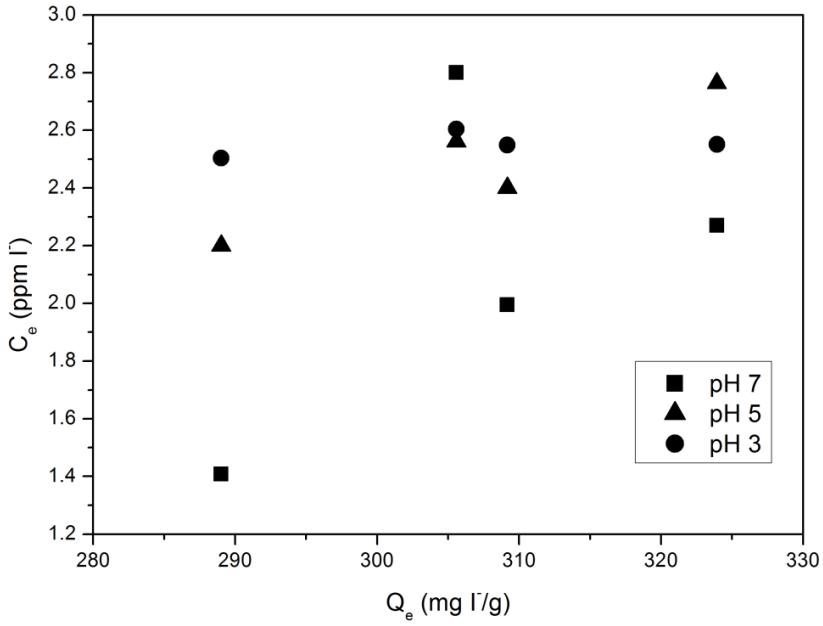

Figure 3-10 – Iodide leaching from 31C-I adsorbent at different pH values. Q_e is the iodide adsorbed by the adsorbent 31C-c and C_e is the I^- equilibrium concentration after 30 h of leaching tests.

The amount of iodide released was fairly similar in the various cases; even the experiment carried out with the most acidic conditions (pH = 3) presented only slightly higher releasing values than those found at pH = 7, despite the disaggregation that the HTs may undergo in these conditions. The experiments conducted at pH = 7 showed a release of about 35% of iodide from the adsorbent, while those carried out at lower pH values presented an iodide release of about 40%. Furthermore, the amount of iodide released in the experiments conducted at lower pH values does not seem to be closely related to the amount of iodide adsorbed in the LDH. The iodide released in this case is always close to 2.5 ppm independent of the initial content of iodide in the adsorbent (31C-I).

Recycling studies were also conducted with the material showing the highest uptake capacity, i.e. 31C-c. After every adsorption run, the resulting material

was recovered from the solution by centrifugation, washed with water and dried overnight at 353 K. The solid was then calcined at 723 K for 5 h in static air and submitted to a new adsorption experiment. The mixed oxide 31C-c was able to be regenerated 3 times, indicating a certain reversibility of both the adsorption and the calcination–reconstruction processes. However, a loss of adsorption capacity was found in the third cycle compared to the fresh material (Table 3-7), dropping from approximately 392 mg I^-/g in the first run to ~ 213 mg I^-/g in the third. One plausible explanation for this behavior may be found in the subsequent calcination steps, which can affect the LDH reconstruction process. Every consecutive calcination/reconstruction step may lead to the formation of undesirable oxides which cannot reincorporate into the LDH structure[264]. The formation of $Mg_2Al_3O_4$ spinel may also occur after the first calcination cycle[232], affecting the reconstruction process and therefore the anion sorption capacity. An additional X-ray analysis performed in this sample after three cycles of adsorption revealed a very poor crystalline material (Figure 3-11). The background of the diffractogram also indicates a great amount of amorphous species. The diffractogram shows the typical lines corresponding to a layered material and, as previously found, the existence of various layered phases is observed, since the PXRD patterns show splitted peaks in the (00l) harmonics. These should correspond to the intercalation of hydroxyl species in the interlayer that compete with iodide species during the adsorption, and even to carbonate species from possible CO_2 contamination produced during the subsequent treatments and manipulation of the sample. Since the crystallinity of this sample is very poor, it is difficult to determine every possible extra-phase in the sample; however, reflection lines different to LDH have been identified noticing structural changes in the material. These lines could be attributed to an oxyhydroxy aluminum phase and an MgAl oxide poorly crystallized. This change in the structural composition of the sample may be responsible for the loss in the adsorption capacity of the adsorbent.

Table 3-7 – Removal capacity of 31C-c after different adsorption-regeneration cycles

Cycle	Uptake capacity mg I^-/g HTc	Adsorbed I^- %
1	392.2	57
2	383.1	52
3	213.3	30

T = 303 K; [I^-] = 3000 ppm; [31C-c] = 4.5 g/L

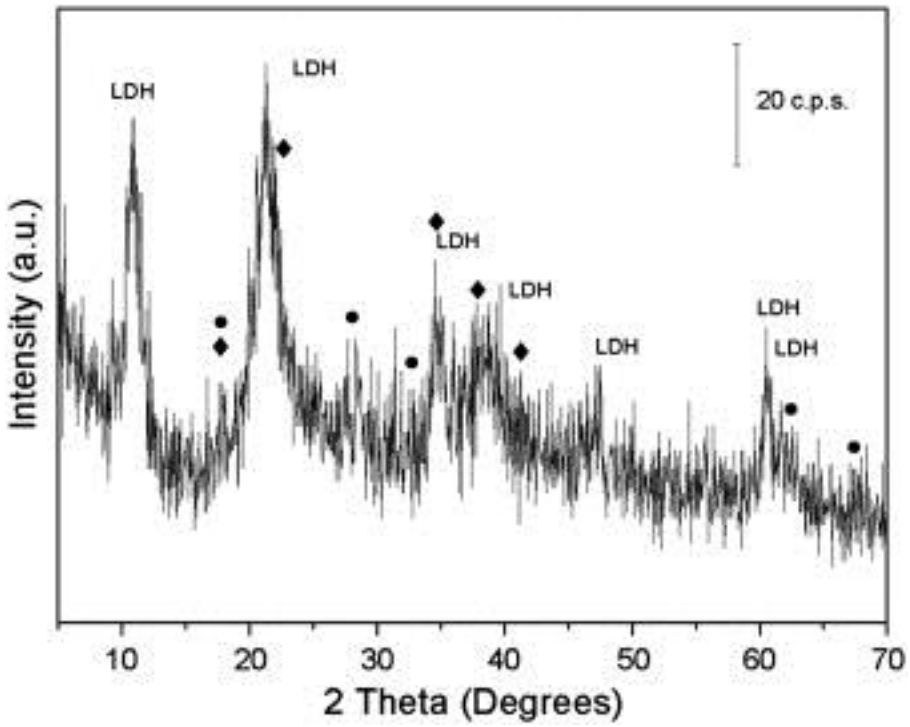

Figure 3-11 – PXRD of sample 31C-I after three cycles of adsorption. (●) represents reflections by a MgAl oxide phase and (♦) represents reflections by a AlO(OH) phase.

3.3. LDHs as storage materials

As abovementioned, there are some few examples in the literature on the use of LDHs as storage materials for wastes from nuclear industry. In this section it is presented the synthesis and deep characterization of several iodine containing LDHs with the following compositions: Mg_3Al-IO_3, $Ca_{1.5}Mg_{1.5}Al$-IO_3, Ca_3Fe-IO_3, $Ca_{1.5}Mg_{1.5}Fe$-IO_3, Mg_3Fe-IO_3, Mg_3Al-I, and $Ca_{1.5}Mg_{1.5}Al$-I.

Our objective was to study the applicability of different LDHs as matrices for the long-term storage of radioactive iodine and identify the different factors influencing on the viability of its applicability in nuclear repositories. For that, different synthesis methods, such as coprecipitation, anionic exchange and reconstruction were applied to study the differences in the iodine incorporation mechanisms (if any) and to exam the method that leads to the highest incorporation of either iodide or iodate into the LDH. The local structure environment of incorporated iodine was studied using the I K X-ray absorption edge by EXAFS spectroscopy. Both, the thermal stability and resistance to leaching with MilliQ water and brine were studied as important parameters affecting the applicability and feasibility of proposed LDH matrices for the long-term storage of radioactive iodine.

In addition, the simultaneous adsorption of Cs and I was also studied using two calcined Mg_3Al-CO_3 LDH. ^{137}Cs and ^{129}I are volatile fission products[265]. Iodine radioisotopes (^{131}I and ^{129}I, principally) are volatile at elevated temperatures, and in an accident situation in which the fuel overheats and the cladding fails, the iodine may be released to air as happened in Chernobyl[266,267] and Fukushima[268,269] nuclear accidents and subsequently be breathed in or deposited on vegetation; Cs is also volatile at elevated temperatures (temperatures higher than those at which iodine is volatile), and the radioisotope ^{137}Cs may get released under accident situations like in Chernobyl[266,267] or Fukushima[268,269]. In the work presented in this section,

LDHs are studied as a possible matrix to retain both ions from a solution using a single adsorbent material.

3.3.1. Synthesis of LDHs

3.3.1.1. Materials

MilliQ water (18 MΩ·cm) was used for preparation of all solutions. Magnesium nitrate hexahydrate ($Mg(NO_3)_2 \cdot 6H_2O$, Merck, 99.99%), calcium nitrate tetrahydrate ($Ca(NO_3)_2 \cdot 4H_2O$, Merck, ACS), aluminum nitrate nonahydrate ($Al(NO_3)_3 \cdot 9H_2O$, Merck, 98.5% and Sigma Aldrich, 98%), iron nitrate nonahydrate ($Fe(NO_3)_3 \cdot 9H_2O$, Merck, ACS), sodium hydroxide (NaOH, Merck, 99%), sodium carbonate (Na_2CO_3, Fluka, 99.5%), potassium iodate (KIO_3, Sigma Aldrich, 98%), potassium iodide (KI, Aldrich, 99%), sodium sulphate decahydrate ($Na_2SO_4 \cdot 10H_2O$, Fluka, 99%), magnesium chloride hexahydrate ($MgCl_2 \cdot 6H_2O$, Merck, 99%), and nitric acid (HNO_3, Merck, 99.0%) were used for the synthesis of the LDHs, Table 3-8.

3.3.1.2. Synthesis by coprecipitation

MgAl LDHs were synthesized by adopting the method described elsewhere[270]. An aqueous solution containing $Mg(NO_3)_2 \cdot 6H_2O$ and $Al(NO_3)_3 \cdot 9H_2O$ was dropwise added into a solution of either KIO_3 or KI under vigorous stirring. The pH was maintained at around 12 by the addition of a 5 M NaOH solution. The amounts of iodate or iodide were two times stoichiometrically in excess in order to increase iodine incorporation. Solution was stirred overnight. The synthesized LDH powders were separated from the reaction solution by filtration and washed five times with ca. 200 mL of MilliQ water. All synthesized LDHs were dried in the oven at 333 K overnight. Samples were labeled according to their composition ($M(II)_nM(III)_m$-X), tables 3-8 and 3-9.

3.3.1.3. Synthesis by anionic exchange

$Ca_{1.5}Mg_{1.5}Al–C_6H_5COO$ LDH (**16**) was synthesized under nitrogen gas flow as described above. For iodine incorporation via anionic exchange, 5.0 g of **16** were placed in contact with 0.12 M KIO_3 or 0.12 M KI solutions, respectively during 10 days under stirring. The iodine/benzoate ratio was two to favor iodine incorporation. The amount of incorporated I^- or IO_3^- was determined by ionic chromatography (IC), table 3-10.

3.3.1.4. Synthesis by reconstruction

To study the iodine incorporation by reconstruction, Mg_3Al-CO_3 LDH (**15**) was synthetized as described above. An alkaline solution of 0.38 M Na_2CO_3 was used to reach the maximum carbonate quantity in the interlayer space. This material was calcined at 723 K during five hours, and after that stored in inert atmosphere. To find the maximum of iodide or iodate incorporation by reconstruction, 0.1 g of obtained LDH **15** were placed in contact with a series of iodide or iodate solutions from 50 to 3000 ppm during ca. one week, Table 3-11, Figures 3-13 and 3-14.

3.3.1.5. Heating experiment

Thermal stability of the synthesized iodide and iodate containing samples (**1** – **6**) was analyzed by heating materials at 453 K during 17 hours. The amount of iodine in LDHs after thermal treatment was determined by digesting samples in the concentrated HNO_3 and measuring with IC, while structural changes were studied by PXRD, Table 3-14.

3.3.1.6. Leaching experiment

Leaching experiments were carried out with two samples, Mg_3Al-IO_3 (**1**) and Ca_3Fe-IO_3 (**5**), in MilliQ water and brine (0.1 M Na_2SO_4 and 1 M $MgCl_2$) at different contact time, Figure 3-16. Modified Q-brine composition was chosen as an example of possible ions present in the Asse salt mine (Lower Saxony, Germany), which is used as a test site for a deep underground radioactive waste repository[271]. For that purpose 0.5 g of samples **1** and **5** were placed in

contact with MilliQ water or brine solution under stirring in closed glass bottles. After the corresponding contact time, an aliquot of the solution was measured by IC for iodine content.

3.3.1.7. Simultaneous adsorption of cesium and iodide

Cs^+ and I^- adsorption experiments were carried out with two previously calcined samples as precursors. Mg_3Al-CO_3 samples (**15** and **17**), differenced by the use of Na_2CO_3 during the synthesis of LDH **15**, previously described, and the lack of it during the obtaining of LDH **17**. The precursors were calcined at 723 K during five hours, and after that stored in inert atmosphere. Typically, 10.00 g of each sample was in contact with 0.1 L of a $7.5 \cdot 10^{-2}$ M CsI solution for 1 hour. After this, a part of the samples was calcined at 723 K f 5 hours in static air. The solid samples were dissolved in HNO_3 and analyzed by ICP-OES to determine iodine and cesium incorporation.

3.3.2. Results and discussion

3.3.2.1. Adsorption by coprecipitation

Samples **1** – **9**, **16a, 16b** and **17** (Table 3-8) were prepared by coprecipitation, incorporating iodine directly during synthesis. The corresponding reference materials with nitrate in the interlayer space (Samples **9 – 14**, **16**) were also synthesized. The ICP-OES analyses of samples **1** and **3** showed that the Mg/Al molar ratios presented in the solid are similar to those of the starting parent solutions, i.e. 3/1, and that both iodate and iodide were incorporated into these materials in the amounts showed in Table 3-9. In table, it can be seen that ternary materials prepared with Ca and Mg as divalent cations present a Mg/M(III) molar ratio slightly higher than expected. In these cases, the trivalent cation could not be fully incorporated into the materials' structure(s) during the coprecipitation, which will explain the higher Mg/M(III) molar ratios found in solid samples regarding to the initial molar ratios in the parent solutions. Samples **5** and **6** showed lower M(II)/M(III) ratios due to a low Ca^{2+} incorporation, as also occur in reference nitrate

materials (samples **10-14**). Comparing the reference samples, the calcium amount is especially low in sample **11**. The low calcium amounts found in all the calcium-containing samples may be related, first, with the higher size of Ca^{2+} (with an ionic radius equal to 0.98 Å) which is rather large for octahedral coordination in the holes of brucite-like layers, compared to Mg^{2+} (with an ionic radius equal to 0.65 Å). Second, with the solubility of $Ca(OH)_2$ (K_{sp}=5.02·10^{-6} mol/L), higher than the solubility of the corresponding hydroxides of Mg, Fe or Al, and due to the washing of the materials the calcium was eliminated from the solids[272].

Table 3-8 – Synthesis conditions of LDH prepared by coprecipitation from alkaline aqueous solution at 23°C and pH ≈ 10 – 12.

N	Sample name	M(II)	M(III)	M(II)/M(III)	Guest
1	Mg_3Al-IO_3	Mg	Al	3/1	IO_3^-
2	$Ca_{1.5}Mg_{1.5}Al$-IO_3	Ca, Mg		1.5/1.5/1	
3	Mg_3Al-I	Mg		3/1	I^-
4	$Ca_{1.5}Mg_{1.5}Al$-I	Ca, Mg		1.5/1.5/1	
5	Ca_3Fe-IO_3	Ca	Fe	3/1	IO_3^-
6	$Ca_{1.5}Mg_{1.5}Fe$-IO_3	Ca, Mg		1.5/1.5/1	
7	Mg_3Fe-IO_3	Mg		3/1	
8	Ca_3Fe-I	Ca	Fe	3/1	I^-
9	$Ca_{1.5}Mg_{1.5}Fe$-I	Ca, Mg		1.5/1.5/1	
10	Mg_3Al-NO_3	Mg	Al	3/1	NO_3^-
11	$Ca_{1.5}Mg_{1.5}Al$-NO_3	Ca, Mg		1.5/1.5/1	
12	Ca_3Fe-NO_3	Ca	Fe	3/1	
13	$Ca_{1.5}Mg_{1.5}Fe$-NO_3	Ca, Mg		1.5/1.5/1	
14	Mg_3Fe-NO_3	Mg		3/1	
15	Mg_3Al-CO_3	Mg	Al	3/1	CO_3^{2-}
15a	Mg_3Al-IO_3	Mg	Al	3/1	IO_3^-
15b	Mg_3Al-I	Mg	Al	3/1	I^-
16	$Ca_{1.5}Mg_{1.5}Al$- C_6H_5COO	Ca, Mg	Al	1.5/1.5/1	$C_6H_5COO^-$
16a	$Ca_{1.5}Mg_{1.5}Al$-IO_3	Ca, Mg	Al	1.5/1.5/1	IO_3^-
16b	$Ca_{1.5}Mg_{1.5}Al$-I	Ca, Mg	Al	1.5/1.5/1	I^-
15c	Mg_3Al-I	Mg	Al	3/1	I^-, Cs^+
17	Mg_3Al-CO_3	Mg	Al	3/1	CO_3^{2-}
17a	Mg_3Al-CO_3	Mg	Al	3/1	I^-, Cs^+

Table 3-9 – Stoichiometries of LDH determined by ICP-OES

N	ratio M(II)/M(III)	I in sample[1] g/g	Empirical formula	I in the sample % in mass
1	2.91	0.1610	$[Mg_{2.90}Al(OH)_{n/a}](IO_3)_{0.50}$	16.1
2	2.21	0.2000	$[Ca_{0.47}Mg_{1.75}Al(OH)_{n/a}](IO_3)_{0.83}$	20.0
3	2.95	0.0280	$[Mg_{2.95}Al(OH)_{n/a}]I_{0.08}$	2.8
4	1.51	0.0096	$[Ca_{0.01}Mg_{1.51}Al(OH)_{n/a}]I_{0.02}$	1.0
5	0.81	0.2118	$[Ca_{0.81}Fe(OH)_{n/a}](IO_3)_{0.82}$	21.2
6	2.44	0.1704	$[Ca_{0.65}Mg_{1.79}Fe(OH)_{n/a}](IO_3)_{0.88}$	17.0
7	2.26	0.2283	$[Mg_{2.26}Fe(OH)_{n/a}](IO_3)_{0.61}$	22.8
8	n/a	n/a	n/a	n/a
9	1.76	0.0140	$[Ca_{0.06}Mg_{1.70}Fe(OH)_{n/a}]I_{0.04}$	1.4
10	2.94	0	$[Mg_{2.94}Al(OH)_{n/a}](NO_3)_{n/a}$	0
11	1.55	0	$[Ca_{0.02}Mg_{1.53}Al(OH)_{n/a}](NO_3)_{n/a}$	0
12	n/a	n/a	n/a	n/a
13	2.55	0	$[Ca_{1.04}Mg_{1.52}Fe(OH)_{n/a}](NO_3)_{n/a}$	0
14	2.40	0	$[Mg_{2.40}Fe(OH)_{n/a}](NO_3)_{n/a}$	0

[1] in the form of either iodide or iodate

All samples showed higher iodate uptake when compared to iodide adsorption. For instance, we have found an uptake of 0.2283 g of IO_3^- per gram of material (sample **7**) in the case of iodate *vs.* 0.028 g I^- g^{-1} material in the case of iodide (sample **3**), Table 3-10.

Comparing the I/M(III) ratios in analogous samples (i.e. Mg_3Al-IO_3 (**1**) and Mg_3Al-I (**3**)) it was found that sample **1** incorporated about 6 times more iodine than **3**, confirming that incorporation of iodate was higher than incorporation of iodide, as previously found by other authors[273]. Ca/Mg/Al ratios in $Ca_{1.5}Mg_{1.5}$Al-IO_3 (**2**) and $Ca_{1.5}Mg_{1.5}$Al-I (**4**) showed marked deviations from their theoretical ratios, Table 3-9.

PXRD analysis of sample **4** showed absence of phases with calcium and the typical reflections of hydrotalcite and gibbsite (represented in Figure 3-12, summary of phases presented in Table 3-10). In case of $Ca_3Fe\text{-}IO_3$ (**5**) and $Ca_{1.5}Mg_{1.5}Fe\text{-}IO_3$ (**6**) samples, high iodine incorporation was reached and their PXRD diffractograms of **5** and **6** showed no insights of (003) and (006) reflections, which would be indicative of the formation of the LDH structure. However, bruggenite $Ca(IO_3)_2\cdot(H_2O)$ was identified in both samples and, additionally, calcium iodate hydrate was identified in sample **6**. X-ray diffractograms of samples **1**, **3, 4** and **9** showed that these samples presented a LDH structure with a poor crystallinity, specially samples **1** and **9** (Figure 3-12). Sample **4** showed also reflections that corresponds to gibbsite, $Al(OH)_3$. The presence of bruggenite, in samples **2**, **5** and **6**, suggest that, in the typical used synthesis conditions, the LDH formation was hindered through precipitation of the iodate phase. Hence, LDH precipitation is not produced when iodate and calcium are present in the parent solution simultaneously. This also occurs in the case of $Ca_3Fe\text{-}I$ (**8**), where PXRD analysis revealed a very amorphous material with some small reflections corresponding to iron and calcium phases (goethite and calcite, respectively) and iodide oxide.

Table 3-10 – Diffractogram analysis of samples from coprecipitation.

Sample	JCPDS Phase	Name of the phase	Symbol
1	89-0460	Hydrotalcite (displaced)	◇
2	76-2134	Bruggenite, syn	o
	88-1356	Calcium iodate hydrate	+
3	89-0460	Hydrotalcite (displaced)	◇
4	89-0460	Hydrotalcite (displaced)	◇
	07-0324	Gibbsite	Δ
5	76-2134	Bruggenite, syn	o
6	76-2134	Bruggenite, syn	o
	88-1356	Calcium iodate hydrate	+
7	89-0460	Hydrotalcite (displaced)	◇
8	72-1937	Calcite	×
	81-0464	Goethite, syn	✱
	52-0319	Iodine oxide	‖
9	89-0460	Hydrotalcite (displaced)	◇

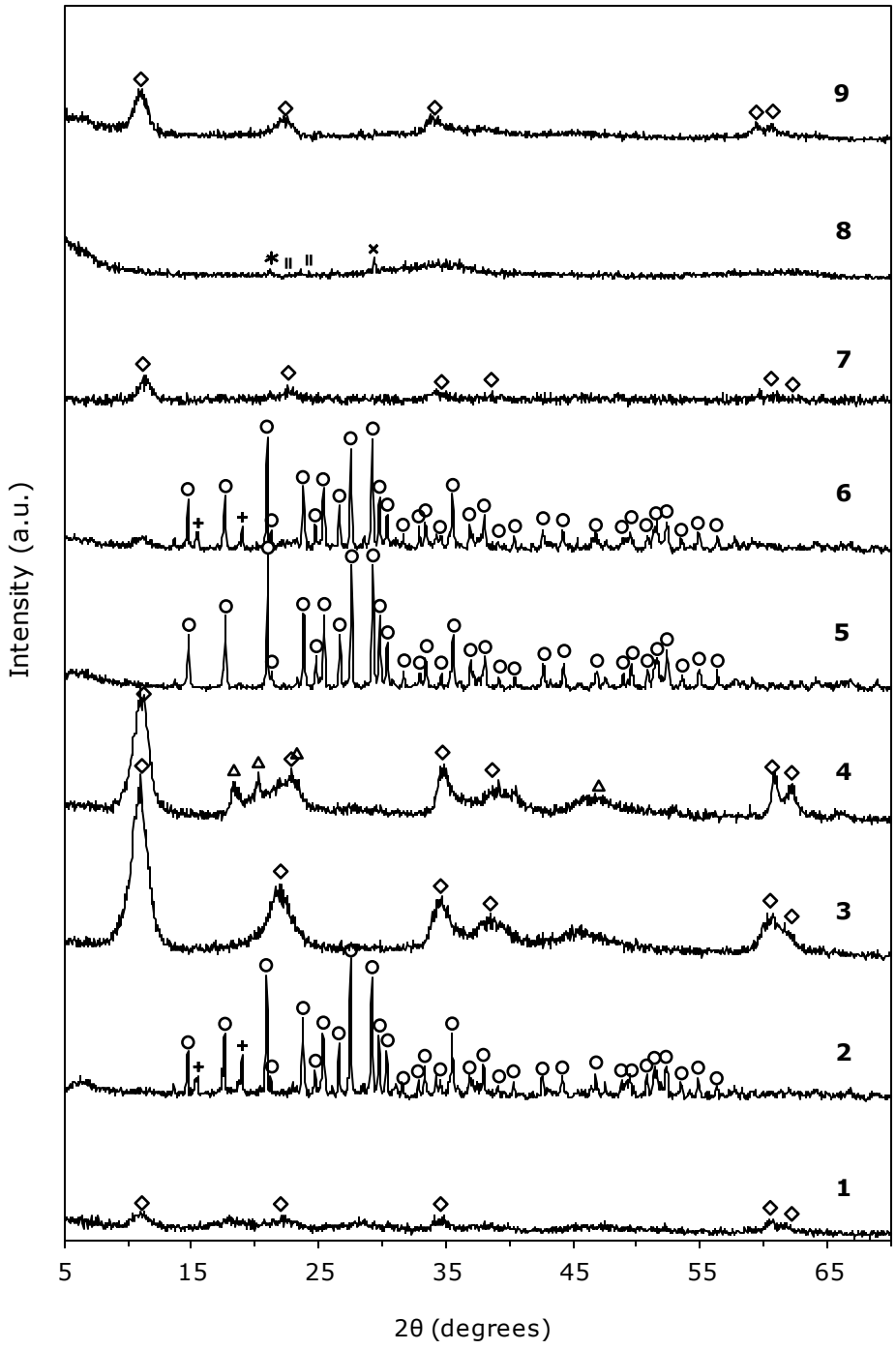

Figure 3-12 – XRD diffractograms of the synthesized samples.

3.3.2.2. Adsorption by anionic exchange

Anionic exchange implies that a less strongly bounded bulky anion is exchanged for another anion, having higher selectivity to LDH. Benzoate was chosen as exchangeable anion due to its large size and relatively weak interaction within LDH interlayer space. The evolution of the basal spacing with chosen intercalated anions is increasing from ~7.6 Å for hydroxide to ~15 Å for benzoate, following the sequence $OH^- < I^- < IO_3^- < C_6H_5COO^-$ [143]. It is accepted that X-ray diffractograms show no more regular long-range ordering of the layers when basal spacing is higher than 11 Å[143]. The results of exchanging benzoate by iodide or iodate anions are showed in Table 3-11. Higher incorporation of iodate *vs.* iodide, was obtained (0.322 g for IO_3^- and 0.202 g for I^- per gram of sample, respectively). A favoring exchange towards iodate is most probably due to the difference in size and charge density of the anions (iodate has pyramidal structure[274] with an anionic radius of 181 pm; iodide diameter is 412 pm[275,276]), as well as the ability of iodate to form hydrogen bonds with hydroxide groups and water molecules in the interlayer space of LDH. According to Miyata, the ion selectivity of monovalent anions is in the order $OH^- > F^- > Cl^- > Br^- > NO_3^- > I^-$, and supports low iodide selectivity[137].

Table 3-11 – Results of anionic exchange of 5 g of sample 16 with IO_3^- and I^- after 10 days

Anion	Initial anion mass	Mass incorporated in sample	Weight in sample
	g	g	%
IO_3^-	5.0689	1.2322	20
I^-	3.6779	0.6554	12

3.3.2.3. Adsorption by reconstruction

A series of solutions with different concentrations of iodate and iodide were prepared to study the maximum uptake of iodate or iodide by sample **15** through reconstruction of calcined $Mg_3Al\text{-}CO_3$ LDH, Table 3-12. In both cases iodate/iodide uptake depends on the initial concentration of the anion in

solution. Iodate adsorption increased steadily in the studied concentration range reaching a maximum value of 1.165 g of iodate per 1 g of initial LDH, whereas iodide adsorption was 0.439 g per 1 g of LDH at the same conditions (Table 3-12). These results were analyzed with the help of Langmuir and Freundlich isotherm models to obtain the best fitting isotherm. These two models are the most common isotherms to describe the solid-liquid adsorption system. Below it is displayed the adsorption isotherms of both iodide and iodate on sample **15** (Figure 3-13).

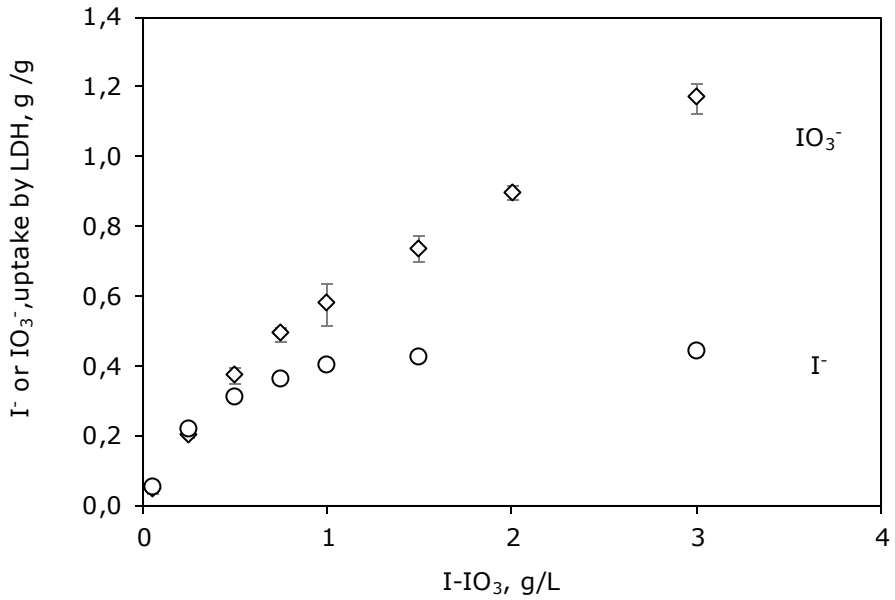

Figure 3-13 – Adsorption isotherms of iodate and iodide anions adsorbed onto LDH.

A)

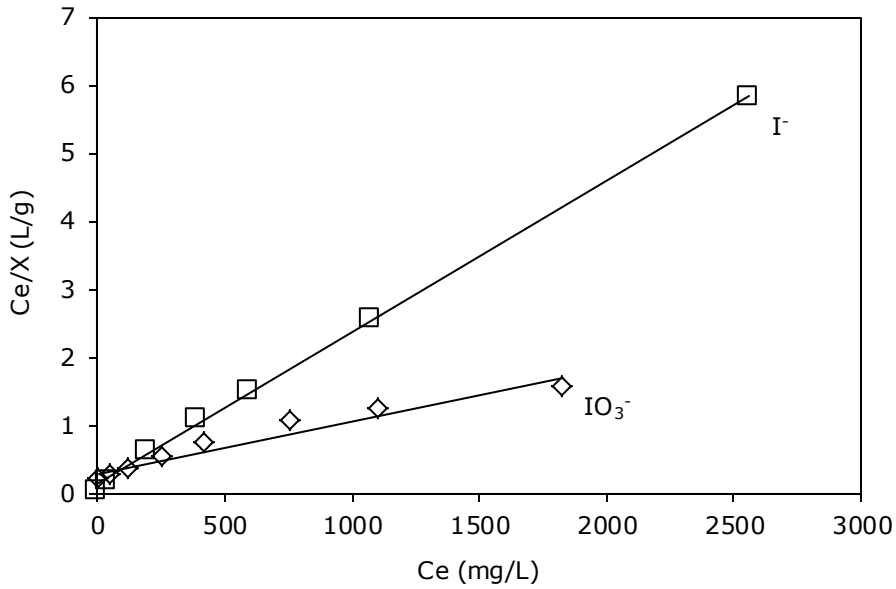

B)

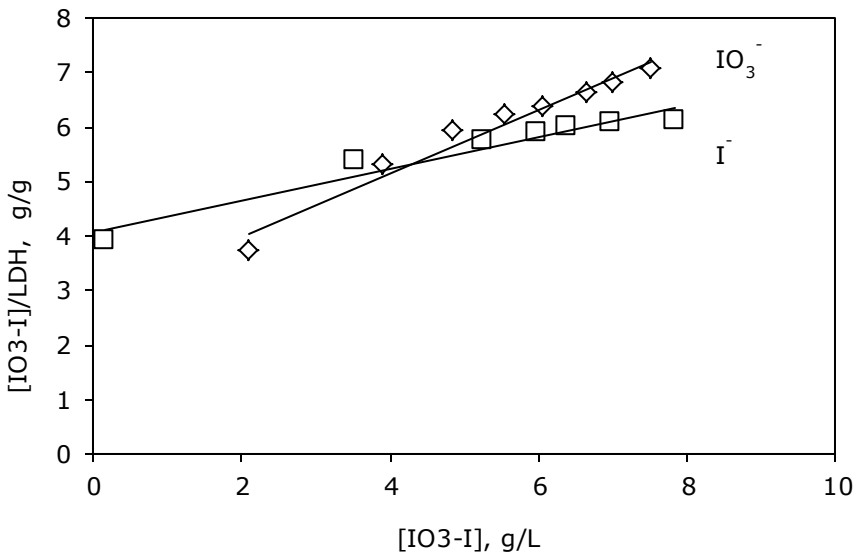

Figure 3-14 – a) Langmuir linear regression, eq. (3), where the slope = $1/Q_m$ and the intercept = $1/(K_L \cdot Q_m)$; b) Freundlich linear regression, eq. (6), where slope is 1/n and intercept is $\ln K_F$.

Table 3-12 – The results of adsorption experiments of IO_3^- or I^- onto sample 15. Results from IC waters analysis.

Entry	Initial X^- g/L	Final IO_3^- g/L	I in mass for IO_3^- g/g	Final I^- g/L	I in mass for I^- g/g
1	3.000	1.826	1.165	2.559	0.439
2	2.000	1.102	0.895	n/a	n/a
3	1.500	0.763	0.733	1.076	0.423
4	1.000	0.424	0.574	0.596	0.402
5	0.750	0.259	0.489	0.392	0.357
6	0.500	0.126	0.372	0.192	0.307
7	0.250	0.049	0.199	0.034	0.214
8	0.050	0.008	0.042	0.001	0.049

The experimental results were fitted into the Langmuir equation with a confidence limit of 99.89% in the case of iodide and 95.10% in the case of iodate (Figure 3-14 and Table 3-13). The Langmuir equilibrium constants were found to be 383.13 L/g and 58.65 L/g for iodate and iodide, respectively. Despite Langmuir isotherm model has extensively been used to describe the solid-liquid adsorption system, it has been observed that Langmuir equation does not provide the best fitting isotherm for the case of iodate adsorption, obtaining a correlation coefficient of 0.95. In addition, the shape of the isotherm (Figure 3-13) seems to suggest that the adsorption is not produced as a single monolayer over the adsorbate, since the adsorption limit (plateau) is not achieved. Such a shape rather looks like a Freundlich system, where the isotherm does not present a clear limit of adsorption, i.e., the plateau is not reached. Calculus showed that this system was better fitted to a Freundlich adsorption model with a correlation coefficient of 0.97 (Table 3-13).

The free Gibbs energy (ΔG^0) was calculated using equation 3-5. The higher K_L and lower ΔG^0 values obtained for iodate indicate its higher affinity for the LDH.

$$\Delta G^0 = -RT\ln(K_L) \qquad \text{(Eq. 3-5)}$$

where R is the universal gas constant, T is the temperature (K) and K_L is the Langmuir equilibrium constant. The calculated free Gibbs energy values are $\Delta G^0 = -147.79$ kJ/mol and $\Delta G^0 = -101.16$ kJ/mol for iodate and iodide, respectively. The negative values of the calculated free Gibbs energy indicate that the adsorption process takes place spontaneously under the experimental conditions.

Table 3-13 – Langmuir and Freundlich isotherm parameters for adsorption of iodated or iodide on calcined MgAl hydrotalcites.

Adsorbent, anion	Langmuir				Freundlich		
	Q_m g I^-/g $_{HTc}$	K_L	R^2	ΔG^0 kJ/mol	K_F	n	R^2
Mg_3Al, IO_3	1.165	383.13	0.951	-147.79	16.55	1.71	0.965
Mg_3Al, I	0.439	58.65	0.999	-101.16	57.97	3.41	0.938

3.3.2.4. Heating experiment

The results of thermal stability experiments with samples **1 – 7** are showed in Table 3-14. ICP-OES was used to measure the iodine released from the digested samples after the calcination treatment. The iodine loss found (i.e. either iodide or iodate) was between the 64 – 90% range after heating the samples at 453 K for 17 h.

Ca_3Fe-IO_3 (**5**) showed the lowest iodine release (iodate) with a total mass loss of about 17%. In spite of that, only a 36% of the initially incorporated iodate remained in the sample after heating.

In general, the experiments showed that incorporated iodate and iodide are easily removed from the adsorbent when they are submitted to a soft thermal treatment. This indicates that both iodate and iodide are rather poorly bounded in the interlayer space through hydrogen bonds and van der Waals' interactions and both are released to a high extent at relatively low temperature.

Table 3-14 – The results of heating experiments at 453 K for 17h in static.

Sample	Mass loss	IO_3/I initial	IO_3/I remaining in sample	I that remains after heating
	%	% in mass	% in mass	%
1	10	16.13	3.95	23
2	15	21.00	5.84	28
3	13	2.94	0.64	20
4	13	1.04	n/a	n/a
5	17	21.18	7.54	36
6	16	17.38	5.06	29
7	13	22.85	5.51	24

Table 3-15 – Diffractogram analysis of samples from heating experiments at 453 K for 17h in static air.

Sample	JCPDS Phase	Name of the phase
1-H453	-	-
2-H453	076-2134	Bruggenite, syn
	28-0221	Lautarite, syn
3-H453	89-0460	Hydrotalcite (displaced)
4-H453	89-0460	Hydrotalcite (displaced)
5-H453	76-2134	Bruggenite, syn
6-H453	76-2134	Bruggenite, syn
7-H453	89-0460	Hydrotalcite (displaced)

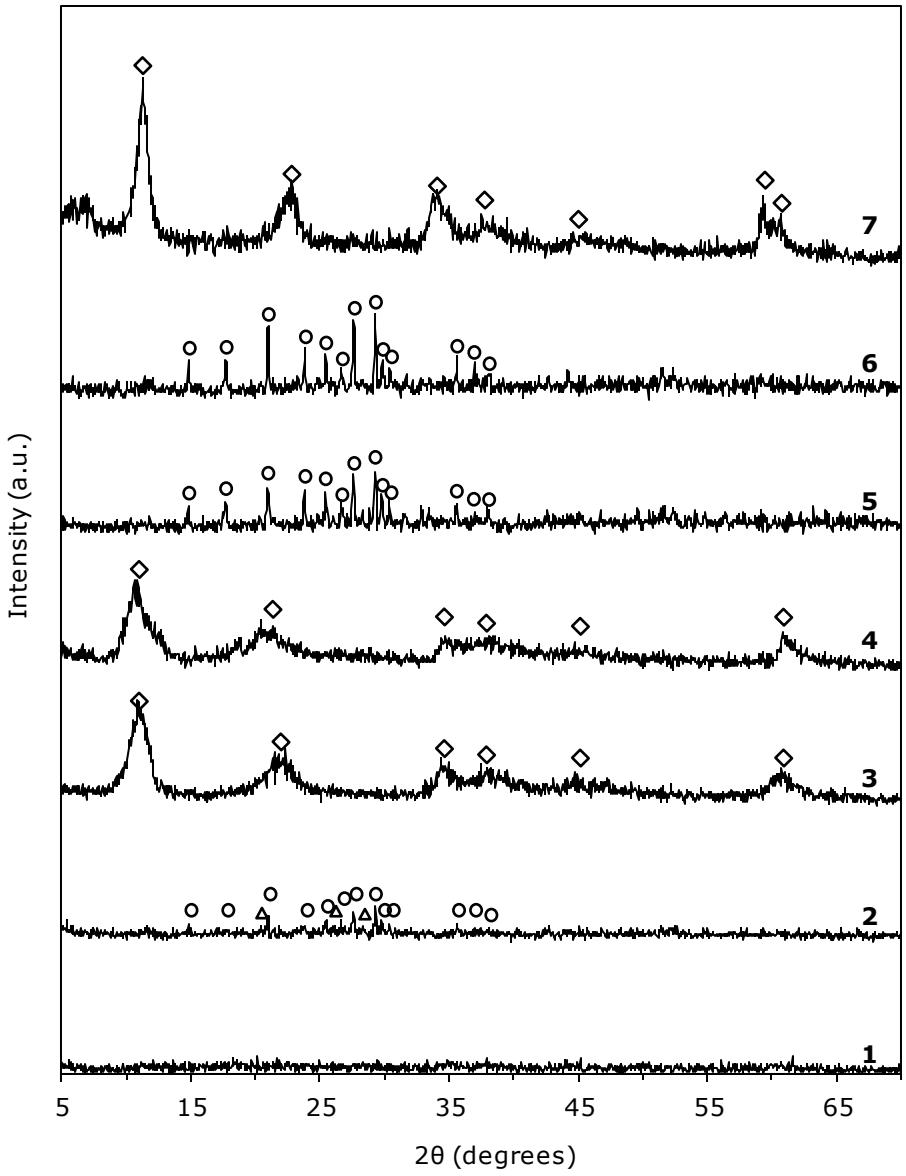

Figure 3-15 – Diffractograms of samples after heating at 453K. Simbols: ◇, hydrotalcite; ○, bruggenite; △, lautarite.

3.3.2.5. Leaching experiment

Leaching tests with sample **1** were performed in two aqueous media: milliQ water and brine (0.1 M Na_2SO_4 and 1 M $MgCl_2$). The results of leaching experiments showed that the iodate release is significantly faster in brine than in MilliQ water, which could be explained by the substitution of iodate with chloride ions present in the brine solution. After ca. 14 days in MilliQ water, about 60% of iodate was resealed to the aqueous medium, meanwhile in brine solution the leaching ups to 94% after one day. After 31 days in MilliQ, only 10% of iodate was still incorporated in the sample, Figure 3-16.

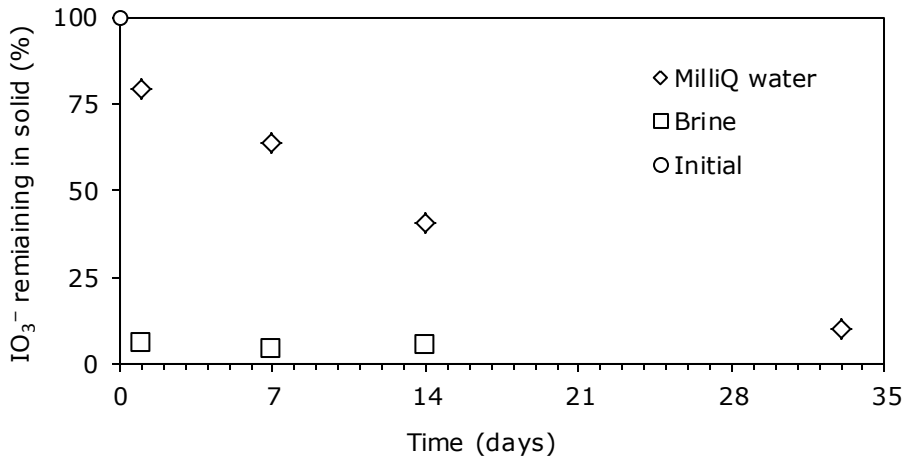

Figure 3-16 – Leaching experiments of sample 1 with MilliQ water. Circle: initial concentration; square: results in brine solution; diamonds: results in milliQ water.

3.3.2.6. Simultaneous adsorption of Cs and I

Results of ICP-OES analysis of the samples are shown in Table 3-16. Both samples presented iodide incorporation, being this higher for sample **17** (synthetized without sodium carbonate). On the contrary, cesium had a very low incorporation in both samples, demonstrating that the incorporation capacity of cations to the LDH is very low, as expected, with a significant difference respect to the amount of adsorbed iodide, meaning this that these ions are adsorbed separately. Major iodide adsorption in sample **17a** compared with **16c** adsorption capacity seems to be influenced by the sodium carbonate used during coprecipitation of the later. Cross *et al.*[277] have reported

that residual sodium (from Na_2CO_3 in this case) in LDHs is difficult to remove and make the basicity of the LDH stronger, affecting to the iodide adsorption, a weak base.

Due to these results, calcined LDH does not seem to be suitable materials for simultaneous adsorption of I^- and Cs^+.

Table 3-16 - ICP-OES results of CsI adsorption.

Sample	I	Cs
	g/g	g/g
16c	$6.86 \cdot 10^{-3}$	$9.00 \cdot 10^{-6}$
16c_c	$7.65 \cdot 10^{-3}$	$9.00 \cdot 10^{-6}$
17a	$1.38 \cdot 10^{-1}$	$1.00 \cdot 10^{-5}$
17c_c	$3.22 \cdot 10^{-2}$	$9.00 \cdot 10^{-6}$

3.3.2.7. EXAFS at the iodine K-edge

In order to investigate local structure environment around the incorporated iodide and iodate into LDH, EXAFS measurements were performed using the iodine K X-ray absorption edge. These studies will help to the understanding of the iodide/iodate uptake and release mechanisms of the adsorbent materials.

The data treatment is done using EXAFSPAK program. First was performed a polynomial pre-edge subtraction that consists in the removal of the background signal to isolate an X-ray absorption spectrum for the absorbing atom alone (iodine).

The next step is a spline subtraction – a stiff but flexible curve of several polynomials mathematically knotted together – to fit EXAFS region of the raw data.

Normalization is used to put the EXAFS on a proper amplitude scale. The difference between this extrapolation and the background-corrected spectrum at the edge is the step height or edge step. This step is proportional to the total amount of the absorbing element in the sample. The data are then divided by the size of the edge step, to normalize the EXAFS to a unit edge, which compensates for uncertainties in the concentration and sample thickness.

Extraction and the k3-weighting of the EXAFS function was made to change from energy scale in eV to wave number scale in $Å^{-1}$.

Fourier transform (FT) resulting in a pseudo-radial distribution function which changes scale from the wavenumber to distance between the atoms but not corrected for a phase shift, which is usually 0.5 Å.

FT provides the peaks corresponding to the distances between the absorbing atoms (iodine) to the near neighbors. Using the KIO_3 crystallographic structure provided by the crystal structure database (ICSD) as the reference, the distances are fitted.

The EXAFS spectra of all iodate-LDH samples and the reference potassium iodate showed the presence of white line, whereas all iodide-LDH samples and the reference potassium iodide did not, as can be seen in Figure 3-17. This indicates that there were no oxidation state changes during EXAFS data collection; therefore, iodate -or iodide-LDH samples could be distinguished. The Fourier transform, FT, of the iodate containing samples (**1**, **5** and **15a**) showed only single I–O scattering path, whereas potassium iodate reference has more complex structure with several scattering paths (Figure 3-18).

The Debye-Waller factor shows how well defined the distance is, i.e. the smaller it is the less is bond distance distribution, meaning that a good fitting has been obtained and, hence we have a well-define bond for the studied systems. The I – O distance of ca. 1.8 Å with fairly low Debye-Waller factor was found for all the measured LDH samples, as well as KIO_3 reference,

indicating low bond distance distribution, Table 3-17. In addition, long range interactions of ~3.7 Å were also found in samples **1** and **15a**, most probably indicating an I•••O distance to hydroxide groups or water molecules present in the interlayer space. This agrees with findings of Aimoz *et al.*[227], who found a I–O distance of ~3.6 Å to interlayer water molecules and hydroxide groups in iodide containing MgAl and ZnAl LDHs. However, the easy removal of both iodate and iodide species from the samples at fairly low temperatures, mostly suggests an interaction with the interlayer water molecules rather than with the hydroxyl groups of the layers, since crystalline water it is removed in the 373-373 K range, whereas OH^- groups are removed at higher temperatures.

Sample **1** was synthesized by coprecipitation, while sample **15a** was obtained by reconstruction of the calcined carbonate sample **15**. However, the oscillations of EXAFS function and the peak positions in Fourier transforms for these samples are very similar, indicating that the mechanism of iodate incorporation into interlayer space of LDH does not depend on the synthesis method.

Table 3-17 – Mean bond distances, d $Å^{-1}$, number of distances, N, and Debye-Waller, σ^2, factors in the EXAFS studies of iodate containing LDH

Sample	Interaction	N	d, $Å^{-1}$	σ^2
KIO_3 ref	I – O	4	1.821±0.024	0.00056
	I – O2	2	2.193±0.139	0.01932
	I···O	6	4.345±0.062	0.0038
	I···I	6	3.926±0.085	0.00724
1	I – O	3	1.812±0.028	0.00078
	I···O	1	3.719±0.053	0.00285
5	I – O	3	1.822±0.028	0.00076
15a	I – O	3	1.823±0.031	0.00096
	I···O	1	3.773±0.062	0.00384

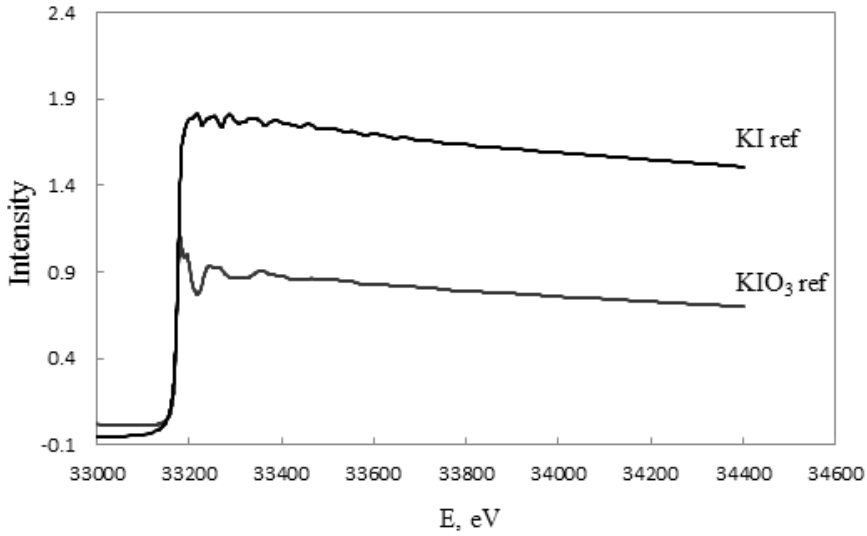

Figure 3-17 – EXAFS spectra of potassium iodide and iodate references

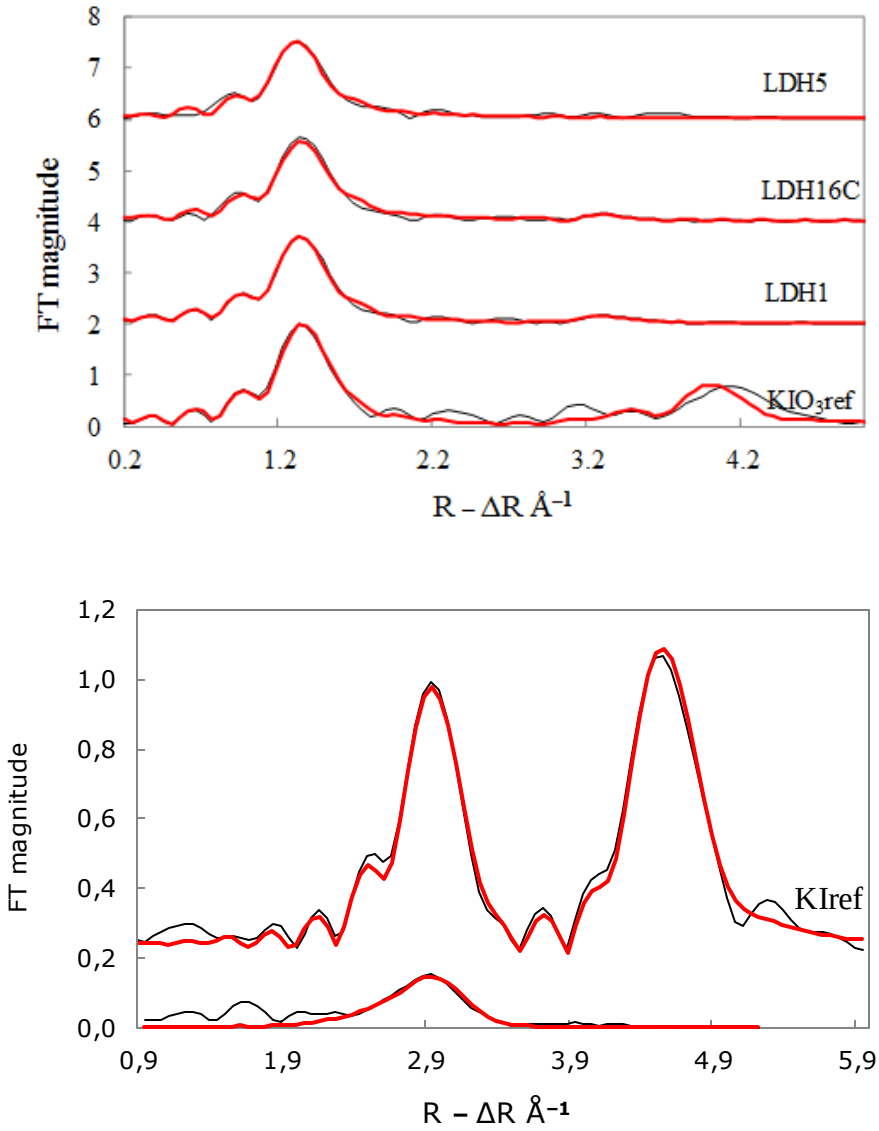

Figure 3-18 – Fourier transforms of iodate (IO_3^-, fig 5a) and iodide (I^-, fig 5b) containing LDHs and potassium iodate reference. Red line – model, black line – experimental. The IO_3^- FT data are offset by +2.

The wonderful thing about science is that it's alive

Richard Feynman

4. General conclusions

UNIVERSITAT ROVIRA I VIRGILI
ON THE USE OF LAYERED DOUBLE HYDROXIDES IN THE MANAGEMENT OF 129I FROM LIQUID NUCLEAR WASTES
Luis Iglesias Pérez
Dipòsit Legal: T 893-2015

4.1. LDH as adsorbent materials

Mg–Al mixed oxides derived from LDHs were used as adsorbents for removing and sequestering iodide anions in water solutions. The experiments were conducted in two different ways. On the one hand, the adsorption of I^- was done by reconstructing the mixed oxide with the aqueous iodide under mechanical stirring, while on the other; the use of ultrasound was applied during the first stage of the adsorption to enhance the uptake capacities of the adsorbents.

The uptake capacity of the different samples was dependent on their Mg/Al molar ratio, and thus samples with an Mg/Al molar ratio of around 3 presented larger adsorption capacities. Magnesium hydroxide (brucite) has not shown adsorption capacity; thus, indicating that iodine was removed from solution by incorporation into the LDHs interlayer space and any other interaction between iodine anions and the adsorbent LDH solid can be discarded. A dependence on the guest anion forming the parent LDH was also observed, and the mixed oxides derived from carbonated LDH presented higher adsorption capacities than those derived from nitrated LDH. This was attributed to the higher surface area of the former, which allows an easier incorporation of the anions to reconstruct the layered structure.

The use of ultrasound resulted in an increase in the adsorption capacity of the samples by a factor of 2 compared to the non-ultrasonicated samples, showing that both the diffusion of the iodide anions and mass transfer were boosted more strongly by this technique, leading to a more efficient process for water remediation.

We have demonstrated that these materials present an acceptable stability in neutral and acidic conditions, and a minimum release of iodide was observed in the used conditions.

4.2. LDH as storage materials

LDH materials, synthesized by coprecipitation, anionic exchange or reconstruction, of different composition were tested for immobilization of iodate and iodide. The reconstruction protocol gave the highest iodate incorporation, ca. 54% vs. ca. 23% reached by coprecipitation. It was found that even if the fraction of iodate incorporated into the host structure was relatively high, the stability of synthesized iodate-LDH was very low. Heating at 453 K leads to nearly 70% of iodine loss. In the same line more than 90% of incorporated iodate was released after one day in brine solution. The iodide was incorporated at lower extent in comparison to iodate, probably due to differences in charge density, size and conformation of IO_3^- and I^- ions.

As expected, the simultaneous adsorption tests of Cs and I showed that Cs^+ did not adsorb on the sample due to the lack of interaction with the LDH.

From all the data obtained, we may conclude that LDHs can be considered as iodine scavengers for a short-term storage, but they are not suitable for a long-term storage of radioactive iodine (in form of I^- or IO_3^-), due to their low thermal stability and ease iodine release in contact with aqueous media (here studied: MilliQ water and brine).

5. Bibliography

UNIVERSITAT ROVIRA I VIRGILI
ON THE USE OF LAYERED DOUBLE HYDROXIDES IN THE MANAGEMENT OF 129I FROM LIQUID NUCLEAR WASTES
Luis Iglesias Pérez
Dipòsit Legal: T 893-2015

1. El-Wakil, M. M., Nuclear Fission Power Plants the State of the Art. In *Alternative Energy Sources*, Manassah, J. T., Ed. Academic Press: 1981; pp 519-605.

2. Magaud, P.; Marbach, G.; Cook, I., Nuclear Fusion Reactors. In *Encyclopedia of Energy*, Cleveland, C. J., Ed. Elsevier: New York, 2004; pp 365-381.

3. *Nuclear Technology Review 2014*. International Atomic Energy Agency: Vienna, Austria, 2014.

4. Breeze, P., Chapter 17 - Nuclear Power. In *Power Generation Technologies (Second Edition)*, Breeze, P., Ed. Newnes: Boston, 2014; pp 353-378.

5. Marques, J. G., Evolution of nuclear fission reactors: Third generation and beyond. *Energy Conversion and Management* **2010,** *51* (9), 1774-1780.

6. Blin-Stoyle, R. J., *Eureka! Physics of Particles, Matter and the Universe*. Institute of Physics Publishing, The Institute of Physics: London, 1997; Vol. 1, p 139-142.

7. Magill, J.; Galy, J., *Radioactivity Radionuclides Radiation*. Springer Berlin Heidelberg: 2005.

8. Stoker, H. S., *General, Organic, and Biological Chemistry*. Cengage Learning: 2012.

9. Stevens, L. G., Injurious effects on the skin. *Br. Med. J* **1896,** *1*.

10. Gilchrist, T. C., A case of dermatitis due to the X-rays. *Bulletin Johns Hopkins Hospital* **1897,** *7*.

11. Wow! Now Chemcraft has Atomic Energy! *Popular Science* December 1947, 1947.

12. Gehe und Co., D., *Gehes Codex der pharmazeutischen Spezialpräparate mit Angaben über Zusammensetzung, Indikationen, Zubereitungsformen und Hersteller*. 1926.

13. Blaufox, M. D., Radioactive artifacts: Historical sources of modern radium contamination. *Seminars in Nuclear Medicine* **1988,** *18* (1), 46-64.

14. Wiesner, B. P., BIOLOGICAL DANGERS FROM ATOMIC FISSION. *The Lancet* **1946,** *247* (6384), 33.

15. Pastore, J. O., The short-term effects of nuclear war: The medical legacy of Hiroshima and Nagasaki. *Preventive Medicine* **1987,** *16* (3), 293-307.

16. Shaeffer, J. R., Radiation injuries, with notes on Hiroshima and Nagasaki. *The American Journal of Surgery* **1957,** *93* (4), 641-643.

17. Harper, R. M.; Tinnacher, R. M., Plutonium. In *Encyclopedia of Ecology*, Jørgensen, S. E.; Fath, B. D., Eds. Academic Press: Oxford, 2008; pp 2845-2850.

18. Amiro, B. D., Environmental Radioactivity. In *Encyclopedia of Physical Science and Technology (Third Edition)*, Meyers, R. A., Ed. Academic Press: New York, 2003; pp 583-599.

19. Federation of Electric Power Companies of Japan (電気事業連合会) http://www.fepc.or.jp

20. Melnick, E. L.; Everitt, B. S., *Encyclopedia of Quantitative Risk Analysis and Assessment*. Wiley: 2008.

21. Walley El-Dine, N., Study of natural radioactivity and the state of radioactive disequilibrium in U-series for rock samples, North Eastern Desert, Egypt. *Applied Radiation and Isotopes* **2008,** *66* (1), 80-85.

22. Chougaonkar, M. P.; Eappen, K. P.; Ramachandran, T. V.; Shetty, P. G.; Mayya, Y. S.; Sadasivan, S.; Venkat Raj, V., Profiles of doses to the population living in the high background radiation areas in Kerala, India. *Journal of Environmental Radioactivity* **2004,** *71* (3), 275-297.

23. *Sexto Plan General de Residuos Radioactivos*. Ministerio de Industria, Turismo y Comercio: 2006.

24. Zucchetti, M., Radioactivity Transfer in Environment and Food by Fokion K. Vosniakos. *Nuclear Physics News* **2013,** *23* (4), 39-39.

25. Dueñas, C.; Fernández, M. C.; Liger, E.; Carretero, J., Natural radioactivity levels in bottled water in Spain. *Water Research* **1997,** *31* (8), 1919-1924.

26. Mola, M.; Palomo, M.; Peñalver, A.; Aguilar, C.; Borrull, F., Distribution of naturally occurring radioactive materials in sediments from the Ebro river reservoir in Flix (Southern Catalonia, Spain). *Journal of Hazardous Materials* **2011,** *198* (0), 57-64.

27. Biermans, G.; Horemans, N.; Vanhoudt, N.; Vandenhove, H.; Saenen, E.; Van Hees, M.; Wannijn, J.; Vives i Batlle, J.; Cuypers, A., An organ-based approach to dose calculation in the assessment of dose-dependent biological effects of ionising radiation in Arabidopsis thaliana. *Journal of Environmental Radioactivity* **2014,** *133* (0), 24-30.

28. Willey, N.; Collins, C., Phytoremediation of soils contaminated with radionuclides. In *Radioactivity in the Environment*, George, S., Ed. Elsevier: 2007; Vol. Volume 10, pp 43-69.

29. Jha, A. N.; Blake, W. H.; Millward, G. E., Preface: environmental radioactivity: implications for human and environmental health. *Journal of Environmental Radioactivity* **2014,** *133* (0), 1-4.

30. Jenkinson, S. B.; McCubbin, D.; Kennedy, P. H. W.; Dewar, A.; Bonfield, R.; Leonard, K. S., An estimate of the inventory of technetium-99 in the sub-tidal sediments of the Irish Sea. *Journal of Environmental Radioactivity* **2014,** *133* (0), 40-47.

31. Organization, W. H., *Preliminary Dose Estimation from the Nuclear Accident After the 2011 Great East Japan Earthquake and Tsunami*. The Organization: 2012.

32. Devillers, C., Payen J.P. and Manesse, D., Activité alpha, beta Neutronique, Spectre d'Emission gamma et Puissance Residuelle d'un Combustible P.W.R. Irradié. *Internal Report CEA/SERMA/S/314* **June 1977**.

33. Ley 24/2005, de 18 de noviembre, de reformas para el impulso a la productividad. *Boletín Oficial del Estado* **2005,** *277 (19th November)*, 37846-37868.

34. Real Decreto 1522/1984, de 4 de julio, por el que se autoriza la constitución de la «Empresa Nacional de Residuos Radiactivos, S. A.» (ENRESA). *Boletín Oficial del Estado* **1984,** *201 (22nd August)*, 24186-24187.

35. Ley 25/1964, de 29 de abril, sobre energía nuclear. *Boletín Oficial del Estado* **1964,** *107 (4th May)*, 5688-5696.

36. Ley 11/2009, de 26 de octubre, por la que se regulan las Sociedades Anónimas Cotizadas de Inversión en el Mercado Inmobiliario. *Boletín Oficial del Estado* **2009,** *259 (27th October)*, 89693-89723.

37. Johnson, A. B. J. *Behavior of spent nuclear fuel in water pool storage*; BNWL-2256; TRN: 78-000073 United StatesTRN: 78-000073Mon Jan 12 07:39:46 EST 2015Dep. NTIS, PC A06/MF A01.PNNL; ERA-03-008314; NTS-78-000499; EDB-78-008097English; 1977; p Medium: ED; Size: Pages: 104.

38. Chapman, N.; Hooper, A., The disposal of radioactive wastes underground. *Proceedings of the Geologists' Association* **2012,** *123* (1), 46-63.

39. García, R.; Catalán, J. P.; Sanz, J., Assessment of radioactive wastes from a DCLL fusion reactor: Disposal in El Cabril facility. *Fusion Engineering and Design* **2014,** *89* (9–10), 2038-2042.

40. Rempe, N. T., Permanent underground repositories for radioactive waste. *Progress in Nuclear Energy* **2007,** *49* (5), 365-374.

41. Compton, K. L.; Novikov, V. M.; Parker, F. L., *Deep Well Injection of Liquid Radioactive Waste at Krasnoyarsk-26: Analysis of hypothetical scenarios*. International Institute for Applied Systems Analysis: 2001.

42. Rybalchenko, A. I.; Pimenov, M. K.; Kurochkin, V. M.; Kamnev, E. N.; Korotkevich, V. M.; Zubkov, A. A.; Khafizov, R. R., Deep Injection Disposal of Liquid Radioactive Waste in Russia, 1963–2002: Results and Consequences. In *Developments in Water Science*, Chin-Fu, T.; John, A. A., Eds. Elsevier: 2005; Vol. Volume 52, pp 13-19.

43. Bates, E. A.; Driscoll, M. J.; Lester, R. K.; Arnold, B. W., Can deep boreholes solve America′s nuclear waste problem? *Energy Policy* **2014,** *72* (0), 186-189.

44. Boehmer-Christiansen, S. A., Dumping nuclear waste into the Sea: International control and the role of science and law. *Marine Policy* **1983,** *7* (1), 25-36.

45. Benn, A. R.; Weaver, P. P.; Billet, D. S. M.; van den Hove, S.; Murdock, A. P.; Doneghan, G. B.; Le Bas, T., Human Activities on the Deep Seafloor in the North East Atlantic: An Assessment of Spatial Extent. *PLoS ONE* **2010,** *5* (9), e12730.

46. Mukerjee, M., Poisoned Shipments: Are Strange, Illicit Sinkings Making the Mediterranean Toxic? *Scientific American* 2010.

47. Lindblom, U. L. F.; Gnirk, P., Alternative Methods of Nuclear Waste Disposal. In *Nuclear Waste Disposal*, Gnirk, U. L., Ed. Pergamon: 1982; pp 10-12.

48. Hanifah, N. A.; Hashim, R., The Madrid Protocol 1991 and its Environmental Impacts towards the Quality of Life. *Procedia - Social and Behavioral Sciences* **2012,** *35* (0), 398-403.

49. Salvatores, M.; Palmiotti, G., Radioactive waste partitioning and transmutation within advanced fuel cycles: Achievements and challenges. *Progress in Particle and Nuclear Physics* **2011,** *66* (1), 144-166.

50. Wootan, D. W., Nelson, J.V., Transmutation of Selected Fission Products in a Fast Reactor. In *AmericanNuclear Society Global '93--FutureNuclear Systems: EmergingFuel Cycles and Waste DmposalOptionsConference*, Westinghouse Hanford Company: Seattle, WA, 1993.

51. Choppin, G. R.; Khankhasayev, M. K., *Chemical Separation Technologies and Related Methods of Nuclear Waste Management: Applications, Problems, and Research Needs*. Springer Netherlands: 1999.

52. Systems, C. S. T. T.; Commission on Geosciences, E. R.; Studies, D. E. L.; Council, N. R., *Nuclear Wastes: Technologies for Separations and Transmutation*. National Academies Press: 1996.

53. Nieder-Westermann, G. H.; Bollingerfehr, W., 14 - Germany: experience of radioactive waste (RAW) management and contaminated site clean-up. In *Radioactive Waste Management and Contaminated Site Clean-Up*, Lee, W. E.; Ojovan, M. I.; Jantzen, C. M., Eds. Woodhead Publishing: 2013; pp 462-488.

54. Conca, J.; Kirchner, T., 22 - Environmental monitoring programs and public engagement for siting and operation of geological repository systems: experience at the Waste Isolation Pilot Plant (WIPP). In *Geological Repository Systems for Safe Disposal of Spent Nuclear Fuels and Radioactive Waste*, Ahn, J.; Apted, M. J., Eds. Woodhead Publishing: 2010; pp 678-718.

55. Jabbar, T.; Wallner, G.; Steier, P., A review on 129I analysis in air. *Journal of Environmental Radioactivity* **2013,** *126* (0), 45-54.

56. Eisenbud, M.; Gesell, T., Chapter 6 - Natural Radioactivity. In *Environmental Radioactivity (Fourth Edition)*, Eisenbud, M.; Gesell, T., Eds. Academic Press: San Diego, 1997; pp 134-200.

57. Rao, U.; Fehn, U., Sources and reservoirs of anthropogenic iodine-129 in western New York. *Geochimica et Cosmochimica Acta* **1999,** *63* (13–14), 1927-1938.

58. Herod, M. N.; Clark, I. D.; Kieser, W. E.; Agosta, S.; Zhao, X.-L., 129I dispersion and sources in Northwest Canada. *Nuclear Instruments and Methods in Physics Research Section B: Beam Interactions with Materials and Atoms* **2013,** *294* (0), 552-558.

59. Suárez, J. A.; Espartero, A. G.; Rodríguez, M., Radiochemical analysis of 129I in radioactive waste streams. *Nuclear Instruments and Methods in Physics Research Section A: Accelerators, Spectrometers, Detectors and Associated Equipment* **1996,** *369* (2–3), 407-410.

60. Tigeras, A.; Bachet, M.; Catalette, H.; Simoni, E., PWR iodine speciation and behaviour under normal primary coolant conditions: An analysis of thermodynamic calculations, sensibility evaluations and NPP feedback. *Progress in Nuclear Energy* **2011,** *53* (5), 504-515.

61. Guidolin, M.; Guseo, R., A nuclear power renaissance? *Technological Forecasting and Social Change* **2012,** *79* (9), 1746-1760.

62. Buraglio, N.; Aldahan, A.; Possnert, G., 129I in lakes of the Chernobyl fallout region and its environmental implications. *Applied Radiation and Isotopes* **2001,** *55* (5), 715-720.

63. Paul, M.; Fink, D.; Hollos, G.; Kaufman, A.; Kutschera, W.; Magaritz, M., Measurement of 129I concentrations in the environment after the Chernobyl reactor accident. *Nuclear Instruments and Methods in Physics Research Section B: Beam Interactions with Materials and Atoms* **1987,** *29* (1–2), 341-345.

64. Hou, X.; Povinec, P. P.; Zhang, L.; Shi, K.; Biddulph, D.; Chang, C.-C.; Fan, Y.; Golser, R.; Hou, Y.; Ješkovský, M.; Jull, A. J. T.; Liu, Q.; Luo, M.; Steier, P.; Zhou, W., Iodine-129 in Seawater Offshore Fukushima: Distribution, Inorganic Speciation, Sources, and Budget. *Environ. Sci. Technol.* **2013,** *47* (7), 3091-3098.

65. Aldahan, A.; Alfimov, V.; Possnert, G., 129I anthropogenic budget: Major sources and sinks. *Appl. Geochem.* **2007,** *22* (3), 606-618.

66. Limited, A. E. o. C.; Miller, H. G.; Oscarson, D. W.; Watson, R. L., *An Evaluation of Potential Additives to a Clay - Based Buffer Material for the Immobilization of I-129*. Whiteshell Nuclear Research Establishment: 1986.

67. Krumhansl, J. L.; Brady, P. V.; Zhang, P.-C., Soil Mineral Backfills and Radionuclide Retention. In *Geochemistry of Soil Radionuclides*, Zhang, P.-C.; Brady, P. V., Eds. Soil Science Society of America: 2002; pp 191-209.

68. Li, D.; Kaplan, D. I.; Knox, A. S.; Crapse, K. P.; Diprete, D. P., Aqueous 99Tc, 129I and 137Cs removal from contaminated groundwater and sediments using highly effective low-cost sorbents. *Journal of Environmental Radioactivity* **2014,** *136* (0), 56-63.

69. Thibault, D. H.; Sheppard, I.; Smith, P. A.; Establishment, W. N. R.; Limited, A. E. o. C., *A Critical Compilation and Review of Default Soil Solid/liquid Partition Coefficients, Kd, for Use in Environmental Assessments*. Whiteshell Nuclear Research Establishment: 1990.

70. Strickert, R.; Friedman, A. M.; Fried, S., The Sorption of Technetium and Iodine Radioisotopes by Various Minerals. *Nuclear Technology* **1980,** *49* (2), 253-266.

71. Balsley, S. D.; Brady, P. V.; Krumhansl, J. L.; Anderson, H. L., Anion Scavengers for Low-Level Radioactive Waste Repository Backfills. *Journal of Soil Contamination* **1998,** *7* (2), 125-141.

72. Gu, B. a. S., R. K. (Robert K.) and U.S. Nuclear Regulatory Commission. *Anion retention in soil possible application to reduce migration of buried technetium and iodine : a review*; Division of Regulatory Applications, Office of Nuclear Regulatory Research, U.S. Nuclear Regulatory Commission: Washington, DC, 1991

73. Dultz, S.; Riebe, B.; Bunnenberg, C., Temperature effects on iodine adsorption on organo-clay minerals: II. Structural effects. *Applied Clay Science* **2005,** *28* (1–4), 17-30.

74. Kaufhold, S.; Pohlmann-Lortz, M.; Dohrmann, R.; Nüesch, R., About the possible upgrade of bentonite with respect to iodide retention capacity. *Applied Clay Science* **2007,** *35* (1–2), 39-46.

75. Artioli, G., Inorganic Compounds and Minerals Studied Using X-Ray Diffraction. In *Encyclopedia of Spectroscopy and Spectrometry (Second Edition)*, Lindon, J. C., Ed. Academic Press: Oxford, 1999; pp 1048-1056.

76. Kvick, Å., Materials Science Applications of X-Ray Diffraction. In *Encyclopedia of Spectroscopy and Spectrometry (Second Edition)*, Lindon, J. C., Ed. Academic Press: Oxford, 1999; pp 1470-1478.

77. Niemantsverdriet, J. W., *Spectroscopy in Catalysis*. Wiley: 2007.

78. Koningsberger, D. C., X-ray absorption: principles, applications, techniques of EXAFS, SEXAFS, and XANES. John Wiley and Sons: United States, 1988.

79. Koningsberger, D. C.; Mojet, B. L.; van Dorssen, G. E.; Ramaker, D. E., XAFS spectroscopy; fundamental principles and data analysis. *Topics in Catalysis* **2000,** *10* (3-4), 143-155.

80. Reich, T.; Bernhard, G.; Geipel, G.; Funke, H.; Hennig, C.; Rossberg, A.; Matz, W.; Schell, N.; Nitsche, H., The Rossendorf beam line ROBL - A dedicated experimental station for XAFS measurements of actinides and other radionuclides. *Radiochim. Acta* **2000,** *88* (9-11).

81. Kominami, H.; Matsuura, T.; Iwai, K.; Ohtani, B.; Nishimoto, S.-i.; Kera, Y., Ultra-highly Active Titanium(IV) Oxide Photocatalyst Prepared by

Hydrothermal Crystallization from Titanium(IV) Alkoxide in Organic Solvents. *Chemistry Letters* **1995,** *24* (8), 693-694.

82. Li, Q.; Lin, B.; Wang, K.; Zhao, M.; Ruan, M., Surface properties of pulverized coal and its effects on coal mine methane adsorption behaviors under ambient conditions. *Powder Technology* **2015,** *270, Part A* (0), 278-286.

83. Zaki, M. I.; Fouad, N. E.; Mekhemer, G. A. H.; Jagadale, T. C.; Ogale, S. B., TiO2 nanoparticle size dependence of porosity, adsorption and catalytic activity. *Colloids and Surfaces A: Physicochemical and Engineering Aspects* **2011,** *385* (1–3), 195-200.

84. Brunauer, S.; Emmett, P. H.; Teller, E., Adsorption of Gases in Multimolecular Layers. *J. Am. Chem. Soc.* **1938,** *60* (2), 309-319.

85. Amelinckx, S., *Handbook of Microscopy: Applications in Materials Science, Solid-state Physics, and Chemistry*. VCH: 1997.

86. Danilatos, G. D., Foundations of Environmental Scanning Electron Microscopy. In *Advances in Electronics and Electron Physics*, Peter, W. H., Ed. Academic Press: 1988; Vol. Volume 71, pp 109-250.

87. http://www.phy.cam.ac.uk.

88. Tyutyunnikov, D.; Burak Özdöl, V.; Koch, C. T., Simultaneous orientation and thickness mapping in transmission electron microscopy. *Ultramicroscopy* **2015,** *150* (0), 37-43.

89. http://www2.warwick.ac.uk/fac/sci/physics/.

90. Goldstein, J., *Scanning Electron Microscopy and X-ray Microanalysis: Third Edition*. Springer US: 2003.

91. Goldstein, J., *Scanning Electron Microscopy and X-ray Microanalysis: A Text for Biologists, Materials Scientists, and Geologists*. Plenum Press: 1992.

92. Singh, A. K.; Mehtab, S., Polymeric membrane sensors based on Cd(II) Schiff base complexes for selective iodide determination in environmental and medicinal samples. *Talanta* **2008,** *74* (4), 806-814.

93. Van Os, E.; Gieling, T. H.; Lieth, J. H., 5 - Technical Equipment in Soilless Production Systems. In *Soilless Culture*, Raviv, M.; Lieth, J. H., Eds. Elsevier: Amsterdam, 2008; pp 157-XI.

94. Evans, A.; James, A. M.; ACOL, *Potentiometry and ion selective electrodes*. Published on behalf of ACOL, Thames Polytechnic, London, by Wiley: 1987.

95. Huang, Z.; Zhu, Z.; Subhani, Q.; Yan, W.; Guo, W.; Zhu, Y., Simultaneous determination of iodide and iodate in povidone iodine solution by ion chromatography with homemade and exchange capacity controllable columns and column-switching technique. *Journal of Chromatography A* **2012,** *1251* (0), 154-159.

96. Mahesh Kumar, G. N., I.; Ajitha, A.; Uma MaheshwaraRao, V., Inductively Coupled Plasma Atomic Emission Spectroscopy: An Overwiew. *International Journal of Pharmaceutical Research & Analysis* **2014,** *4* (8), 470-477.

97. http://www.rohs-cmet.in.

98. Prohaska, C.; Pomazal, K.; Steffan, I., Determination of Ca, Mg, Fe, Cu, and Zn in blood fractions and whole blood of humans by ICP-OES. *Fresenius J Anal Chem* **2000,** *367* (5), 479-484.

99. Trevizan, L. C.; Nogueira, A. R. A.; Nóbrega, J. A., Single vessel procedure for acid vapor partial digestion of bovine liver in a focused microwave: multielement determination by ICP-OES. *Talanta* **2003,** *61* (2), 81-86.

100. Lech, T., ICP OES and CV AAS in determination of mercury in an unusual fatal case of long-term exposure to elemental mercury in a teenager. *Forensic Science International* **2014,** *237* (0), e1-e5.

101. Sivakumar, S.; Khatiwada, C. P.; Sivasubramanian, J., Studies the alterations of biochemical and mineral contents in bone tissue of mus musculus due to aluminum toxicity and the protective action of desferrioxamine and deferiprone by FTIR, ICP-OES, SEM and XRD techniques. *Spectrochimica Acta Part A: Molecular and Biomolecular Spectroscopy* **2014,** *126* (0), 59-67.

102. Baran, A.; Wieczorek, J., Concentrations of heavy metals in hair as indicators of environmental pollution. *E3S Web of Conferences* **2013,** *1*, 21005.

103. Dimpe, K. M.; Ngila, J. C.; Mabuba, N.; Nomngongo, P. N., Evaluation of sample preparation methods for the detection of total metal content using inductively coupled plasma optical emission spectrometry (ICP-OES) in wastewater and sludge. *Physics and Chemistry of the Earth, Parts A/B/C* (0).

104. Hristozov, D.; Domini, C. E.; Kmetov, V.; Stefanova, V.; Georgieva, D.; Canals, A., Direct ultrasound-assisted extraction of heavy metals from sewage sludge samples for ICP-OES analysis. *Anal. Chim. Acta* **2004,** *516* (1–2), 187-196.

105. Chand, V.; Prasad, S., ICP-OES assessment of heavy metal contamination in tropical marine sediments: A comparative study of two digestion techniques. *Microchemical Journal* **2013,** *111* (0), 53-61.

106. Henglein, A., T. J. Mason, J. P. Lorimer: Sonochemistry (Theory, Applications and Uses of Ultrasound in Chemistry), Ellis Horwood Limited. Chichester, and John Wiley and Sons, New York 1988. 252 Seiten, Preis: £ 38.50. *Berichte der Bunsengesellschaft für physikalische Chemie* **1989,** *93* (10), 1150-1151.

107. Mason, T. J., *Practical sonochemistry: user's guide to applications in chemistry and chemical engineering*. E. Horwood: 1991.

108. Suslick, K. S.; Hammerton, D. A.; Cline, R. E., Sonochemical hot spot. *J. Am. Chem. Soc.* **1986,** *108* (18), 5641-5642.

109. Wibetoe, G.; Takuwa, D. T.; Lund, W.; Sawula, G., Coulter particle analysis used for studying the effect of sample treatment in slurry sampling electrothermal atomic absorption spectrometry. *Fresenius J Anal Chem* **1999,** *363* (1), 46-54.

110. Capelo-Martínez, J. L.; Ximénez-Embún, P.; Madrid, Y.; Cámara, C., Advanced oxidation processes for sample treatment in atomic spectrometry. *TrAC Trends in Analytical Chemistry* **2004,** *23* (4), 331-340.

111. Sato, T.; Fujita, H.; Endo, T.; Shimada, M.; Tsunashima, A., Synthesis of hydrotalcite-like compounds and their physico-chemical properties. *Reactivity of Solids* **1988,** *5* (2–3), 219-228.

112. Meyn, M.; Beneke, K.; Lagaly, G., Anion-exchange reactions of layered double hydroxides. *Inorganic Chemistry* **1990,** *29* (26), 5201-5207.

113. Ding, Y.; Alpay, E., Equilibria and kinetics of CO2 adsorption on hydrotalcite adsorbent. *Chemical Engineering Science* **2000,** *55* (17), 3461-3474.

114. Vaccari, A., Clays and catalysis: a promising future. *Applied Clay Science* **1999,** *14* (4), 161-198.

115. Barrabés, N.; Garrido, M. A.; Frare, A.; Monzón, A.; Tichit, D., Pt-MgZnCuAl hydrotalcite-derived catalysts in the reduction of nitrates using continuous and batch reactors. *Catalysis Today* **2011,** *175* (1), 328-337.

116. Miranda, R.-A.; Llorca, J.; Finocchio, E.; Ramis, G.; Medina, F.; Sueiras, J. E.; Segarra, A. M., Novel nanohybrid materials based on l-leucine on hydrotalcite clays: Asymmetric epoxidation reaction of chalcona. *Catalysis Today* **2011,** *172* (1), 48-52

117. Kovanda, F.; Maryšková, Z.; Kovář, P., Intercalation of paracetamol into the hydrotalcite-like host. *Journal of Solid State Chemistry* **2011,** *184* (12), 3329-33353.

118. Bonina, F. P.; Giannossi, M. L.; Medici, L.; Puglia, C.; Summa, V.; Tateo, F., Diclofenac-hydrotalcite: In vitro and in vivo release experiments. *Applied Clay Science* **2008,** *41* (3–4), 165-1714.

119. Yu, X.; Wang, J.; Zhang, M.; Yang, P.; Yang, L.; Cao, D.; Li, J., One-step synthesis of lamellar molybdate pillared hydrotalcite and its application for AZ31 Mg alloy protection. *Solid State Sciences* **2009,** *11* (2), 376-381.

120. Vega, J. M.; Granizo, N.; de la Fuente, D.; Simancas, J.; Morcillo, M., Corrosion inhibition of aluminum by coatings formulated with Al–Zn–vanadate hydrotalcite. *Progress in Organic Coatings* **2011,** *70* (4), 213-219.

121. Pérez-Bernal, M. E.; Ruano-Casero, R. J.; Rives, V., Effect of added zinc on the properties of cobalt-containing ceramic pigments prepared from

layered double hydroxides. *Journal of Solid State Chemistry* **2009,** *182* (9), 2566-2578.

122. Catti, M.; Ferraris, G.; Hull, S.; Pavese, A., Static compression and H disorder in brucite, Mg(OH)2, to 11 GPa: a powder neutron diffraction study. *Phys Chem Minerals* **1995,** *22* (3), 200-206.

123. http://www.public.asu.edu.

124. Ohtsuka, K.; Suda, M.; Tsunoda, M.; Ono, M., Synthesis of metal hydroxide-layer silicate intercalation compounds (metal = Mg(II), Ca(II), Mn(II), Fe(II), Co(II), Ni(II), Zn(II), and Cd(II)). *Chemistry of Materials* **1990,** *2* (5), 511-517.

125. Basu, D.; Das, A.; Stöckelhuber, K. W.; Wagenknecht, U.; Heinrich, G., Advances in layered double hydroxide (LDH)-based elastomer composites. *Progress in Polymer Science* **2014,** *39* (3), 594-626.

126. Besserguenev, A. V.; Fogg, A. M.; Francis, R. J.; Price, S. J.; O'Hare, D.; Isupov, V. P.; Tolochko, B. P., Synthesis and Structure of the Gibbsite Intercalation Compounds $[LiAl_2(OH)_6]X$ {X = Cl, Br, NO_3} and $[LiAl_2(OH)_6]Cl{\cdot}H_2O$ Using Synchrotron X-ray and Neutron Powder Diffraction. *Chemistry of Materials* **1997,** *9* (1), 241-247.

127. Intissar, M.; Holler, S.; Malherbe, F.; Besse, J.-P.; Leroux, F., Incorporation of Ti4+ into layered double hydroxide sheets? The response by X-ray diffraction and absorption study. *Journal of Physics and Chemistry of Solids* **2004,** *65* (2–3), 453-457.

128. Intissar, M.; Malherbe, F.; Prévot, V.; Leroux, F., Evidences of segregated SnO2 type nanoparticles coating layered double hydroxide at moderate temperature. *Journal of Colloid and Interface Science* **2006,** *299* (2), 747-753.

129. Cavani, F.; Trifirò, F.; Vaccari, A., Hydrotalcite-type anionic clays: Preparation, properties and applications. *Catalysis Today* **1991,** *11* (2), 173-301.

130. Radha, A. V.; Kamath, P. V.; Shivakumara, C., Order and disorder among the layered double hydroxides: combined Rietveld and DIFFaX approach. *Acta Crystallographica Section B* **2007,** *63* (2), 243-250.

131. Trave, A.; Selloni, A.; Goursot, A.; Tichit, D.; Weber, J., First Principles Study of the Structure and Chemistry of Mg-Based Hydrotalcite-Like Anionic Clays. *The Journal of Physical Chemistry B* **2002,** *106* (47), 12291-12296.

132. Hofmeister, W.; Platen, H. V., Crystal Chemistry and Atomic Order in Brucite-related Double-layer Structures. *Crystallography Reviews* **1992,** *3* (1), 3-26.

133. Borja, M.; Dutta, P. K., Fatty acids in layered metal hydroxides: membrane-like structure and dynamics. *The Journal of Physical Chemistry* **1992,** *96* (13), 5434-5444.

134. Xiao, Y.; Thorpe, M. F.; Parkinson, J. B., Two-dimensional discrete Coulomb alloy. *Physical Review B* **1999,** *59* (1), 277-285.

135. Khan, A. I.; O'Hare, D., Intercalation chemistry of layered double hydroxides: recent developments and applications. *Journal of Materials Chemistry* **2002,** *12* (11), 3191-3198.

136. Kameda, T.; Takeuchi, H.; Yoshioka, T., Hybrid inorganic/organic composites of Mg–Al layered double hydroxides intercalated with citrate, malate, and tartrate prepared by co-precipitation. *Materials Research Bulletin* **2009,** *44* (4), 840-845.

137. Miyata, S., Anion-exchange properties of hydrotalcite-like compounds. *Clays and Clay Minerals* **1983,** *31* (4), 305-311.

138. Britto, S.; Radha, A. V.; Ravishankar, N.; Kamath, P. V., Solution decomposition of the layered double hydroxide (LDH) of Zn with Al. *Solid State Sciences* **2007,** *9* (3–4), 279-286.

139. Crepaldi, E. L.; Pavan, P. C.; Valim, J. B., Comparative study of the coprecipitation methods for the preparation of Layered Double Hydroxides. *Journal of the Brazilian Chemical Society* **2000,** *11*, 64-70.

140. Bravo-Suárez, J. J.; Páez-Mozo, E. A.; Oyama, S. T., Review of the synthesis of layered double hydroxides: a thermodynamic approach. *Química Nova* **2004,** *27*, 601-614.

141. Gerds, N.; Katiyar, V.; Koch, C. B.; Risbo, J.; Plackett, D.; Hansen, H. C. B., Synthesis and characterization of laurate-intercalated Mg–Al layered double hydroxide prepared by coprecipitation. *Applied Clay Science* **2012,** *65–66* (0), 143-151.

142. Rabenau, A., The Role of Hydrothermal Synthesis in Preparative Chemistry. *Angewandte Chemie International Edition in English* **1985,** *24* (12), 1026-1040.

143. Rives, V. a. e., *Layered Double Hydroxides: present and future*. 1 ed.; Nova Science Pub Inc: New York, 2001.

144. Fornasari, G.; Gazzano, M.; Matteuzzi, D.; Trifirò, F.; Vaccari, A., Structure and reactivity of high-surface-area Ni/Mg/Al mixed oxides. *Applied Clay Science* **1995,** *10* (1–2), 69-82.

145. Carlino, S.; Hudson, M. J., Thermal intercalation of layered double hydroxides: capric acid into an Mg-Al LDH. *Journal of Materials Chemistry* **1995,** *5* (9), 1433-1442.

146. Hussein, M. Z. b.; Long, C. W., Synthesis of organo-mineral nanohybrid material: indole-2-carboxylate in the lamella of Zn–Al-layered double hydroxide. *Materials Chemistry and Physics* **2004,** *85* (2–3), 427-431.

147. Zhao, Y.; Li, F.; Zhang, R.; Evans, D. G.; Duan, X., Preparation of Layered Double-Hydroxide Nanomaterials with a Uniform Crystallite Size Using a New Method Involving Separate Nucleation and Aging Steps. *Chemistry of Materials* **2002,** *14* (10), 4286-4291.

148. Yun, S. K.; Pinnavaia, T. J., Water Content and Particle Texture of Synthetic Hydrotalcite-like Layered Double Hydroxides. *Chemistry of Materials* **1995,** *7* (2), 348-354.

149. Bravo-Suárez, J. J.; Páez-Mozo, E. A.; Oyama, S. T., Intercalation of Decamolybdodicobaltate(III) Anion in Layered Double Hydroxides. *Chemistry of Materials* **2004,** *16* (7), 1214-1225.

150. Liu, J.; Song, J.; Xiao, H.; Zhang, L.; Qin, Y.; Liu, D.; Hou, W.; Du, N., Synthesis and thermal properties of ZnAl layered double hydroxide by urea hydrolysis. *Powder Technology* **2014,** *253* (0), 41-45.

151. Costantino, U.; Marmottini, F.; Nocchetti, M.; Vivani, R., New Synthetic Routes to Hydrotalcite-Like Compounds − Characterisation and Properties of the Obtained Materials. *European Journal of Inorganic Chemistry* **1998,** *1998* (10), 1439-1446.

152. Li, F.; Liu, J.; Evans, D. G.; Duan, X., Stoichiometric Synthesis of Pure MFe2O4 (M = Mg, Co, and Ni) Spinel Ferrites from Tailored Layered Double Hydroxide (Hydrotalcite-Like) Precursors. *Chemistry of Materials* **2004,** *16* (8), 1597-1602.

153. Vogel, A. I., *Vogel's textbook of quantitative chemical analysis*. 5th ed. / ed.; Longman Scientific & Technical ;: Harlow, Essex, England : New York, 1989.

154. Morel-Desrosiers, N.; Pisson, J.; Israeli, Y.; Taviot-Gueho, C.; Besse, J.-P.; Morel, J.-P., Intercalation of dicarboxylate anions into a Zn-Al-Cl layered double hydroxide: microcalorimetric determination of the enthalpies of anion exchange. *Journal of Materials Chemistry* **2003,** *13* (10), 2582-2585.

155. Israeli, Y.; Taviot-Gueho, C.; Besse, J.-P.; Morel, J.-P.; Morel-Desrosiers, N., Thermodynamics of anion exchange on a chloride-intercalated zinc-aluminum layered double hydroxide: a microcalorimetric study. *Journal of the Chemical Society, Dalton Transactions* **2000,** (5), 791-796.

156. Newman, S. P.; Jones, W., Comparative Study of Some Layered Hydroxide Salts Containing Exchangeable Interlayer Anions. *Journal of Solid State Chemistry* **1999,** *148* (1), 26-40.

157. P. Newman, S.; Jones, W., Synthesis, characterization and applications of layered double hydroxides containing organic guests. *New Journal of Chemistry* **1998,** *22* (2), 105-115.

158. Kukkadapu, R. K.; Witkowski, M. S.; Amonette, J. E., Synthesis of a Low-Carbonate High-Charge Hydrotalcite-like Compound at Ambient Pressure and Atmosphere. *Chemistry of Materials* **1997,** *9* (2), 417-419.

159. Ying, X.; Dianqing, L.; Lingling, R.; EVANS, D. G.; Xue, D., Assembly and Structural Characteristics of Supramolecular Salicy late-pillared Hydrotalcites. *Acta Chimica Sinica* **2003,** *61* (2), 267-272.

160. Marchi, A. J.; Apesteguía, C. R., Impregnation-induced memory effect of thermally activated layered double hydroxides. *Applied Clay Science* **1998,** *13* (1), 35-48.

161. Răciulete, M.; Layrac, G.; Tichit, D.; Marcu, I.-C., Comparison of CuxZnAlO mixed oxide catalysts derived from multicationic and hybrid LDH precursors for methane total oxidation. *Applied Catalysis A: General* **2014,** *477* (0), 195-204.

162. Erickson, K. L.; Bostrom, T. E.; Frost, R. L., A study of structural memory effects in synthetic hydrotalcites using environmental SEM. *Materials Letters* **2005,** *59* (2–3), 226-229.

163. Stanimirova, T. S.; Kirov, G.; Dinolova, E., Mechanism of hydrotalcite regeneration. *Journal of Materials Science Letters* **2001,** *20* (5), 453-455.

164. Rocha, J.; del Arco, M.; Rives, V.; A. Ulibarri, M., Reconstruction of layered double hydroxides from calcined precursors: a powder XRD and 27Al MAS NMR study. *Journal of Materials Chemistry* **1999,** *9* (10), 2499-2503.

165. Aloisi, G. G.; Costantino, U.; Elisei, F.; Latterini, L.; Natali, C.; Nocchetti, M., Preparation and photo-physical characterisation of nanocomposites obtained by intercalation and co-intercalation of organic chromophores into hydrotalcite-like compounds. *Journal of Materials Chemistry* **2002,** *12* (11), 3316-3323.

166. You, Y.; Zhao, H.; Vance, G. F., Hybrid organic-inorganic derivatives of layered double hydroxides and dodecylbenzenesulfonate: Preparation and adsorption characteristics. *Journal of Materials Chemistry* **2002,** *12* (4), 907-912.

167. Ogawa, M.; Asai, S., Hydrothermal Synthesis of Layered Double Hydroxide−Deoxycholate Intercalation Compounds. *Chemistry of Materials* **2000,** *12* (11), 3253-3255.

168. Li, F.; Duan, X., Applications of Layered Double Hydroxides. In *Layered Double Hydroxides*, Duan, X.; Evans, D., Eds. Springer Berlin Heidelberg: 2006; Vol. 119, pp 193-223.

169. Boehm, H.-P.; Steinle, J.; Vieweger, C., [Zn2Cr(Oh)6]X·2H2O, New Layer Compounds Capable of Anion Exchange and Intracrystalline Swelling. *Angewandte Chemie International Edition in English* **1977,** *16* (4), 265-266.

170. El Malki, K.; De Roy, A.; Besse, J. P., *New Cu-Cr layered double hydroxyde compound: discussion of pillaring with intercalated tetrahedral anions*. Elsevier: Paris, FRANCE, 1989; Vol. 26.

171. Shedam, M. R.; Venkateswara Rao, A., Effect of temperature on nucleation and growth of cadmium oxalate single crystals in silica gels. *Materials Chemistry and Physics* **1998,** *52* (3), 263-266.

172. Tichit, D.; Rolland, A.; Prinetto, F.; Fetter, G.; de Jesus Martinez-Ortiz, M.; Valenzuela, M. A.; Bosch, P., Comparison of the structural and acid-base properties of Ga- and Al-containing layered double hydroxides obtained by microwave irradiation and conventional ageing of synthesis gels. *Journal of Materials Chemistry* **2002,** *12* (12), 3832-3838.

173. Fetter, G.; Botello, A.; Lara, V. H.; Bosch, P., Detrital Mg(OH)2 and Al(OH)3 in Microwaved Hydrotalcites. *Journal of Porous Materials* **2001,** *8* (3), 227-232.

174. Seida, Y.; Nakano, Y.; Nakamura, Y., Crystallization of Layered Double Hydroxides by Ultrasound and the effect of crystal quality on their surface properties. *Clays and Clay Minerals* **2002,** *50* (4), 525-532.

175. Álvarez, M. G.; Chimentão, R. J.; Barrabés, N.; Föttinger, K.; Gispert-Guirado, F.; Kleymenov, E.; Tichit, D.; Medina, F., Structure

evolution of layered double hydroxides activated by ultrasound induced reconstruction. *Applied Clay Science* **2013,** *83–84* (0), 1-11.

176. Álvarez, M. G.; Plíšková, M.; Segarra, A. M.; Medina, F.; Figueras, F., Synthesis of glycerol carbonates by transesterification of glycerol in a continuous system using supported hydrotalcites as catalysts. *Applied Catalysis B: Environmental* **2012,** *113–114* (0), 212-220.

177. Mok, K. B.; Ross, J. R. H.; Sambrook, R. M., Thermally And Mechanically Stable Catalysts For Steam Reforming And Methanation. A New Concept In Catalyst Design. In *Studies in Surface Science and Catalysis*, G. Poncelet, P. G.; Jacobs, P. A., Eds. Elsevier: 1983; Vol. Volume 16, pp 291-299.

178. Paulhiac, J. L.; Clause, O., Surface coprecipitation of cobalt(II), nickel(II), or zinc(II) with aluminum(III) ions during impregnation of .gamma.-alumina at neutral pH. *J. Am. Chem. Soc.* **1993,** *115* (24), 11602-11603.

179. d'Espinose de la Caillerie, J.-B.; Kermarec, M.; Clause, O., Impregnation of .gamma.-Alumina with Ni(II) or Co(II) Ions at Neutral pH: Hydrotalcite-Type Coprecipitate Formation and Characterization. *J. Am. Chem. Soc.* **1995,** *117* (46), 11471-11481.

180. Merlen, E.; Gueroult, P.; d'Espinose de la Caillerie, J. B.; Rebours, B.; Bobin, C.; Clause, O., Hydrotalcite formation at the alumina/water interface during impregnation with Ni (II) aqueous solutions at neutral pH. *Applied Clay Science* **1995,** *10* (1–2), 45-56.

181. Winter, F.; Koot, V.; van Dillen, A. J.; Geus, J. W.; de Jong, K. P., Hydrotalcites supported on carbon nanofibers as solid base catalysts for the synthesis of MIBK. *Journal of Catalysis* **2005,** *236* (1), 91-100.

182. Álvarez, M. G.; Frey, A. M.; Bitter, J. H.; Segarra, A. M.; de Jong, K. P.; Medina, F., On the role of the activation procedure of supported hydrotalcites for base catalyzed reactions: Glycerol to glycerol carbonate and self-condensation of acetone. *Applied Catalysis B: Environmental* **2013,** *134–135* (0), 231-237.

183. Dussault, L.; Dupin, J. C.; Guimon, C.; Monthioux, M.; Latorre, N.; Ubieto, T.; Romeo, E.; Royo, C.; Monzón, A., Development of Ni–Cu–Mg–Al catalysts for the synthesis of carbon nanofibers by catalytic decomposition of methane. *Journal of Catalysis* **2007,** *251* (1), 223-232.

184. Jong, H. L.; Hye, J. N.; Seog, W. R.; Jung, D. Y., Hybrid assembly of layered double hydroxide nanocrystals with inorganic, polymeric and biomaterials from micro- to nanometer scales. *European Journal of Inorganic Chemistry* **2008,** (36), 5573-5578.

185. Wolters, M.; van Grotel, L. J. W.; Eggenhuisen, T. M.; Sietsma, J. R. A.; de Jong, K. P.; de Jongh, P. E., Combining confinement and NO calcination to arrive at highly dispersed supported nickel and cobalt oxide catalysts with a tunable particle size. *Catalysis Today* **2011,** *163* (1), 27-32.

186. Choudary, B. M.; Madhi, S.; Chowdari, N. S.; Kantam, M. L.; Sreedhar, B., Layered double hydroxide supported nanopalladium catalyst for Heck-, Suzuki-, Sonogashira-, and Stille-type coupling reactions of chloroarenes. *J Am Chem Soc* **2002,** *124* (47), 14127-36.

187. Kantam, M. L.; Roy, S.; Roy, M.; Sreedhar, B.; Choudary, B. M.; De, R. L., Layered double hydroxides supported rhodium(0): An efficient and reusable catalyst for Heck, Suzuki, and Stille reactions of haloarenes. *Journal of Molecular Catalysis A: Chemical* **2007,** *273* (1–2), 26-31.

188. Li, B.; Hu, Y.; Liu, J.; Chen, Z.; Fan, W., Preparation of poly (methyl methacrylate)/LDH nanocomposite by exfoliation-adsorption process. *Colloid Polym Sci* **2003,** *281* (10), 998-1001.

189. Li, F.; Tan, Q.; Evans, D.; Duan, X., Synthesis of carbon nanotubes using a novel catalyst derived from hydrotalcite-like Co–Al layered double hydroxide precursor. *Catal Lett* **2005,** *99* (3-4), 151-156.

190. Kirm, I.; Medina, F.; Rodríguez, X.; Cesteros, Y.; Salagre, P.; Sueiras, J., Epoxidation of styrene with hydrogen peroxide using hydrotalcites as heterogeneous catalysts. *Applied Catalysis A: General* **2004,** *272* (1–2), 175-185.

191. Costantino, U.; Curini, M.; Montanari, F.; Nocchetti, M.; Rosati, O., Hydrotalcite-like compounds as catalysts in liquid phase organic synthesis: I. Knoevenagel condensation promoted by [Ni0.73Al0.27(OH)2](CO3)0.135. *Journal of Molecular Catalysis A: Chemical* **2003,** *195* (1–2), 245-252.

192. Choudary, B. M.; Lakshmi Kantam, M.; Neeraja, V.; Koteswara Rao, K.; Figueras, F.; Delmotte, L., Layered double hydroxide fluoride: a novel solid base catalyst for C-C bond formation. *Green Chemistry* **2001,** *3* (5), 257-260.

193. Rives, V.; Prieto, O.; Dubey, A.; Kannan, S., Synergistic effect in the hydroxylation of phenol over CoNiAl ternary hydrotalcites. *Journal of Catalysis* **2003,** *220* (1), 161-171.

194. Kapoor, M. P.; Matsumura, Y., Liquid-phase methanol carbonylation catalyzed over tin promoted nickel–aluminium layered double hydroxide. *Catalysis Today* **2004,** *93–95* (0), 287-291.

195. Tanabe, K.; Hölderich, W. F., Industrial application of solid acid–base catalysts. *Applied Catalysis A: General* **1999,** *181* (2), 399-434.

196. Climent, M. J.; Corma, A.; Iborra, S.; Primo, J., Base Catalysis for Fine Chemicals Production: Claisen-Schmidt Condensation on Zeolites and Hydrotalcites for the Production of Chalcones and Flavanones of Pharmaceutical Interest. *Journal of Catalysis* **1995,** *151* (1), 60-66.

197. Aramendía, M. a. A.; Borau, V.; Jiménez, C.; Marinas, J. M.; Ruiz, J. R.; Urbano, F., Reduction of α,β-unsaturated aldehydes with basic MgO/M2O3 catalysts (M=Al, Ga, In). *Applied Catalysis A: General* **2003,** *249* (1), 1-9.

198. Bulbule, V. J.; Deshpande, V. H.; Velu, S.; Sudalai, A.; Sivasankar, S.; Sathe, V. T., Heterogeneous Henry reaction of aldehydes: Diastereoselective synthesis of nitroalcohol derivatives over Mg-Al hydrotalcites. *Tetrahedron* **1999,** *55* (30), 9325-9332.

199. Fishel, C. T.; Davis, R. J., Characterization of magnesium-aluminum mixed oxides by temperature-programmed reaction of 2-propanol. *Langmuir* **1994,** *10* (1), 159-165.

200. Li, F.; Zhang, L.; Evans, D. G.; Duan, X., Structure and surface chemistry of manganese-doped copper-based mixed metal oxides derived from layered double hydroxides. *Colloids and Surfaces A: Physicochemical and Engineering Aspects* **2004,** *244* (1–3), 169-177.

201. Carja, G.; Nakamura, R.; Niiyama, H., Copper and iron substituted hydrotalcites: properties and catalyst precursors for methylamines synthesis. *Applied Catalysis A: General* **2002,** *236* (1–2), 91-102.

202. Chen, A.; Xu, H.; Yue, Y.; Hua, W.; Shen, W.; Gao, Z., Hydrogenation of methyl benzoate to benzaldehyde over manganese oxide catalysts prepared from Mg/Mn/Al hydrotalcite-like compounds. *Applied Catalysis A: General* **2004,** *274* (1–2), 101-109.

203. Zhang, L.; Li, F.; Evans, D. G.; Duan, X., Structure and surface characteristics of Cu-based composite metal oxides derived from layered double hydroxides. *Materials Chemistry and Physics* **2004,** *87* (2–3), 402-410.

204. Kumbhar, P. S.; Sanchez-Valente, J.; Figueras, F., Reduction of aromatic nitro compounds with hydrazine hydrate in the presence of the iron(III) oxide-MgO catalyst prepared from a Mg・Fe hydrotalcite precursor. *Tetrahedron Letters* **1998,** *39* (17), 2573-2574.

205. Velu, S.; Swamy, C. S., Effect of substitution of Fe3+Cr3+ on the alkylation of phenol with methanol over magnesium-aluminium calcined hydrotalcite. *Applied Catalysis A: General* **1997,** *162* (1–2), 81-91.

206. Barrault, J.; Derouault, A.; Courtois, G.; Maissant, J. M.; Dupin, J. C.; Guimon, C.; Martinez, H.; Dumitriu, E., On the catalytic properties of mixed oxides obtained from the Cu-Mg-Al LDH precursors in the process of hydrogenation of the cinnamaldehyde. *Applied Catalysis A: General* **2004,** *262* (1), 43-51.

207. Holgado, M. J.; Labajos, F. M.; Montero, M. J. S.; Rives, V., Thermal decomposition of Mg/V hydrotalcites and catalytic performance of the products in oxidative dehydrogenation reactions. *Materials Research Bulletin* **2003,** *38* (14), 1879-1891.

208. Yoo, J. S.; Bhattacharyya, A. A.; Radlowski, C. A., De-SOx catalyst: an XRD study of magnesium aluminate spinel and its solid solutions. *Industrial & Engineering Chemistry Research* **1991,** *30* (7), 1444-1448.

209. Corma, A.; Palomares, A. E.; Rey, F., Optimization of SOx additives of FCC catalysts based on MgO-Al2O3 mixed oxides produced from hydrotalcites. *Applied Catalysis B: Environmental* **1994,** *4* (1), 29-43.

210. Lee, S. K.; Mogi, G.; Kim, J. W., The competitiveness of Korea as a developer of hydrogen energy technology: The AHP approach. *Energy Policy* **2008,** *36* (4), 1284-1291.

211. Bhattacharyya, A.; Chang, W. D.; Kleefisch, M. S.; Udovich, C. A., Catalyst prepared from nickel-containing hydrotalcite-like precursor compound. Google Patents: 1998.

212. Bhattacharyya, A.; Chang, W. D.; Kleefisch, M. S.; Udovich, C. A., Method for preparing synthesis gas using nickel catalysts. Google Patents: 1997.

213. Takehira, K.; Shishido, T.; Wang, P.; Kosaka, T.; Takaki, K., Autothermal reforming of CH4 over supported Ni catalysts prepared from Mg–Al hydrotalcite-like anionic clay. *Journal of Catalysis* **2004,** *221* (1), 43-54.

214. Lee, K.; Lee, W., Partial Oxidation of Methane to Syngas over Calcined Ni–Mg/Al Layered Double Hydroxides. *Catal Lett* **2002,** *83* (1-2), 65-70.

215. Morioka, H.; Shimizu, Y.; Sukenobu, M.; Ito, K.; Tanabe, E.; Shishido, T.; Takehira, K., Partial oxidation of methane to synthesis gas over supported Ni catalysts prepared from Ni–Ca/Al-layered double hydroxide. *Applied Catalysis A: General* **2001,** *215* (1–2), 11-19.

216. Rives, V.; Angeles Ulibarri, M. a., Layered double hydroxides (LDH) intercalated with metal coordination compounds and oxometalates. *Coordination Chemistry Reviews* **1999,** *181* (1), 61-120.

217. Giannelis, E. P.; Nocera, D. G.; Pinnavaia, T. J., Anionic photocatalysts supported in layered double hydroxides: intercalation and

photophysical properties of a ruthenium complex anion in synthetic hydrotalcite. *Inorganic Chemistry* **1987,** *26* (1), 203-205.

218. Schmassmann, A.; Tarnawski, A.; Gerber, H. A.; Flogerzi, B.; Sanner, M.; Varga, L.; Halter, F., Antacid provides better restoration of glandular structures within the gastric ulcer scar than omeprazole. *Gut* **1994,** *35* (7), 896-904.

219. Tarnawski, A. S.; Tomikawa, M.; Ohta, M.; Sarfeh, I. J., Antacid talcid activates in gastric mucosa genes encoding for EGF and its receptor. The molecular basis for its ulcer healing action. *Journal of Physiology Paris* **2000,** *94* (2), 93-98.

220. Rives, V.; del Arco, M.; Martín, C., Layered double hydroxides as drug carriers and for controlled release of non-steroidal antiinflammatory drugs (NSAIDs): A review. *Journal of Controlled Release 169* (1–2), 28-39.

221. Li, B.; He, J.; Evans, D. G.; Duan, X., Enteric-coated layered double hydroxides as a controlled release drug delivery system. *International Journal of Pharmaceutics* **2004,** *287* (1–2), 89-95.

222. Choy, J.-H.; Kwak, S.-Y.; Park, J.-S.; Jeong, Y.-J.; Portier, J., Intercalative Nanohybrids of Nucleoside Monophosphates and DNA in Layered Metal Hydroxide. *J. Am. Chem. Soc.* **1999,** *121* (6), 1399-1400.

223. Choy, J.-H.; Kwak, S.-Y.; Park, J.-S.; Jeong, Y.-J., Cellular uptake behavior of [[gamma]-32P] labeled ATP-LDH nanohybrids. *Journal of Materials Chemistry* **2001,** *11* (6), 1671-1674.

224. Aisawa, S.; Takahashi, S.; Ogasawara, W.; Umetsu, Y.; Narita, E., Direct Intercalation of Amino Acids into Layered Double Hydroxides by Coprecipitation. *Journal of Solid State Chemistry* **2001,** *162* (1), 52-62.

225. Nakayama, H.; Wada, N.; Tsuhako, M., Intercalation of amino acids and peptides into Mg–Al layered double hydroxide by reconstruction method. *International Journal of Pharmaceutics* **2004,** *269* (2), 469-478.

226. Hwang, S. H.; Han, Y. S.; Choy, J. H., Intercalation of functional organic molecules with pharmaceutical, cosmeceutical and nutraceutical functions into layered double hydroxides and zinc basic salts. *Bulletin of the Korean Chemical Society* **2001,** *22* (9), 1019-1022.

227. Aimoz, L.; Taviot-Guého, C.; Churakov, S. V.; Chukalina, M.; Dähn, R.; Curti, E.; Bordet, P.; Vespa, M., Anion and Cation Order in Iodide-Bearing Mg/Zn–Al Layered Double Hydroxides. *The Journal of Physical Chemistry C* **2012,** *116* (9), 5460-5475.

228. Theiss, F. L.; Sear-Hall, M. J.; Palmer, S. J.; Frost, R. L., Zinc aluminium layered double hydroxides for the removal of iodine and iodide from aqueous solutions. *Desalination and Water Treatment* **2012,** *39* (1-3), 166-175.

229. Maria Bastianini, D. C., Chiara Bisio, Leonardo Marchese, Umberto Costantino, Riccardo Vivani and MOrena Nocchetti, On the Intercalation of the Iodine-Iodide Couple on Layered Double Hydroxides with Different Particle Sizes. *Inorganic Chemistry* **2012,** *51*, 2560-2568.

230. Liang, L.; Li, L., Adsorption behavior of calcined layered double hydroxides towards removal of iodide contaminants. *J. Radioanal. Nucl. Chem.* **2007,** *273* (1), 221-226.

231. Zhang, J.; Zhang, F.; Ren, L.; Evans, D. G.; Duan, X., Synthesis of layered double hydroxide anionic clays intercalated by carboxylate anions. *Materials Chemistry and Physics* **2004,** *85* (1), 207-214.

232. Prasanna, S. V.; Kamath, P. V.; Shivakumara, C., Interlayer structure of iodide intercalated layered double hydroxides (LDHs). *Journal of Colloid and Interface Science* **2010,** *344* (2), 508-512.

233. Kulyukhin, S. A.; Krasavina, E. P.; Gredina, I. V.; Rumer, I. A.; Mizina, L. V., Sorption of cesium, strontium, and yttrium radionuclides from the aqueous phase on layered double hydroxides. *Radiochemistry* **2008,** *50* (5), 493-501.

234. Chibwe, K.; Jones, W., Intercalation of organic and inorganic anions into layered double hydroxides. *Journal of the Chemical Society, Chemical Communications* **1989,** (14), 926-927.

235. Toraishi, T.; Nagasaki, S.; Tanaka, S., Adsorption behavior of IO3− by CO32−- and NO3−-hydrotalcite. *Applied Clay Science* **2002,** *22* (1–2), 17-23.

236. Ogawa, M.; Kuroda, K., Photofunctions of Intercalation Compounds. *Chemical Reviews* **1995,** *95* (2), 399-438.

237. Valim, J.; Kariuki, B. M.; King, J.; Jones, W., Photoactivity of Cinnamate-Intercalates of Layered Double Hydroxides. *Molecular Crystals and Liquid Crystals Science and Technology. Section A. Molecular Crystals and Liquid Crystals* **1992,** *211* (1), 271-281.

238. Takagi, K.; Shichi, T.; Usami, H.; Sawaki, Y., Controlled photocycloaddition of unsaturated carboxylates intercalated in hydrotalcite clay interlayers. *J. Am. Chem. Soc.* **1993,** *115* (10), 4339-4344.

239. Shichi, T.; Takagi, K.; Sawaki, Y., Stereoselectivity control of [2 + 2] photocycloaddition by changing site distances of hydrotalcite interlayers. *Chemical Communications* **1996,** (17), 2027-2028.

240. Jayashree, R. S.; Kamath, P. V., Modified Nickel Hydroxide Electrodes: Effect of Cobalt Metal on the Different Polymorphic Modifications. *Journal of The Electrochemical Society* **2002,** *149* (6), A761-A764.

241. Chen, H.; Wang, J. M.; Pan, T.; Xiao, H. M.; Zhang, J. Q.; Cao, C. N., Effects of coprecipitated zinc on the structure and electrochemical performance of Ni/Al-layered double hydroxide. *International Journal of Hydrogen Energy* **2002,** *27* (5), 489-496.

242. Chen, H.; Wang, J. M.; Pan, T.; Zhao, Y. L.; Zhang, J. Q.; Cao, C. N., Physicochemical Properties and Electrochemical Performance of Al-substituted α-$Ni(OH)_2$ with Additives for Ni-Metal Hydride Batteries. *Journal of The Electrochemical Society* **2003,** *150* (11), A1399-A1404.

243. Jayashree, R. S.; Vishnu Kamath, P., Layered double hydroxides of Ni with Cr and Mn as candidate electrode materials for alkaline secondary cells. *Journal of Power Sources* **2002,** *107* (1), 120-124.

244. Sakaebe, H.; Uchino, H.; Azuma, M.; Shikano, M.; Higuchi, S., Cycleability of Ni–Fe hydroxides in nonaqueous electrolyte. *Solid State Ionics* **1998,** *113–115* (0), 35-41.

245. Mousty, C.; Therias, S.; Forano, C.; Besse, J.-P., Anion-exchanging clay-modified electrodes: synthetic layered double hydroxides intercalated with electroactive organic anions. *Journal of Electroanalytical Chemistry* **1994,** *374* (1–2), 63-69.

246. Therias, S.; Mousty, C., Electrodes modified with synthetic anionic clays. *Applied Clay Science* **1995,** *10* (1–2), 147-162.

247. Liao, C.-S.; Ye, W.-B., Structure and conductive properties of poly(ethylene oxide)/layered double hydroxide nanocomposite polymer electrolytes. *Electrochimica Acta* **2004,** *49* (27), 4993-4998.

248. Vaccari, A., Preparation and catalytic properties of cationic and anionic clays. *Catalysis Today* **1998,** *41* (1–3), 53-71.

249. van der Ven, L.; van Gemert, M. L. M.; Batenburg, L. F.; Keern, J. J.; Gielgens, L. H.; Koster, T. P. M.; Fischer, H. R., On the action of hydrotalcite-like clay materials as stabilizers in polyvinylchloride. *Applied Clay Science* **2000,** *17* (1–2), 25-34.

250. Miyata, S.; Kuroda, M., Method for inhibiting the thermal or ultraviolet degradation of thermoplastic resin and thermoplastic resin composition having stability to thermal or ultraviolet degradation. Google Patents: 1981.

251. Wang, X.; Zhang, Q., Effect of hydrotalcite on the thermal stability, mechanical properties, rheology and flame retardance of poly(vinyl chloride). *Polymer International* **2004,** *53* (6), 698-707.

252. Rives, V.; Pérez-Bernal, M. E.; Ruano-Casero, R. J.; Nebot-Díaz, I., Development of a black ceramic pigment from non stoichiometric hydrotalcites. *Journal of the European Ceramic Society* **2012,** *32* (5), 975-987.

253. Fraccarollo, A.; Cossi, M.; Marchese, L., DFT simulation of Mg/Al hydrotalcite with different intercalated anions: Periodic structure and solvating effects on the iodide/triiodide redox couple. *Chemical Physics Letters* **2010,** *494* (4–6), 274-278.

254. Moreira, F. K. V.; Pedro, D. C. A.; Glenn, G. M.; Marconcini, J. M.; Mattoso, L. H. C., Brucite nanoplates reinforced starch bionanocomposites. *Carbohydrate Polymers* **2013,** *92* (2), 1743-1751.

255. Palmer, S. J.; Frost, R. L., Use of hydrotalcites for the removal of toxic anions from aqueous solutions. *Industrial and Engineering Chemistry Research* **2010,** *49* (19), 8969-8976.

256. Pfeiffer, H.; Martínez-Dlcruz, L.; Lima, E.; Flores, J.; Vera, M. A.; Valente, J. S., Influence of Mg/Al ratio on the thermokinetic rehydration of calcined Mg-Al layered double hydroxides. *Journal of Physical Chemistry C* **2010,** *114* (18), 8485-8492.

257. Velu, S.; Ramkumar, V.; Narayanan, A.; Swamy, C. S., Effect of interlayer anions on the physicochemical properties of zinc-aluminium hydrotalcite-like compounds. *Journal of Materials Science* **1997,** *32* (4), 957-964.

258. Chang, Q.; Zhu, L.; Luo, Z.; Lei, M.; Zhang, S.; Tang, H., Sono-assisted preparation of magnetic magnesium–aluminum layered double hydroxides and their application for removing fluoride. *Ultrasonics Sonochemistry* **2011,** *18* (2), 553-561.

259. Ramesh, T. N.; Rajamathi, M.; Kamath, P. V., Ammonia induced precipitation of cobalt hydroxide: observation of turbostratic disorder. *Solid State Sciences* **2003,** *5* (5), 751-756.

260. Evans, D.; Slade, R. T., Structural Aspects of Layered Double Hydroxides. In *Layered Double Hydroxides*, Duan, X.; Evans, D., Eds. Springer Berlin Heidelberg: 2006; Vol. 119, pp 1-87.

261. Hall, K. R.; Eagleton, L. C.; Acrivos, A.; Vermeulen, T., Pore- and Solid-Diffusion Kinetics in Fixed-Bed Adsorption under Constant-Pattern

Conditions. *Industrial & Engineering Chemistry Fundamentals* **1966,** *5* (2), 212-223.

262. Jansson-Charrier, M.; Guibal, E.; Roussy, J.; Delanghe, B.; Le Cloirec, P., Vanadium (IV) sorption by chitosan: Kinetics and equilibrium. *Water Research* **1996,** *30* (2), 465-475.

263. Sonawane, S.; Chaudhari, P.; Ghodke, S.; Phadtare, S.; Meshram, S., Ultrasound assisted adsorption of basic dye onto organically modified bentonitenanoclay. *Journal of Scientific and Industrial Research* **2009,** *68* (2), 162-167.

264. Hibino, T.; Tsunashima, A., Characterization of repeatedly reconstructed Mg-Al hydrotalcite-like compounds: Gradual segregation of aluminum from the structure. *Chemistry of Materials* **1998,** *10* (12), 4055-4061.

265. Biard, B., Quantitative analysis of the fission product distribution in a damaged fuel assembly using gamma-spectrometry and computed tomography for the Phébus FPT3 test. *Nuclear Engineering and Design* **2013,** *262* (0), 469-483.

266. Mironov, V.; Kudrjashov, V.; Yiou, F.; Raisbeck, G. M., Use of 129I and 137Cs in soils for the estimation of 131I deposition in Belarus as a result of the Chernobyl accident. *Journal of Environmental Radioactivity* **2002,** *59* (3), 293-307.

267. Gómez-Guzmán, J. M.; Holm, E.; Enamorado-Báez, S. M.; Abril, J. A.; Pinto-Gómez, A. R.; López-Gutiérrez, J. M.; García-León, M., Pre- and post-Chernobyl accident levels of 129I and 137Cs in the Southern Baltic Sea by brown seaweed Fucus vesiculosus. *Journal of Environmental Radioactivity* **2013,** *115* (0), 134-142.

268. Yoshida, N.; Kanda, J., Tracking the Fukushima Radionuclides. *Science* **2012,** *336* (6085), 1115-1116.

269. Chino, M.; Nakayama, H.; Nagai, H.; Terada, H.; Katata, G.; Yamazawa, H., Preliminary Estimation of Release Amounts of 131I and 137Cs Accidentally Discharged from the Fukushima Daiichi Nuclear Power Plant into the Atmosphere. *Journal of Nuclear Science and Technology* **2011,** *48* (7), 1129-1134.

270. Tao, Q.; Zhang, Y.; Zhang, X.; Yuan, P.; He, H., Synthesis and characterization of layered double hydroxides with a high aspect ratio. *Journal of Solid State Chemistry* **2006,** *179* (3), 708-715.

271. Metz, V.; Schüßler, W.; Kienzler, B.; Fanghänel, T., Geochemically derived non-gaseous radionuclides source term for the Asse salt mine - assessment for the use of a $Mg(OH)_2$-based backfill material. *Radiochimica Acta* **2004,** *92*, 819 - 825.

272. Zhou, J.; Xu, Z. P.; Qiao, S.; Liu, Q.; Xu, Y.; Qian, G., Enhanced removal of triphosphate by MgCaFe-Cl-LDH: Synergism of precipitation with intercalation and surface uptake. *Journal of Hazardous Materials* **2011,** *189* (1–2), 586-594.

273. Pless, J.; Benjamin Chwirka, J.; Krumhansl, J., Iodine sequestration using delafossites and layered hydroxides. *Environ Chem Lett* **2007,** *5* (2), 85-89.

274. Chan, L. Y. Y.; Einstein, F. W. B., The Crystal Structure of KIO3.HIO3. *Canadian Journal of Chemistry* **1971,** *49* (3), 468-476.

275. Marcus, Y., *Ion properties*. Marcel Dekker: New York, 1997.

276. Lucy, C. A., Factors affecting selectivity of inorganic anions in capillary electrophoresis. *Journal of Chromatography A* **1999,** *850* (1–2), 319-337.

277. Cross, H. E.; Brown, D. R., Entrained sodium in mixed metal oxide catalysts derived from layered double hydroxides. *Catalysis Communications* **2010,** *12* (3), 243-245.

UNIVERSITAT ROVIRA I VIRGILI
ON THE USE OF LAYERED DOUBLE HYDROXIDES IN THE MANAGEMENT OF 129I FROM LIQUID NUCLEAR WASTES
Luis Iglesias Pérez
Dipòsit Legal: T 893-2015

Publications

Article

L. Iglesias, M.G. Álvarez, R.J. Chimentão, J.L. Leganés, F.Medina; On the role of ultrasound and mechanical stirring for iodide adsorption by calcined layered double hydroxides; Applied Clay Science 91–92 (2014) 70–78.

Submitted article

L. Iglesias, C.s Walther, F. Medina, M.G. Álvarez, A. Hölzer, N. Torapava, Are LDH phases suited as host matrices for radioactive iodine storage?, Journal of Radioanalytical and Nuclear Chemistry, submitted December 2014

Conference contributions

Poster: L. Iglesias, F. Medina; Desarrollo de un nuevo material adsorbente de isótopos radiactivos de difícil medida, 36 Reunión Anual de la Sociedad Nuclear Española, Santiago de Compostela, 2010.

Oral presentation: L. Iglesias, F. Medina; Estudio de la capacidad de adsorción de un material selectivo orientado a isótopos radioactivos; 37 Reunión Anual de la Sociedad Nuclear Española, Burgos, 2011

Oral presentation: L. Iglesias, F. Medina; Uso de dawsonitas como adsorbentes selectivos de aniones en procesos de limpieza de residuos nucleares, 38 Reunión Anual de la Sociedad Nuclear Española, Cáceres, 2012.

Oral presentation: L. Iglesias, F. Medina, M.G. Álvarez, R.J. Chimentão; Estudio comparativo de la capacidad de retención de yoduro por diferentes hidrotalcitas; 39 Reunión Anual de la Sociedad Nuclear Española, Reus, 2013.

Poster: L. Iglesias, F. Medina, M.G. Álvarez; Materiales adsorbentes selectivos para la adsorción y concentración de radioisótopos de difícil medida; VI Jornadas de I+D en gestión de residuos radiactivos, Cuenca, 2014.

Oral presentation: L. Iglesias, M. G. Álvarez, F. Medina; Use of adsorbent materials to clean up waters from nuclear power plants; 7th European Meeting on Chemical Industry and Environment, Tarragona, 2015.

UNIVERSITAT ROVIRA I VIRGILI
ON THE USE OF LAYERED DOUBLE HYDROXIDES IN THE MANAGEMENT OF 129I FROM LIQUID NUCLEAR WASTES
Luis Iglesias Pérez
Dipòsit Legal: T 893-2015

On preferential use of blue color:

Urania, muse of Exact Sciences and Astronomy in Greek Mythology, usually represented dressed in blue.

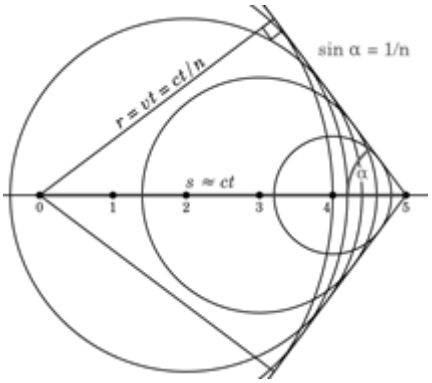

Cherenkov radiation occurs when charged particles are moving faster than the speed of light through a dielectric medium. The characteristic blue glow of an underwater nuclear reactor, where ^{129}I is generated, is due to Cherenkov radiation.

UNIVERSITAT ROVIRA I VIRGILI
ON THE USE OF LAYERED DOUBLE HYDROXIDES IN THE MANAGEMENT OF 129I FROM LIQUID NUCLEAR WASTES
Luis Iglesias Pérez
Dipòsit Legal: T 893-2015